Durham E-Theses

Observations of Cerenkov radiation produced in large cosmic ray showers at 1500m above sea-level

Shearer, J.A.L.

How to cite:

Shearer, J.A.L. (1980) *Observations of Cerenkov radiation produced in large cosmic ray showers at 1500m above sea-level*, Durham theses, Durham University. Available at Durham E-Theses Online: http://etheses.dur.ac.uk/7436/

OBSERVATIONS OF CERENKOV RADIATION PRODUCED

IN LARGE COSMIC RAY SHOWERS AT 1500M
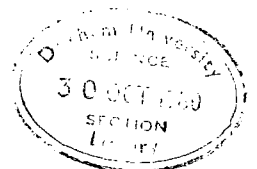
ABOVE SEA-LEVEL

by

J.A.L. SHEARER, B.Sc., M.Sc.

A thesis submitted to the University of Durham in
accordance with the regulations for admittance to
the Degree of Doctor of Philosophy.

Department of Physics
University of Durham

June 1980

ACKNOWLEDGEMENTS

ABSTRACT   (ii)

An experiment designed to measure Cerenkov radiation from
cosmic ray extensive air showers was deployed at Dugway, Utah
from October 1977 to March 1980. This thesis is concerned with
Cerenkov light measurements made at Dugway during the second
season of observation from October 1978 to March 1979.

An introduction to cosmic rays and extensive air showers
is followed by a review of previous studies (both theoretical and
experimental) of Cerenkov radiation from EAS. Particular attention
is given to Cerenkov light parameters which relate to the depth
of electron cascade maximum. A detailed account of the design and
performance of the array of Cerenkov light detectors is then given,
combined with an account of the first season of observation from
October to December 1977.

The calibration of the equipment during the second season of
observation is discussed, indicating the sensitivity of the
equipment to a light flux. This is followed by a description of
the procedure employed to reduce the data from the experiment. A
small sample of the recorded showers was selected to form the
basis of a preliminary analysis presented in this thesis.
Analysis of this sample of showers enabled the average character-
istics of Cerenkov radiation from showers of energy 5×10^{16} –
5×10^{17} eV to be determined.

The study of the average characteristics of Cerenkov radiation
indicated that the lateral distribution of photon density, the
peak height and FWHM of the Cerenkov pulses were sensitive to
the zenith angle and energy of the showers. From the lateral
distribution of photon density a primary energy estimator was
established. Consistency was found between the preliminary

results presented here and computer simulations. There were also favourable comparisons between the results of the Dugway experiment and similar measurements made at other establishments. A survey of vertically incident computer simulations of extensive air showers indicated that the basic assumptions behind the recently introduced elongation theorem may not be valid.

Finally, a review of the future work of the Dugway experiment is presented.

TABLE OF CONTENTS

.

CHAPTER ONE

The Cosmic Radiation

1-1 Introduction

Although most of the information about the observable
universe comes from studies of the cosmic electromagnetic
spectrum, there does exist another source of energy from the
cosmos - a background radiation of energetic particles. The
cosmic radiation, since its discovery by C.T.R. Wilson in
1901, has provided physicists with a number of basic problems.
Firstly, what is its astrophysical nature, i.e. its origin
and consituent particles? Secondly, what information can it
provide on the physics of particle interactions at ultra-high
energies? These two aspects of the study have become known
as the large and small scale quests.

The particles arrive at the earth over a large gamut
of energy from 100's of MeV to energies in excess of
10^{20}eV; cosmic particles with energies less than 100 MeV
can be regarded as being a local phenomena. At the lower
end of the energy spectrum the radiation consists of high
energy γ rays, electrons and atomic nuclei; at the higher end
the composition is unknown.

In the past, until the advent of particle accelerators,
the radiation provided the only means of studying high energy
particle interactions. Consequently it was from studies of
the cosmic radiation that many of the early discoveries in
particle physics were made; e.g. the positron which was
discovered using cloud chambers to observe the cosmic radiation,
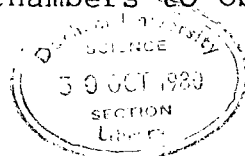
Anderson (1932). The muon also owes much of its theoretical

and experimental treatment to studies of cosmic radiation.

Particle accelerators have now reached energies previously only

attainable by studies of the radiation, consequently most

attention has been devoted recently to studying its astro-

physical nature. Studies of the radiation can be divided into

the following broad areas:-

(1) The Energy Spectrum

(2) The mass spectrum

(3) A search for anisotropies in the arrival
directions of the radiation.

By combining the results of studies of these three

aspects of the radiation it is hoped that its origin can be

ascertained.

1-2 Extensive Air Showers

As was stated above the energy of the cosmic radiation

spans over 11 orders of magnitude; it has been found that the

flux of the radiation can be expressed as a simple power law

of its energy. The integral flux can be expressed thus:

$$N \, (> E) \propto E^{\gamma}$$

where E is the radiation's energy. The exponent of the energy

spectrum, γ , has been observed to vary from -1.6 at low

energies to -2.2 at 5×10^{15} eV and possibly back to -1.6 at

energies beyond 5×10^{19} eV. The observed energy spectrum

is shown in figure 1-1. From this spectrum the flux at

10^{11} eV can be found to be $3.2 \mathrm{m}^{-2} \mathrm{s}^{-1} \mathrm{ster}^{-1}$ going down to

$1.6 \times 10^{-8} \mathrm{m}^{-2} \mathrm{s}^{-1} \mathrm{ster}^{-1}$ at 10^{16} eV, or $0.5 \mathrm{m}^{-2} \mathrm{yr}^{-1} \mathrm{ster}^{-1}$.

At low energies direct observation of the primary radiation

y-axis: Differential Flux $(m^{-2} s^{-1} sr^{-2} eV)$

x-axis: Primary Energy (eV)

a) Haverah Park

b) Volcano Ranch

c) Sydney
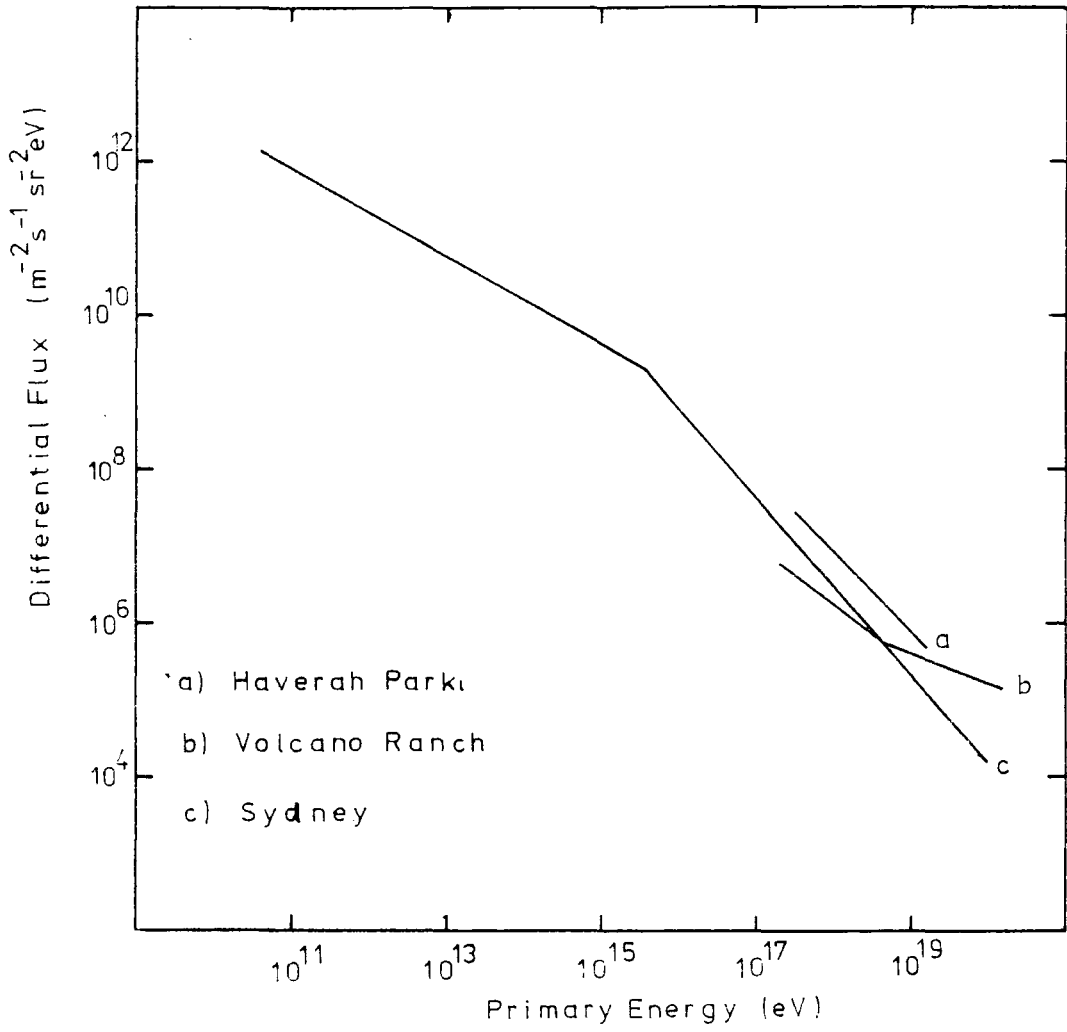
(i.e. before any significant interactions with atmospheric nuclei) is possible using the conventional tools of particle physics, e.g. nuclear emulsion stacks, flown in balloons. However, at higher energies the flux is so low that either exceptionally large detectors or experiments lasting an inordinately long time are required, if the radiation is to be observed directly. A natural large detector does however exist, namely the atmosphere. By studying the secondary radiation following interactions between the cosmic ray particles and atmospheric nuclei, the nature of the primary can be established. Following any particle interaction, a certain amount of the energy will be translated laterally to the direction of the initial particle. In addition Coulomb scattering of particles causes a lateral development. The cascades from the interactions between primary cosmic ray particles and air nuclei therefore have a spatial extent of kilometres at sea-level. By sampling the distribution of secondary particles at ground level, it is possible to detect high energy cosmic rays at a suitable rate, using detectors of modest sensitive area. The showers of secondary particles have become known as an Extensive Air Showers (EAS).

A simplified development of an EAS proceeds as follows. Firstly, accelerator studies indicate that after primary particle-air nucleus collisions, the majority of particles produced will be pi-mesons. Following the initial interaction the primary will not lose its identity and will continue with approximately half of its energy, to interact further and produce more pions. The average distance between interactions

is known from accelerator studies to be in the range 50-80g cm^{-2}.

Fluctuations in this value produce variations in the development

of EAS. The charged pions will either interact with air nuclei

to produce more pions, or will decay to muons which have a

high probability of surviving to the observational plane. All

neutral pions produced will decay almost instantaneously

(10^{-16}s) to 2 γ rays, which will each produce an electron-

positron pair. The electrons and positrons will, via bremsstrahlung

create more photons and so an electromagnetic cascade develops.

The muonic and electromagnetic components of an EAS are contin-

ually replenished by the hadronic cascade following the primary

through the atmosphere. The predicted average sea-level dis-

tribution of electrons and muons for 10^{17}eV primaries of

mass A = 1 and 56 are shown in figures 1-2 and 1-3. These

figures are derived from recent computer simulations carried

out by the University of Durham group, Gaisser et al (1978).

The core of a shower on the observation plane can be

determined by sampling the distribution of particles at ground

level. Then assuming a monotonic relationship between an

observable parameter, usually particle density, and core distance,

the centre of symmetry can be deduced. At the core the hadronic

cascade, which is of limited spatial extent, can be sampled

using flash-tube arrays, spark chambers etc. Away from the core

the electron and muon distribution can be measured using

scintillators or similar particle detectors. At Haverah Park,

for example, the array for the study of $\approx 10^{17}$eV showers

consists of 7 large area ($34m^2$ or $10m^2$) deep water Cerenkov

detectors. These 7 detectors are deployed to produce an array

of sensitive area approximately $1km^2$.
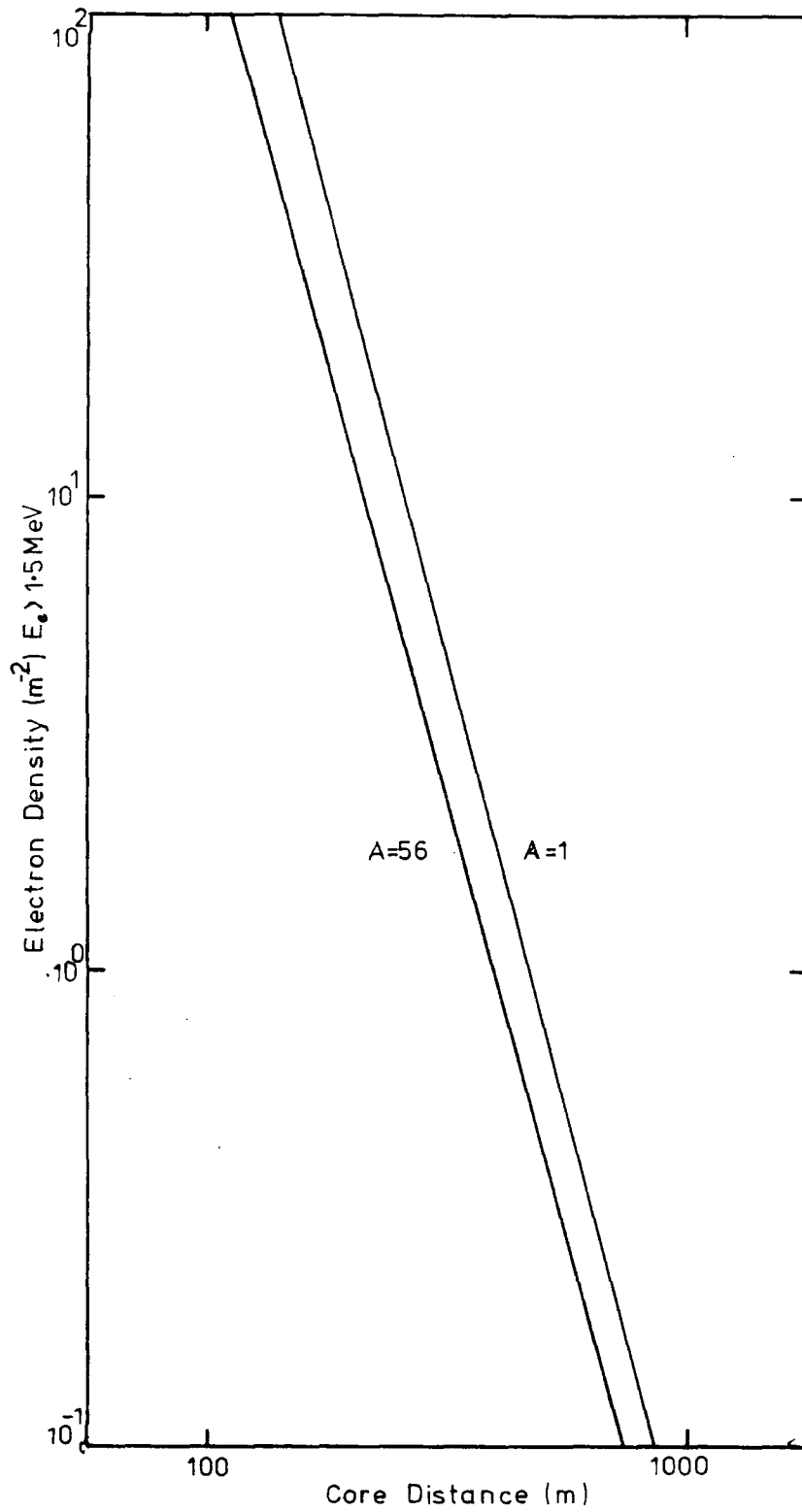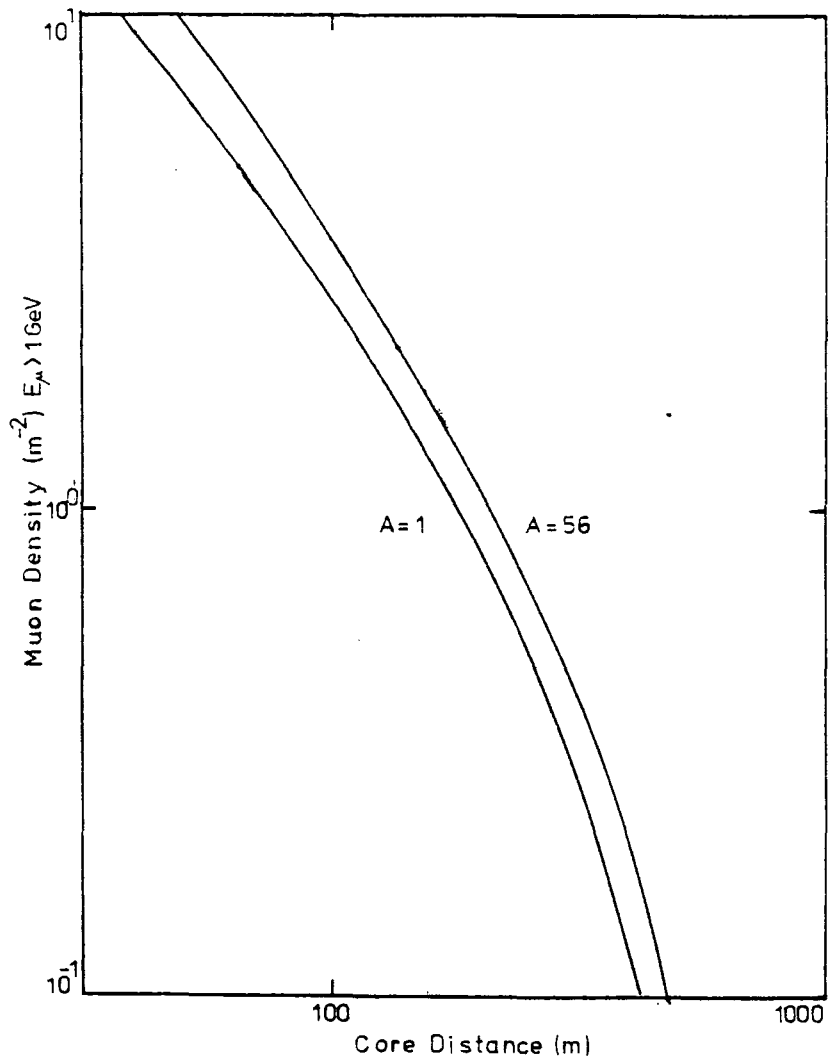
The cascades described above also produce visible light and other electromagnetic radiation during their passage through the atmosphere. The main production processes are those yielding Cerenkov radiation and scintillation light; or interactions between the electromagnetic cascade and the geomagnetic field producing radio-emission. These processes have the advantage that the photon density observed at ground level relates to the total contribution of all the particles which have existed within the shower. This differs from other techniques which essentially only sample a small and localized proportion of the longitudinal cascade. Utilisation of these techniques is becoming increasingly important to the study of cosmic rays. A study of one of these, atmospheric Cerenkov radiation, will be discussed in detail in the following chapters of this thesis.

1-3   The Energy Spectrum

The integral energy spectrum shown in figure 1-1 has two distinct features; the changes in slope at 5×10^{15} eV and 5×10^{19} eV. The former has been well measured by various groups, but the latter, due to the small number of events at this energy, is still speculative and has not yet been fully established.

The change in slope at 5×10^{15} eV (the 'knee' in the energy spectrum) has been given various interpretations. The most popular explanation to date has concerned the diffusion of the primary particles out of the galaxy. The charged particles will gyrate in the galactic magnetic field, average field strength approximately $3 \mu G$, the

Larmor radius of a proton of energy 10^{18}eV in a field of
this strengh is 1/3rd kpc, equal to the dimensions of the
galaxy. This theory predicts that at about 10^{15}eV the
radius of gyration is sufficiently large to allow the escape
of protons from the galaxy. The energy at which escape
is possible is proportional to the charge on the particles,
so that it would be expected that the average mass of the
particles in the primary beam will become heavier beyond
about 5×10^{15}eV. According to this theory the change in
slope reflects the different production spectra for particles
of different mass, Juliusson (1975). At higher energies,
where it would be expected that even the highest mass
primaries would have escaped from the galaxy, the spectrum
becomes dominated by extragalactic particles. This theory
has various modifications, e.g. the suggestion by Strong
et al (1974) where a universal distribution is enhanced about
5×10^{15}eV by a contribution of galactic particles mainly from
pulsars. The theory that different mass primaries diffuse
out of the galaxy at different energies, has the problem
that the rigidity for containment appears to be greater for
protons than for iron nuclei, Hillas (1979). Interpretation
of the flattening of the energy spectrum beyond 5×10^{19}eV,
if established, is complicated by interactions between the
particles and, e.g. the 2.7^{O}K universal microwave background,
which should cause a rapid steepening of the spectrum.

Other explanations for the spectral shape involve changes
in the physics of high energy interactions at 5×10^{15}eV, or
changes at source in the acceleration and absorption processes

of the particles. Until the primary mass can be established

accurately in the EAS region of the energy spectrum, none of

these suggestions can be accurately determined.

1-4   The Arrival Direction of the Primary Radiation

The cosmic radiation has been observed to be highly

isotropic; only after many years of careful observation has

any anisotropy been observed. In the following discussion

only non-local anisotropies will be considered, i.e. not those

caused by interplanetary magnetic fields and solar modulation

effects. Although the source of the radiation probably con-

sists of a number of discrete objects, the deflection of the

radiation in the galactic magnetic field results in a smearing

of the arrival directions. Marsden et al (1976) observed

a correlation between a marked anisotropy at low energies

(10^{11}-10^{12}eV) and the local galactic spiral arm; this ob-

servation has been interpreted as being possibly caused by

a temporary enhancement of particles from the Vela pulsar,

Osborne et al (1977). At higher energies (approximately

10^{17}eV) the results from Havarah Park, Pollack and Watson

(1977), indicate an anistropy which changes with energy;

a full explanation of this has not yet been given, Lloyd-

Evans et al (1979). At the highest energies, because of the

low number of events, the results from several arrays have

to be combined. Krasilnikov (1979) has compared the results

of the world's four largest arrays; Haverah Park, Yakutsk,

Sydney and Volcano Ranch. Considering the 58 largest

showers with assigned primary energy $\rangle 5\times10^{19}$eV, Krasilnikov

observed 3 distinct regions where the intensity was increased -

the 2 galactic poles and the local spiral arm. No firm

conclusion is yet obtainable although an extragalactic origin appears to be the most satisfactory explanation for the particles of the highest energy.

1-5   The Mass Spectrum

The mass of the primary radiation although accurately measured at energies less than a few 10^{13}eV, has not yet been determined at air shower energies. The major problem is the extrapolation of measurements made at the observational level (at sea-level approximately 30 radiation lengths after the initial interaction) to the primary particle. The extrapolation requires a knowledge of the physics of the interactions at least 3 orders of magnitude beyond the capabilities of the present generation of accelerators. It is a circular problem since knowledge of the mass of the primary beam and the physics of particle interactions are mutually dependant. At lower energies the particles can be observed directly, before any significant interactions with the atmosphere. Here the mass has been accurately determined to the extent of observing the isotopic distribution of various elements. The exact abundance distribution gives vital information on the prevelant conditions existing at and between the source and the earth, e.g. the process of nucleosynthesis at the source regions of the radiation and the amount of matter traversed.

Table 1-1 shows the average observed distribution of the primary radiation atmosphere compared to the expected source abundance distribution, from Hillas (1975). Of particular interest is the enhancement of elements in the range $Z=3-5$. This enhancement is attributed to spallation of the source

TABLE 1-1

The observed mass distribution of low energy cosmic rays, from Hillas (1975), normalised to Z=6.

Z	Observed Mean	Extrapolated Pre-Spallation Composition
1	7×10^5	$2\text{-}5 \times 10^5$
2	37500	26000
3	141	-
4	89	-
5	249	-
6	1000	1000
7	246	110 ± 20
8	895	1070 ± 20
9	17	-
10	162	160 ± 20
11	26	8 ± 4
12	187	230 ± 20
13	29	20 ± 10
14	143	204 ± 30
15	6	0-6
16	33	30 ± 6
17	6	
18	14	7 ± 5
19	8	
20	22	22 ± 8
21	5	-
22	14	-
23	7	-
24	16	3 ± 3
25	6	0-6
26	96	205 ± 30
27	3	
28	4	8 ± 2

material by collisions with interstellar gas; the low charge
elements being the daughter products of the fragmentation.
The abundance of the radio-active isotope Be^{10} provides
indications of the propagation of the radiation at low
energies. Webber et al (1973) for example showed, by consider-
ing the abundance of Be^{10} compared to the more common and
stable Be^9 and Be^7, that the escape life time of cosmic
rays lies between the limits $3.4^{+3.4}_{-1.3}$ million years.

Beyond the region where direct observations are
possible the picture is not yet clear. Any interpretation
of EAS results depend heavily upon the various models for
the high energy particle interactions. Figure 1-4 high-
lights this problem by showing the calculated muon lateral
distribution for 2 models and 2 masses, here the distribution
for an iron shower is seen to be superimposed upon the
distribution for a proton shower using the other model.
No experiment has yet been able to produce results which
are totally independant of the model of the interactions
used in the interpretation, although recent experiments
studying many parameters within showers are beginning to
rule out particular models, but are not yet in a position
to categorically estimate the mass. The present indications
have been summarised by Gaisser et al (1978); these authors
made comparison between the results from many arrays, within
the energy band $10^{15}-10^{19}$eV, and the expectations of
computer simulations based upon the Feynman hypothesis of
scaling for the pion-momentum distribution. Assuming the
validity at EAS energies of the Feynman hypothesis, they con-

Muon Density E > 0.3 GeV (metres^{-2})

Core Distance (metres)

A=1
−− Landau E$^{1/4}$
□□ Scaling
A=56
··· Landau E$^{1/4}$
ooo Scaling
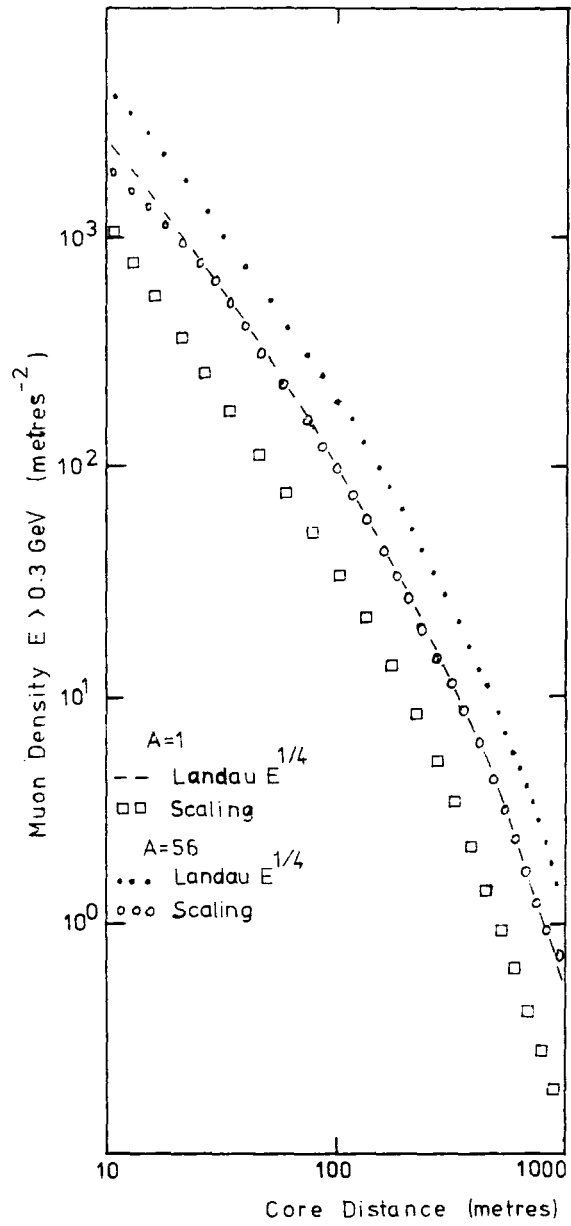
cluded that the results from most experiments were consistent with a heavy (i.e. predominantly iron) primary beam,at an energy approximately 10^{17}eV.

The most promising technique of determining the mass independently of any model of the nuclear physics, is that of studying the fluctuations in the development of individual showers. Although the exact degree of fluctuations for a particular mass depends on the nuclear physics of the interactions, it is possible to consider .the problem on a broad basis. Wide fluctuations indicate a low mass, probably protons, narrow fluctuations a high mass, probably iron nuclei. Figure 1-5 shows the expected extreme fluctuations in the development of a shower for an iron and proton initiated showers; the model used in the calculation was that of Feynman Scaling. The narrow range of fluctuations for an iron shower results from the breakdown of the primary nucleus into daughter nuclei; these proceed to initiate essentially independent air showers. The energy from the primary is thus injected more smoothly into an EAS. Results from experiments studying fluctuations are varied, but the main concensus appears to indicate a mixed composition, Hillas (1975). Whether the composition is exactly the same as that at lower energies remains an open question; protons are almost certainly present, but the degree of enhancement of heavy nuclei has not yet been established.

Determination of the mass of the primary beam is probably the most important aspect of the radiation, yet to be established, if the origin of the radiation is to be elucidated.
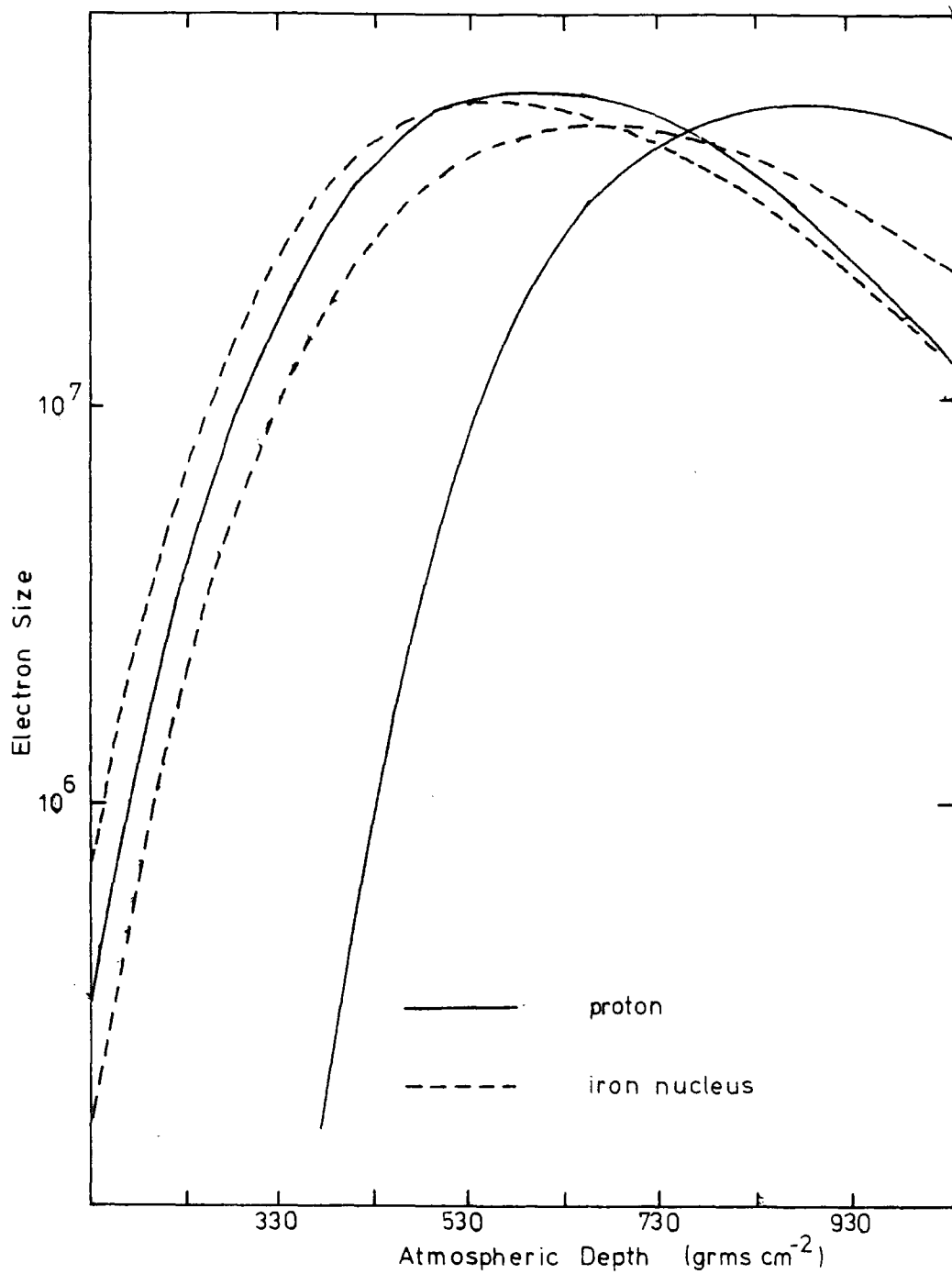
Until this has been determined the theories explaining the
observed energy spectrum will remain speculative. The
exact distribution will enable the conditions surrounding the
source regions of the radiation to be established. Further,
knowledge of the mass will enable the physics of particle
interactions to be determined beyond the capabilities of
present and possibly future generations of particle accelerators.

1-6   This Work

The scope of this work is to report on the construction,
operation and preliminary results of an experiment, situated
in the U.S.A., and designed to measure atmospheric Cerenkov
radiation from EAS initiated by primaries of energy app-
roximately 10^{17}eV. It will be shown that this experiment
has the capability of measuring Cerenkov radiation to a
high precision; sufficient for a future determination of
the development of EAS, as seen in the produced Cerenkov
light.

Chapter 2 discusses the role of Cerenkov radiation in
EAS giving a theoretical basis for the production of the
radiation, including a synopsis of the recent simulations of
Cerenkov light from the University of Durham group. Finally,
a summary of recent experimental work is given.

Chapter 3 describes in detail the construction of the
new experiment, indicating briefly the results from the
first season of observation.

Chapter 4 describes the calibration procedures used to
determine the response of the equipment to a light flux.
The data reduction procedure is also discussed.

Chapter 5 presents the average results from the second season of observations. The observed correlations between various deduced shower parameters are given.

Chapter 6 compares the early results of this experiment with computer simulations and the work of other groups.

Finally, Chapter 7 discusses the results of this experiment, and indicates the direction of future work from the University of Durham group.

CHAPTER TWO

Cerenkov Radiation in Extensive Air Showers

2-1   Introduction

Atmospheric Cerenkov radiation has been used as a tool
in making measurements of EAS since the pioneering work of
Jelley and Galbraith in the early 1950's. P.M.S. Blackett
suggested that Cerenkov radiation from cosmic ray particles in
the atmosphere would make a significant contribution to the night
sky brightness, Blackett (1948). Jelley and Galbraith extended
this proposal by considering Cerenkov emission from EAS when a
large number of charged particles are present with energies above
the Cerenkov threshold in air. Using a photomultiplier with
simple optics and a small array of Geiger-Muller tubes, they
found a coincidence of 22 out of 50 triggers between an optical
pulse and one or more of the Geiger-Muller tubes, Galbraith and
Jelley (1953). Later work at the Pic Du Midi observatory in-
dicated that the light was polarised and had a spectrum consistent
with Cerenkov radiation, Galbraith and Jelley (1955). Similar
work in the Soviet Union confirmed this conclusion, Chudakov
et al (1960). Since this work, studies of the radiation have
provided valuable insights into understanding the development of
the electromagnetic longitudinal cascade in EAS.

2-2   Basic Theory

Electromagnetic radiation is produced whenever a charged
particle traverses a dielectric medium with a velocity in
excess of the phase velocity of light in that medium. The

first experimental studies of the radiation by Cerenkov (1934; 1937) were followed by a satisfactory theoretical explanation by Frank and Tamm (1937) based on classical electromagnetic theory. The present summary of the radiation and its characteristics is based upon the earlier reviews of Jelley (1958; 1967) and Boley (1964).

A charged particle passing through a medium will set up a transient polarization of the medium around the particle track which results in the emission of electromagnetic radiation. If the particle is travelling faster than the phase velocity of light in the medium, this radiation will be in phase from all portions of the particle track and will produce a resultant field. The relationship between the angle of emission, θ , of the radiation and the particle's velocity, βc , was shown to be:-

$$\cos\theta = \frac{1}{\beta\eta} \qquad \text{Equation 2-1}$$

where η was the refractive index of the medium. From this 3 conditions follow:

(1) Only particles for which $\beta\eta > 1$ can produce the radiation, i.e. for a given refractive index there is a given threshold velocity

$$\beta_{min} = \frac{1}{\eta} \qquad \text{Equation 2-2}$$

(2) For ultra-relativistic particles, $\beta = 1$, there is a maximum angle of emission given by:

$$\theta_{max} = \cos^{-1} (1/\eta) \qquad \text{Equation 2-3}$$

(3) Cerenkov radiation can occur only at those frequencies for which $\eta > 1$ - i.e. x-rays and γ rays are not produced by the radiation.

Frank and Tamm (1937) calculated the energy lost dE, due to the production of Cerenkov photons of wavelengths between λ_1, and λ_2, by a particle of charge ze, in traversing a path length dl as:-

$$\frac{dE}{dL} = 4\pi^{-2}z^2 \int_{\lambda_1}^{\lambda_2} (1 - \frac{1}{\beta^2\lambda}) \frac{d\lambda}{\lambda^3}$$ Equation 2-4

From this it can be seen that the production of Cerenkov photons is inversely proportional to the square of the wavelength of the photons- indicating that the emission spectrum of the radiation will peak towards the U.V. and blue regions. Further that the production is also proportional to the square of the charge of the radiating particle.

From equations 2-2 and 2-3 it can be shown that; in the atmosphere where η = 1.00029 the maximum emission angle of the radiation is 1.3° also the threshold energy for electrons at S.T.P. is 21MeV, (4.3 GeV for muons). In an EAS, about 85% of the electrons surviving to sea level have energies above the Cerenkov threshold; Boley (1964) has shown that about 4×10^5 photons are emitted for each electron reaching sea-level. This amplification factor allows for Cerenkov radiation to be detected without the statistical problems inherent in measurements of the particles in EAS. Table 2-1, from Jelley (1967), shows that the Cerenkov effect will dominate over other possible production processes.

The unique aspect of the Cerenkov light arriving at ground level in an EAS, is that it is not proportional to the local particle density, (as are measurements of other aspects of EAS), but to the integral of the electromagnetic cascade over

TABLE 2-1

Radiation Processes

For air at STP and radiation in the region 4000-6000Å
(From Jelley (1967))

Process	Assumptions	Angular Distribution	Energy loss dw/dl $(eVcm^{-1})$
Cerenkov	$E_e = 100$ MeV	$\sim 1.3^{\circ}$	≈ 0.8
Ionization +Recombi- nation	Lifetime of the states $< 5.10^{-8}$ sec	Istotropic	8.10^{-3}
Synchroton	$E_e \approx 3.10^{10}$ eV	In Vacuo (Mc^2/E)	1.3×10^{-7}
	$E_e \approx 10^9$ eV	In Air 1.3°	$\approx e^{-50}$
Bremsstrahlung	$\bar{Z} = 9$ $E_e = 100$ MeV	Same as for Synchrotron radiation	$< 4.10^{-5}$

its complete history. In principle the characteristics of the light at ground level reflect the overall development of the shower through the at·mosphere.

2-3 Computer Simulations of Cerenkov Radiation in EAS

The characteristics of Cerenkov Radiation produced by EAS from primaries of high energy, ($E_p = 10^{15}$-10^{18}eV) have been calculated by a number of groups. In this summary particular attention will be given to the work by the Durham group presented in a number of papers, e.g. Protheroe (1977) and Hammond et al (1978). This work, based on the Feynman hypothesis of scaling for the pion-momentum distribution, Feynman (1969), gives an insight into those aspects of the radiation which are observable and can give information on the development of the longitudinal cascade. It is important to note here that the production of Cerenkov radiation in EAS is inexorably linked to the electromagnetic cascade and it is this cascade which is of importance to studies of Cerenkov radiation in EAS.

2-3-1 The Calculation

The hadron cascade resulting from primaries of varying mass, A = 1, 4 and 56, and different energies $E_p = 10^{15} - 10^{18}$eV were calculated using the scaling hypothesis. The neutral pions predicted from this distribution were then followed to produce electromagnetic cascades. These cascades were described by approximation A of cascade theory for the high energy particles and using a rigorous Monte-Carlo technique for the low energy particles. The Cerenkov radiation from these cascades was followed down to the observation level, including the effects of Rayleigh scattering, aerosol attenuation and ozone absorption. Further, the Cerenkov radiation reaching ground

level was folded with the response of various detecting systems.
By this means the response of various experiments could be
calculated allowing a detailed comparison between simulations
and observations.

2-3-2   The Lateral Distribution of Cerenkov Radiation

Figure 2-1, from Protheroe & Turver (1977) shows the expected
lateral distribution of Cerenkov radiation resulting from
primaries of differing energies and masses. The distributions
are seen to be broader for increasing mass and decreasing
energy, consistent with the depth of cascade maximum becoming
further away from the observation plane. Further studies
indicated that the form of the structure function was solely
dependent on the depth of maximum for the electron cascade
and not dependant on the mass or energy of the primary,
Hammond et al (1978).

2-3-3   The Cerenkov Light Pulse Profiles

The computer simulation calculated the expected pulse
profiles at various distances from the axis of the shower.
The pulses were described by their:-

(1) rise time (10% - 90% levels on the leading edge).

(2) top time (90% - 90% levels)

(3) fall time (90% - 50% levels on the falling edge).

(4) full width at half maximum (FWHM), (50%-50% levels).

Of these the rise time and FWHM at large core distances were
found to increase monotonically with increasing depth of
maximum. The other two parameters were related to the depth
of maximum, though in a more complicated manner. Figure 2-2
shows the predicted variation of the FWHM with core distance
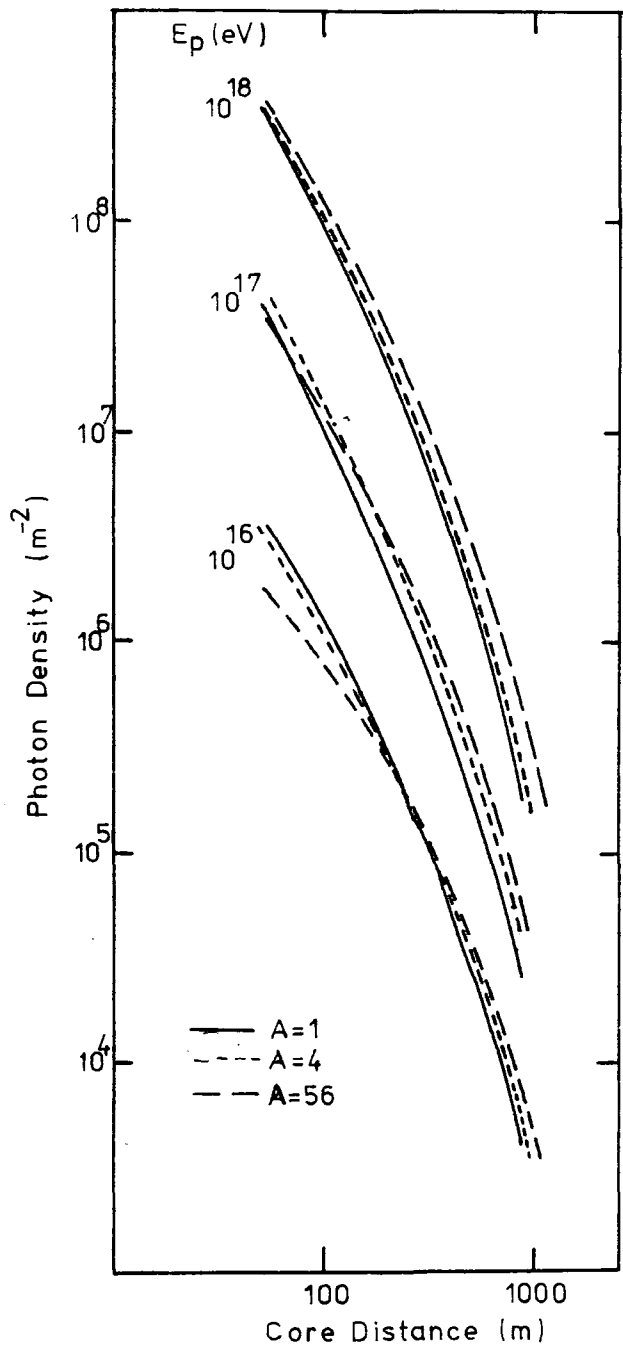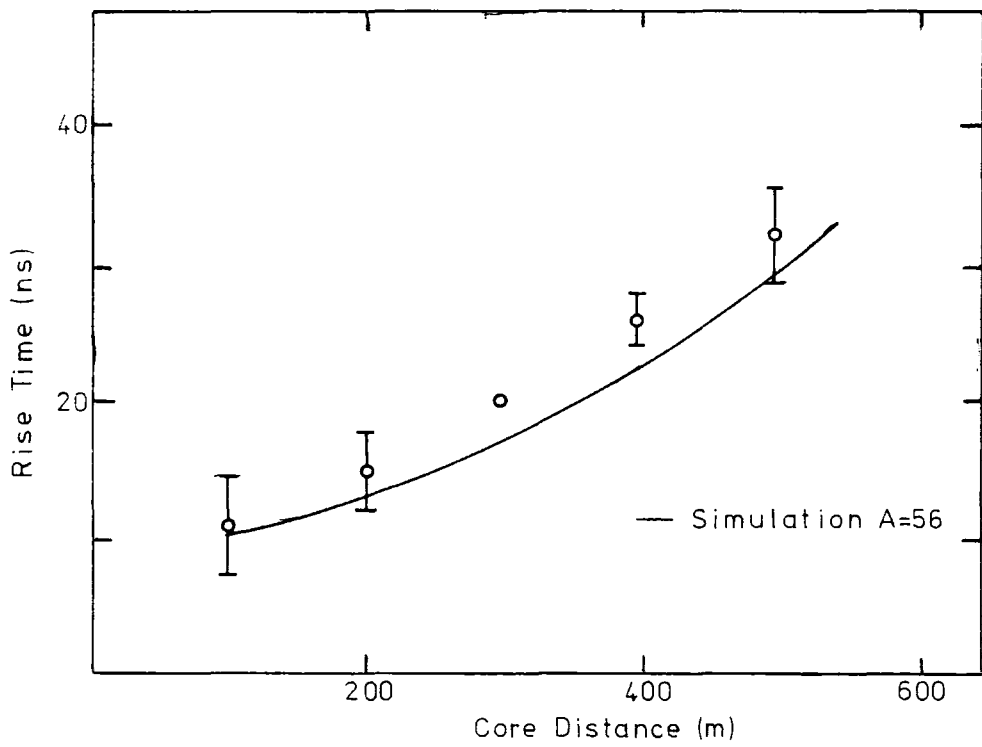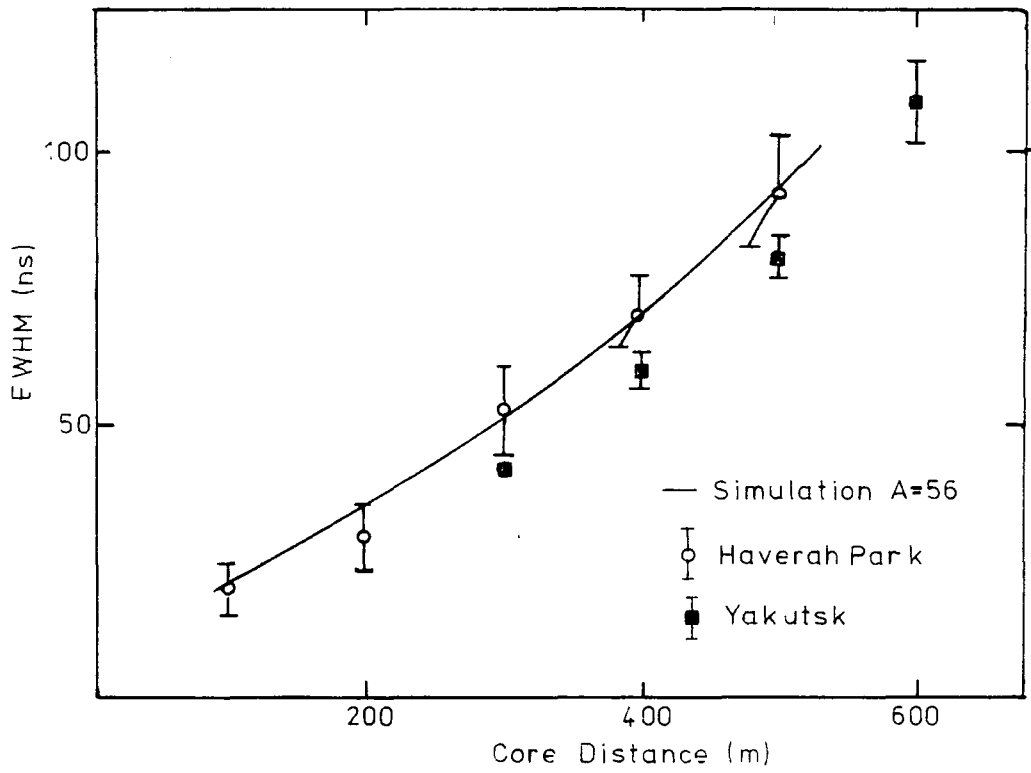
and figure 2-3 the variation of the rise time with core

distance for a shower with a depth of maximum of about 700g

cm^{-2} (produced in this model by a 10^{17}eV iron nucleus). The
figures also show the broadening of the
pulses with increasing core distance. An overall broadening of

the pulse also arises from increases in the depth of development

of the electron cascade in the atmosphere.

2-3-4   The Radius of Curvature of the Cerenkov light front

This series of simulations indicated that the radius

of curvature of Cerenkov light front (defined by the 10%

level on the leading edge) originated high into the atmosphere.

Essentially it was found that beyond 150m the first light to

arrive at the observation level was that which was first

produced. At other levels through the pulse the arrival

sequence mapped the production depths of the light. Figure 2-4

shows the spherical fronts defined by the different levels

through the Cerenkov pulse. Further, it was shown that the

centre of curvature of these spherical fronts corresponded

to the positions in the atmosphere of the various percentage

levels in the longitudinal cascade of observed Cerenkov

radiation.

2-3-5   Computer Simulations Summary

It was confirmed from this series of computer simulations

that the following quantities were sensitive to changes in

shower development:-

(1)   The lateral distribution of the radiation.

(2)   The pulse profiles, specifically the FWHM and

the rise time.

(3)   The radius of curvature of the light front.

FIGURE 2-5

The observed lateral distribution of pulse area,
compared with the results of simulations having the
indicated depths of maxima, from Wellby (1977).

In particular these quantities relate to depth of the electromagnetic cascade maximum. Studies of Cerenkov radiation should be capable of accurately determining the depth of cascade maximum and hence giving indications of the validity of the various models used to describe the high energy particle interactions. Studies of fluctuations of Cerenkov light from a large number of showers should indicate the fluctuations in cascade development, and hence give an indication of the mass of the primary beam.

2-4-1 The Lateral Distribution of Pulse Area

Figure 2-5 shows the observed variation of pulse area against core distance for showers with primary energy estimation $\rho(500)_{VE}$ = 2.0 and 0.2 m^{-2}. (The showers' energy are expressed using the Haverah Park parameter indicating the particle density 500m from the axis of the shower). Also indicated are the lateral distributions calculated from showers having the indicated depth of maxima. The structure function used to describe the lateral distribution was:-

$$\phi(r) \propto r^{\gamma}$$

where r was the core distance and ϕ the photon density. The exponent, γ , was found from a multiple regression to vary with zenith angle, θ , and primary energy as

$$\gamma = 1.99 - 3.55 \cos\theta - 0.28 \log_{10}(\rho(500)_{VE})$$

This result was consistent with a broadening of the lateral distribution as the depth of maximum moved away from the observation plane.

2-4-2 The Pulse Profiles

Figure 2-2 shows the variation of the FWHM with core

Core Distance (m)

Energy = 10^{18} eV
$D_{max} = 810 \, g \, cm^{-2}$

Energy = 10^{18} eV
$D_{max} = 610 \, g \, cm^{-2}$

$\rho(500) = 2 \cdot 0 \, m^{-2}$

$\rho(500) = 0 \cdot 2 \, m^{-2}$

Photon Density (m^{-2})

10^{8}

10^{7}

10^{6}

100   200   500

Core Distance (m)
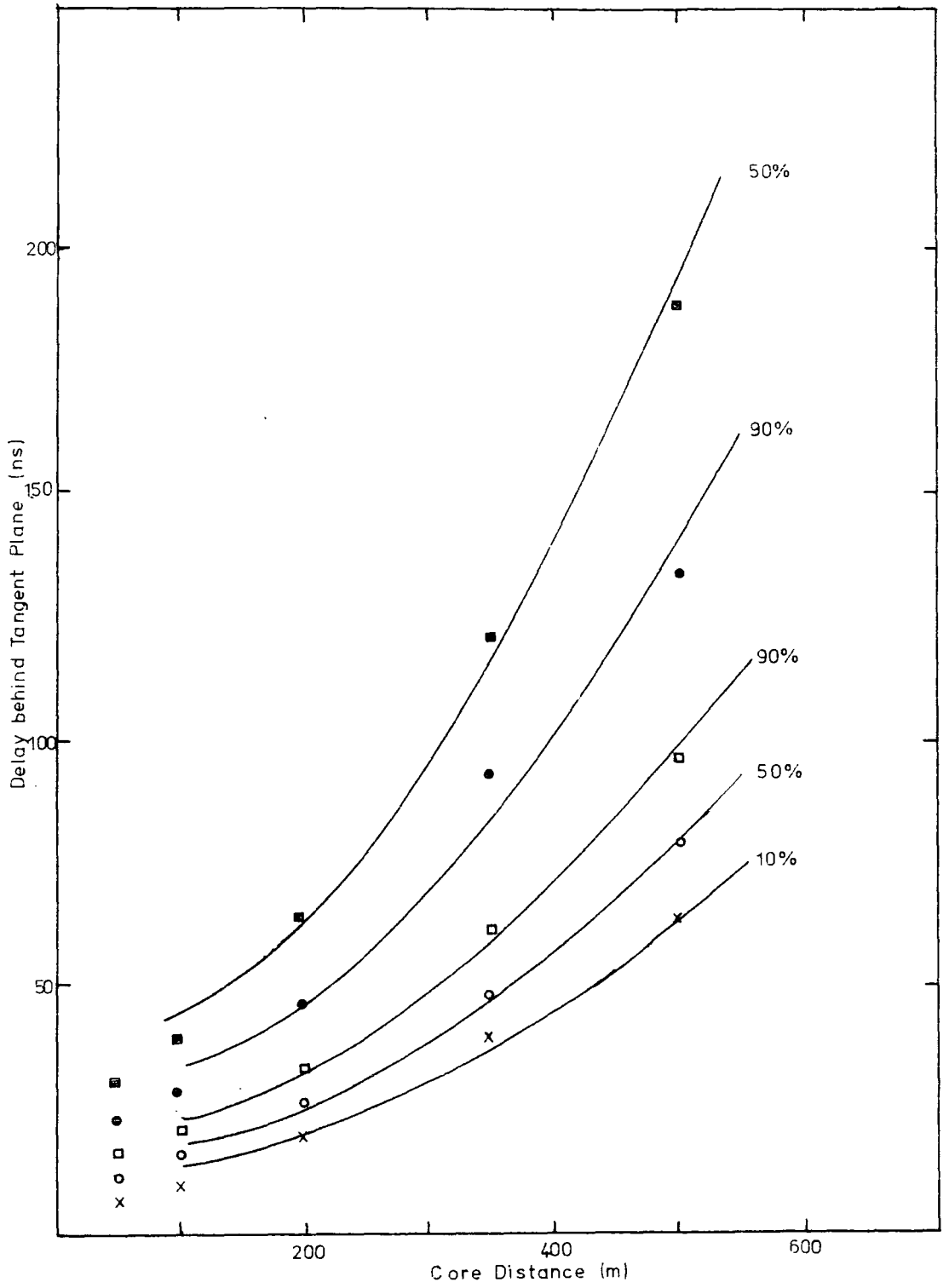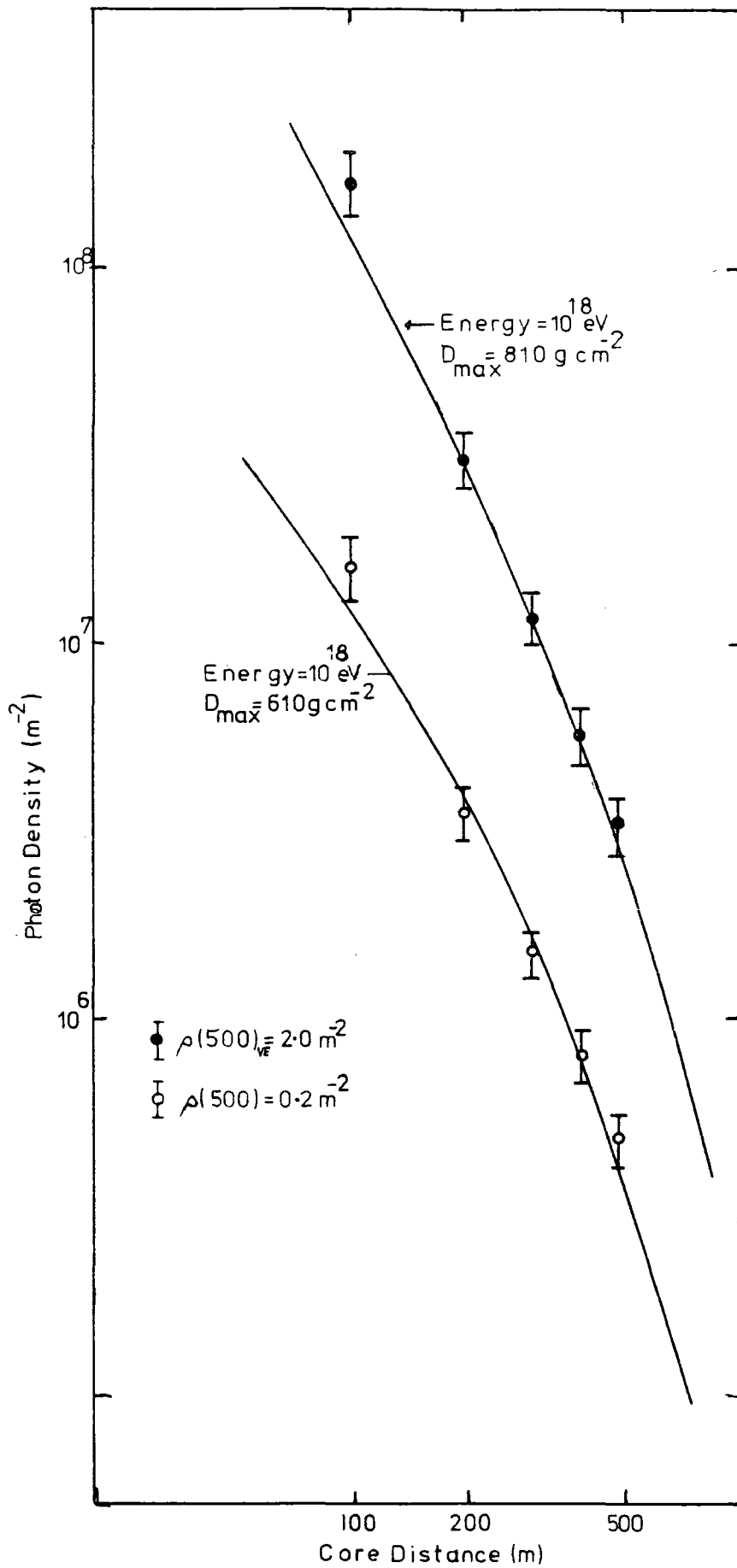
distance, the expectations from simultations for A = 56,

and the results from Kalmykov et al (1976). The two sets of

observations are consistent (the Soviet work had the effect

of instrumental broadening removed from the pulses) with

expectations of simulations for a shower with a depth of

maximum of about 700g cm^{-2} based upon the scaling hypothesis

with primaries which are iron nuclei . The variation of the

FWHM at 400m from the axis of the showers with zenith angle and

primary energy was found from a multiple regression to be:-

FWHM (400m) = 16.84 + 52.96 cos θ + 9.92 log$_{10}$ (ρ (500))ns.

These data are consistent with the depth of maximum moving away

from the observation plane giving a narrower pulse of light.

2-4-3 Imaging of the Longitudinal Cascade

The computer sumulations described in section 2-3

indicated that the radii of curvature of the various percentage

levels through the observed pulses should be directly related

to the development of the longitudinal cascade through the

atmosphere. Orford and Turver (1976) tested this proposal

experimentally; figure 2-6 shows the 'images' of the longitudinal

cascade of Cerenkov light derived from a set of showers

recorded at Haverah Park with zenith angles up to 40°. This

example illustrates how Cerenkov radiation can provide an accurate

means of determining depths of cascade maximum on an individual

shower-by-shower basis.

2-4-4 Observations-Summary

The observations made at Haverah Park indicated, with the

small sample of showers analysed, that measurements of

Cerenkov radiation using simple equipment could indicate accurately

FIGURE 2-6

The inferred longitudinal cascade of Cerenkov
radiation inferred from studies of pulse profiles,
from Orford and Turver (1976).
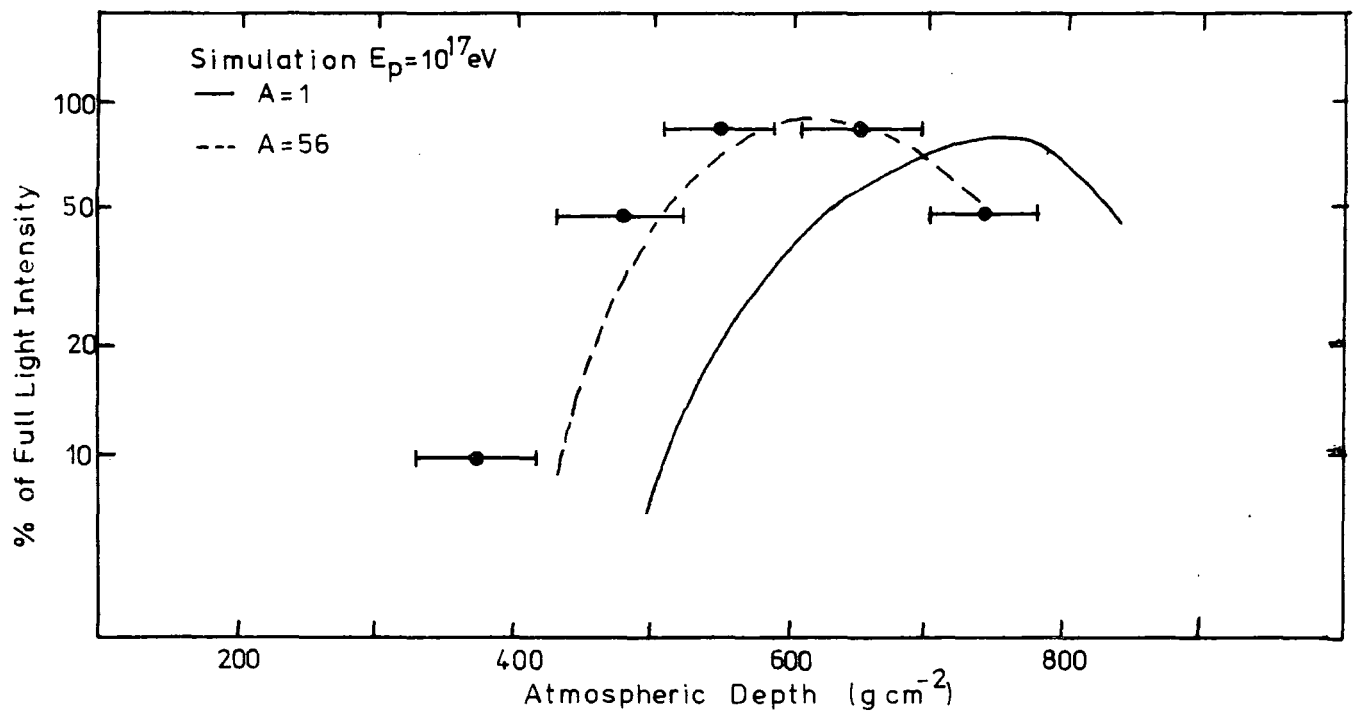
how showers develop. In the future it is expected that studies
of Cerenkov radiation will make a substantial contribution to
studies of the fluctuations in shower development and hence
a determination of the mass of the primary cosmic ray beam.

CHAPTER THREE

The New Atmospheric Cerenkov Light Detector Array

3-1 Introduction

This chapter describes in detail the design and operating conditions of the array of detectors deployed since Summer 1977 at Dugway, Utah. The first sections describe the construction and operating procedures prevalent during the first season of observation from August to December 1977. The last section describes the modifications made prior to the second season which extended from August 1978 to March 1979. It was the purpose of the first season of observation to complete the commissioning of the array and to show, by studying a small set of recorded showers, that the array responded sensibly to EAS.

The experimental design commenced in 1974 following the successful pioneer experiment at Haverah Park; the possibilities for cascade development studies noted there demanded a new system with an improved frequency response. Prior to the work at Dugway the photomultiplier and housing of the new detectors were tested at the Volcano Ranch array at Albuquerque, New Mexico in April, 1976.

3-2 Equipment Design

The Haverah Park Atmospheric Cerenkov Light Detector Array has been described in detail by Wellby (1977). This array had 8 RCA 4522 photomultipliers, of sensitive area $122cm^2$ which were co-located with the deep water Cerenkov detectors of the particle detector array. Each photomultiplier viewed the night sky directly, the opening angle being limited by the

tube housing so that light incident within 60° of the vertical was detected. The output signal from each photomultiplier was amplified by a factor of 100 and passed down high quality co-axial cable to a central recording station. Here the signal from each photomultiplier was displayed on oscilloscopes and photographed on fast recording film. The response to a 2 ns wide pulse (from a NE 130 light pulser) was found to have a rise time of 9 ns and a FWHM of 18 ns. According to Wellby (1977) the timing resolution was found to be such that measurements were possible for:-

(1) arrival time to better than 7 ns

and   (2) pulse shape to better than 5 ns.

The new experiment required an improved response if more detailed information of the longitudinal cascade was to be obtained. Using the Haverah Park technique of delay cables and recording oscilloscopes it was thought that without excessive cost the bandwidth could not be significantly improved. To overcome these problems a digital recording experiment was designed. The basic technique would be to analyse certain aspects of Cerenkov light pulses at each photomultiplier. This information would then be stored in situ in digital format, before transmission to a central station, where it could be stored indefinitely on suitable medium, i.e. magnetic tape.

The first problem here was to choose parameters which could be digitised with the available instrumentation, and which could be used to build a better picture of the pulses than could be achieved with an analogue system. The first two

parameters to be recorded were obvious - the arrival time of the light and the light pulse area. These were easily measureable to the necessary precision. To obtain a record of the pulse shape two systems were considered. First, to measure the rise time and FWHM using discriminators and time-to-amplitude converters. Second, to measure the charge sequentially through the pulse in narrow time intervals, after which the pulse shape could be reconstructed using fitting procedures. The latter option was chosen, as it would give more information and flex- ibility than a rise time and FWHM measure, and it could be achieved with the electronics systems available in 1976.

To summarise, the following information was to be avail- able from each detector:-

> (1) Arrival time of the light,
>
> (2) Pulse Area,
>
> (3) Pulse structure from narrow (10ns) sequential measures of the charge through the pulse.

Figure 3-1 shows an arrangement of the time intervals (slices)to digitise the shape of a pulse of FWHM approximately 20ns.

3-3   The Cerenkov Light Detector Array

3-3-1   The Photomultiplier System

Figure 3-2 shows schematically the analogue signal paths within each detector. The same type of photomultipliers, RCA 4522, as used at Haverah Park were used in this experiment; the response of this type of photomultiplier to a light flux has been described by Wellby (1977) and Orford et al (1977). This use of the similar photomultiplier allowed for a direct comparison between

FIGURE 3-1

An arrangement of slice positions to measure the pulse

shape of narrow pulses (FWHM 20ns).
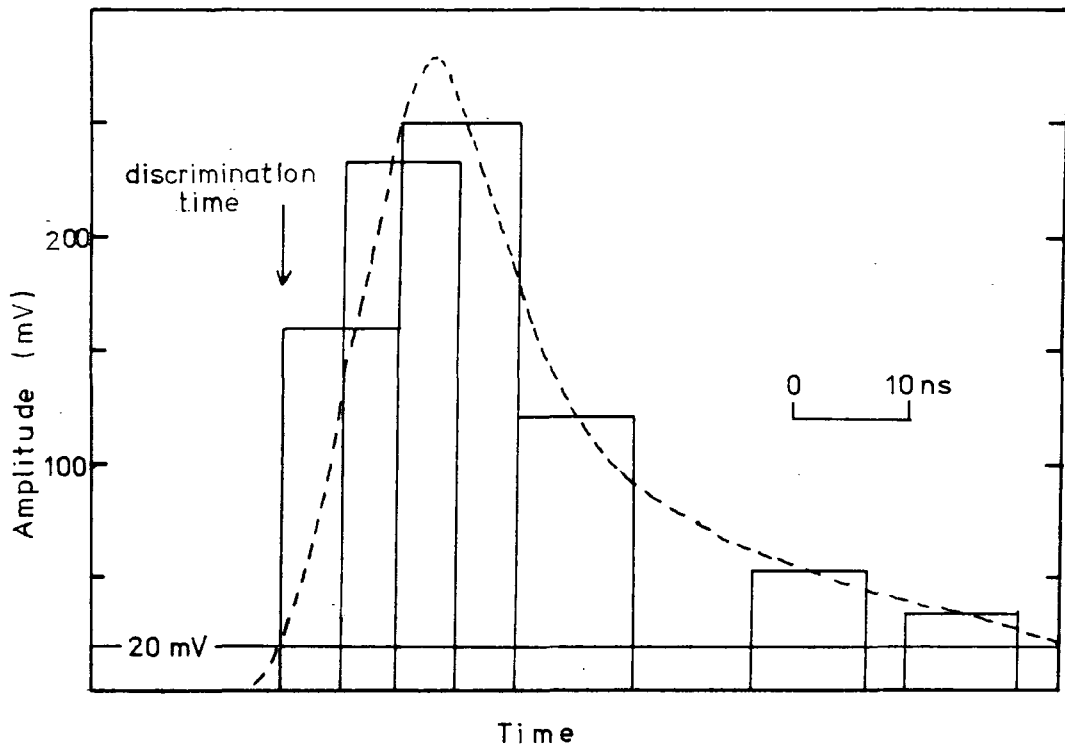
FIGURE 3-2

The Analogue Signal Paths within the Detector
Electronic System.

FIGURE 3-3

The pulse shape and arrival timing digitisation
system.

FIGURE 3-4

The Data Acquisition System.

PMT

×10
VV100

×10
VV100

FAN-OUT

to QTC

to discriminator

DC output for EHT trip and
anode current monitoring

DISC.

Delay
Shaper

QTC

Fanout

AMP.
×100
×10
×100

to Scaler

START

DUMP

time
stretcher

STOP

Output
Interface

to
centre

⟩ analogue
⟩⟩ digital (NIM)
⟩⟩⟩ digital (TTL)

QTC

SCALER

Bits

Clock

OUTPUT
INTER-
FACE

to
centre

from
time stretcher

DISC.

reset

EAS Commit
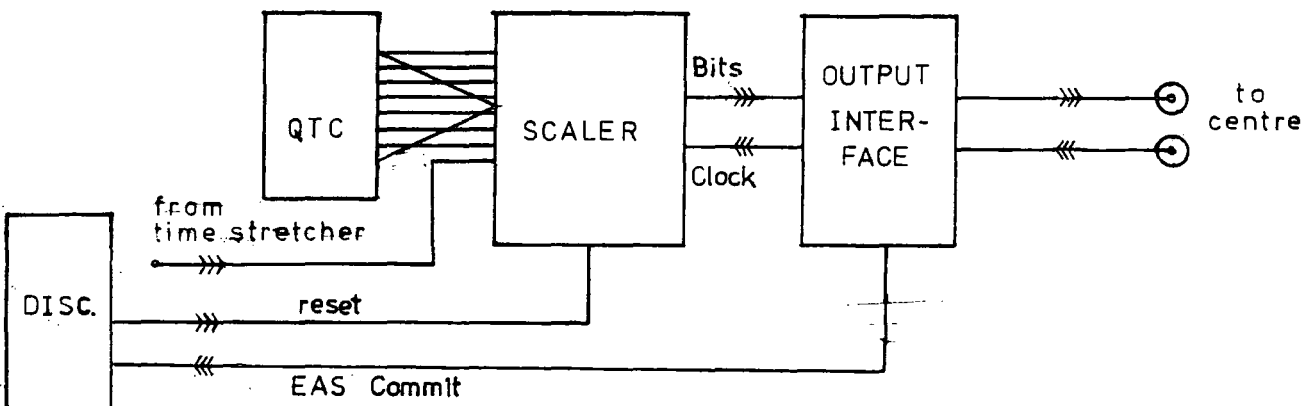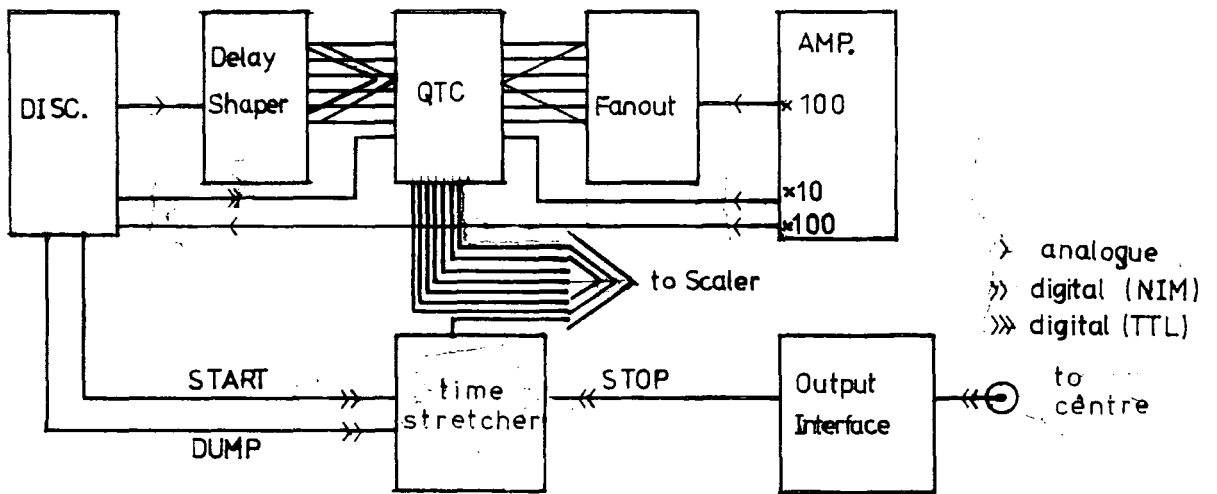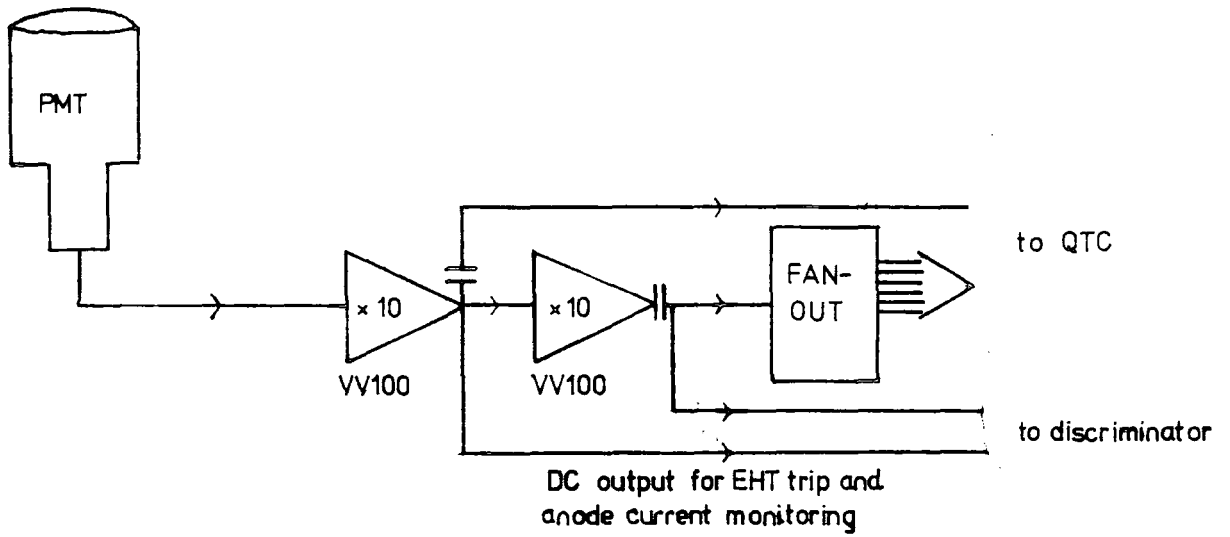
this experiment and the measurements made with the array at

Haverah Park. The photomultipliers in the new experiment

were however, operated at a lower photocathode potential and the

signal was taken from the 11th dynode. The photomultiplier signal

was amplified by x100 using a combination of a discrete 100MHz

amplifier and a VV100 photomultiplier amplifier, (Le Croy

Instruments Inc., New York). This system provided the necessary

overall gain which was comparable to that employed in the Haverah

Park system. After being amplified the signal was split, one

channel going to a discriminator, the other to an 8-way fanout

which formed the basis of the simultaneous analysis of various

aspects of the pulse. The fanout was an 8-way emitter follower

which had a bandwidth in excess of 100 MHz.

For a comparison with the Haverah Park system, the response

of the photomultiplier, amplifier and fanout system to a 2ns

wide light pulse was an output signal whose FWHM was 6.7 ns with

a rise time of 6.2 ns , including the bandwidth of the recording
oscilloscopes.

3-3-2   The Threshold Discrimination System

After being amplified the signal from each photomultiplier

was discriminated using an NE529A fast discriminator. All timing

occurred relative to the time at which this discriminator threshold

was exceeded. If the signal exceeded a threshold of 20mV a series

of gating signals were generated. First, pulses were generated

to start the time stretcher, described below, and to initiate

gates to measure the charge sequentially through the pulse.

Secondly, a pulse was sent to the central recording station to

generate the array trigger. If, after a set time, no EAS

coincidence was made the discriminator initiated the clearance of

the system in readiness for another light pulse. The system was 'dead' for approximately 10μs after receiving a light flash- allowing for a maximum discrimination rate of about 1kHz before the dead time would become significant.

The propagation time through the discriminator was 20ns with a jitter of about 1ns. A positive feed back system ensured that the discrimination delay was the same for large and small pulses. Figure 3-3 shows schematically the digitising electronics for the season 1978/79, (the small differences between this and the first season are described in section 3-7).

3-3-3 Charge to Time Converter System

The heart of the digitising electronics was a seven channel charge-to-time converter (QTC). This module sampled the charge sequentially through the photomultiplier signal and measured the integrated pulse and has been described by Stubbs and Waddoup (1977). The unit was gated on by six narrow (10ns) NIM standard pulses; the time of arrival of these gating pulses could be altered by set amounts to allow for the QTC to measure the charge in narrow sequential segments of the pulses. These gate pulses were generated in a delay shaper module; the width and the delay of the pulses being determined by trimming cables and were accurate to $\pm$200ps. The integral of the pulse was obtained using a simple R-C integrator, the output of which was sampled by the QTC. The 7 parallel TTL outputs from the QTC were then passed to the scaler - see section 3-3-5.

3-3-4 Time of Arrival Determination

The arrival time of each pulse was determined by using a time stretcher. This was necessary as the scaling rate

employed throughout the experiment, was 20MHz - giving a
resolution of 50ns (which was worse than could be achieved with
an analogue system). The arrival time at each detector
relative to the other detectors was measured by stretching the
interval between the arrival of the light pulse at each detector
and an arbitrary time later, before scaling. The two pulses used
to start and stop the time stretcher were the Cerenkov pulse, if
it had surpassed the discrimination level and a pulse whose time
of arrival was accurately known at all detectors.

By using a module described by Waddoup and Stubbs (1975),
a pulse could be formed, the length of which was approximately
75 times the time between a start pulse (light pulse on a detector),
and a stop pulse (EAS coincidence pulse). The stretching factor
of 75 allowed for relative arrival times to be measured to better
than 1ns. Calibration of this unit indicated that the expected
instrumental error on any measurement would be approximately 0.5ns,
(see the next chapter for a more detailed account of the
calibration of all aspects of the equipment).

3-3-5 Scalers

After each pulse was analysed the 8 outputs described above
(six slices and the pulse area from the QTC and arrival time
from the time stretcher) were scaled using 8-bit scalers. The
scaler unit, described by Waddoup and Stubbs (1977), was an 8-way
parallel in, serial out 8-bit scaler. The scaling rates could be
set at 1.25, 2.5, 5, 10 or 20 MHz. The basic design was modified
to produce one 16-bit word for timing, five 8-bit words for
4 slices and the integrator, and, for the remaining 2 slices,
4-bit words.

Figure 3-4 shows a schema of the digital clocking side. The bits were clocked out as a serial string of synchronised 1 ms pulses through an output buffer to a central digital multiplexer. The data were clocked from there into computer storage, and then to magnetic tape.

3-3-6 Detector Housing

Figures 3-5a and 3-5b show photographs of a detector. Each detector consisted of an aluminium box of dimensions, 60 x 55 x 90cm, which contained the electronics and photomultiplier tube. The detectors were thermostatically controlled and could maintain a temperature of 20^OC during the cold desert winters. Each set of detector electronics dissipated about 250 watts during normal running, which could be increased by a further 120 watts from a heating element. Fans provided cooling and allowed the detector interiors to be maintained at the ambient air temperature during the hot desert summers. (The ambient air temperatures in which the equipment operated ranged from $> 100^O$ F in summer to $< 0^O$F in winter). Internal baffles in each detector ensured a uniform circulation of air within the detectors. The photomultiplier, which viewed the night sky directly through a 1/8 inch perspex window, was housed behind the electronics crate. During the day a blind was automatically drawn across the field of view of the photomultiplier to reduce the bleaching effect of sunlight on the photocathode. The photomultiplier was surrounded by a Mumetal shield to minimise the effect of geomagnetic and local magnetic anomalies on its performance.

The environmental status of each detector was monitored during the operation of the array. Two measures of the temperature

FIGURE 3-5

A Cerenkov Light Detector of the Dugway Experiment
showing the photomultiplier housing and digitising
electronics.

thermostat — blind control
— Discriminator
— Fanout
outlet fan — — Delay Shapers
— QTC
— Time Stretcher
— Amplifier
— Scaler
— Output Interface
— EHT PSJ
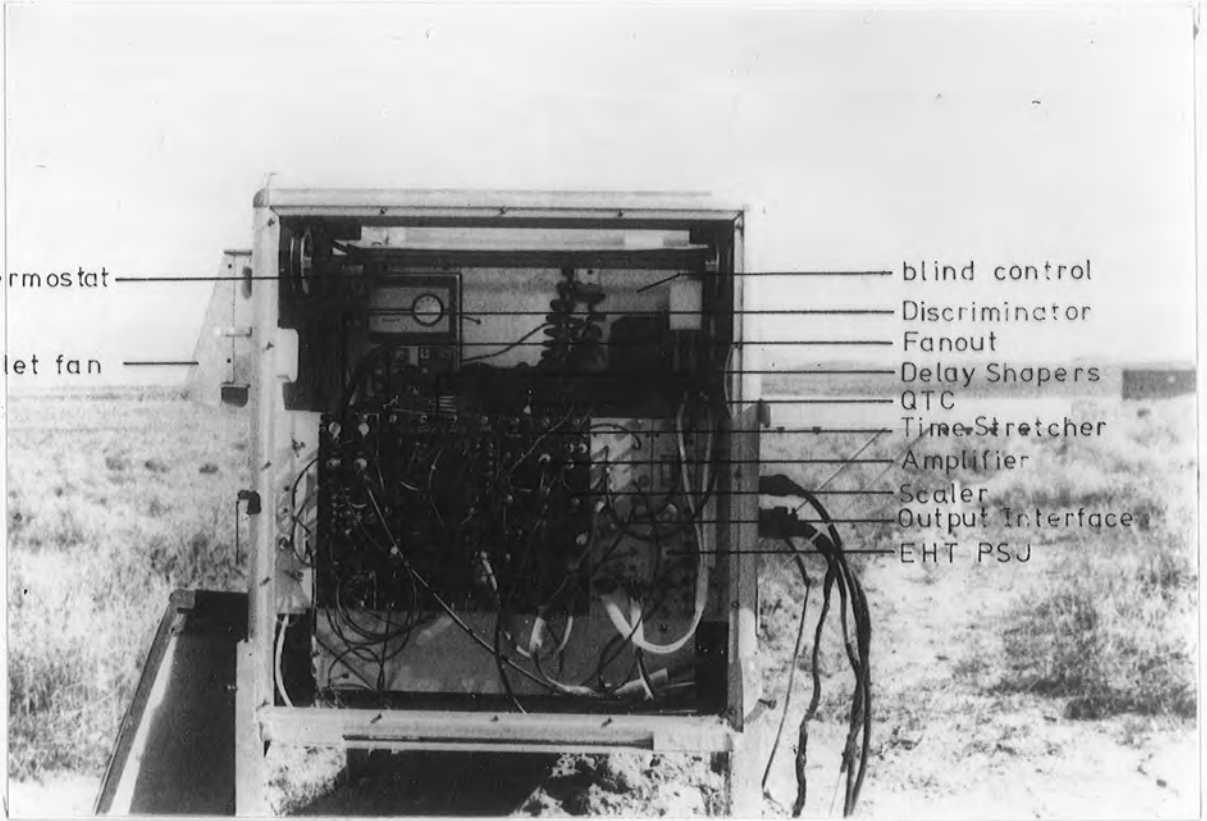
blind

PMT crate

MU Metal
shield

inlet fan

cable house
to centre
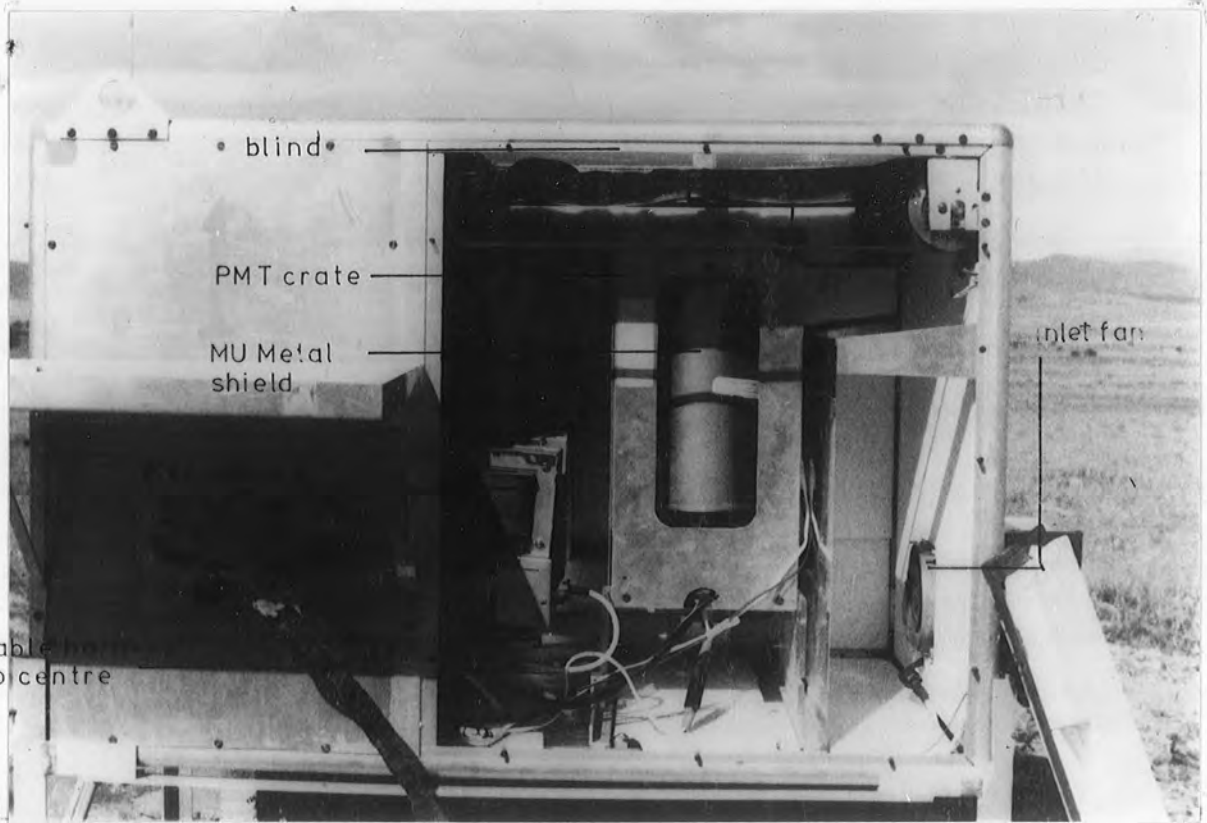
were made, one 5 cms from the photomultiplier tube face and one inside the electronics package. Each set of power lines was monitored. Also the detectors 'status' was recorded, i.e. whether the photomultiplier was powered on, whether the blind was drawn and whether the EHT power supply was on. This 'housekeeping' information was passed to the central station as a set of voltages, which were read into the central computer via a multiplexed analogue-to-digital converter.

3-3-7 The Central Control System

Each detector was controlled from the central station where the data were stored, the EAS event trigger made up and the detectors' performances monitored. The heart of the system was a Tektronix 4051 computer programmed in BASIC which stored the data and controlled the array during operating periods.

An event trigger was made when the central detector (1) and any 2 of the 200 metre detectors (see figure 3-6) responded in coincidence. The coincidence window was approximately 1.8 μs, allowing showers incident at any zenith angle to be recorded. The trigger pulse was sent to each detector simultaneously – thus allowing for synchronisation of the timing information from each detector. The trigger pulse was sent a fixed time (approximately 200ns) after the arrival at the centre of the pulse from the last coinciding detector. The jitter on the time of the trigger pulse was less than 10 ns, but for any analysis of arrival direction, the relative time of each detector firing was of importance, and this jitter was thus inconsequential. As well as a fast trigger the coincidence unit sent a string of 65 1 ms pulses to each detector to clock back the digital data.

After reading the data into store the computer performed various checks on the quality of the data. If the event was 'good' it was stored on magnetic tape along with a calibration event and a summary of the environmental status of each detector. The calibration was performed by illuminating a light emitting diode in the field of view of each photomultiplier. The simultaneous detection of the L.E.D. flash by each detector generated an apparent coincidence and the 'event' was recorded in the usual manner. The total 'dead' time during the recording of an event was about twelve seconds (at a rate of 15 hr^{-1};this meant the system was dead for only 5% of the time). As well as controlling the array the central station also monitored the sky brightness using a d.c. coupled 2" diameter photomultiplier.

3-4   Array Layout and Siting

The array was situated at Dugway Proving Grounds in Utah, U.S.A., latitude 40° 12 'N, longitude 112° 49 'W at 1451 metres above sea level, mean vertical depth into the atmosphere 862 g cm^{-2}. The climate was that of inland desert, giving clear skies, but with a large temperature variation (a 20°C diurnal temperature swing with an observed variation between 0° and 30°C average daily temperature from September to March). This site, chosen for its favourable cloud cover and clear skies, was on flat terrain, and was approximately 40 miles from the nearest town, thus minimising the effect of scattered man-made light interfering with the experiment.

The detectors were laid out as shown in figure 3-6. This layout was chosen on the basis of computer simulated showers, which indicated that this geometry gave the largest number of

FIGURE 3-6

The Dugway Cerenkov Light Array for the season 1977.

2

North

Y

7

37° φ

5 ←————200 m————→ N □ 1
X

C

4

400 m

6

3
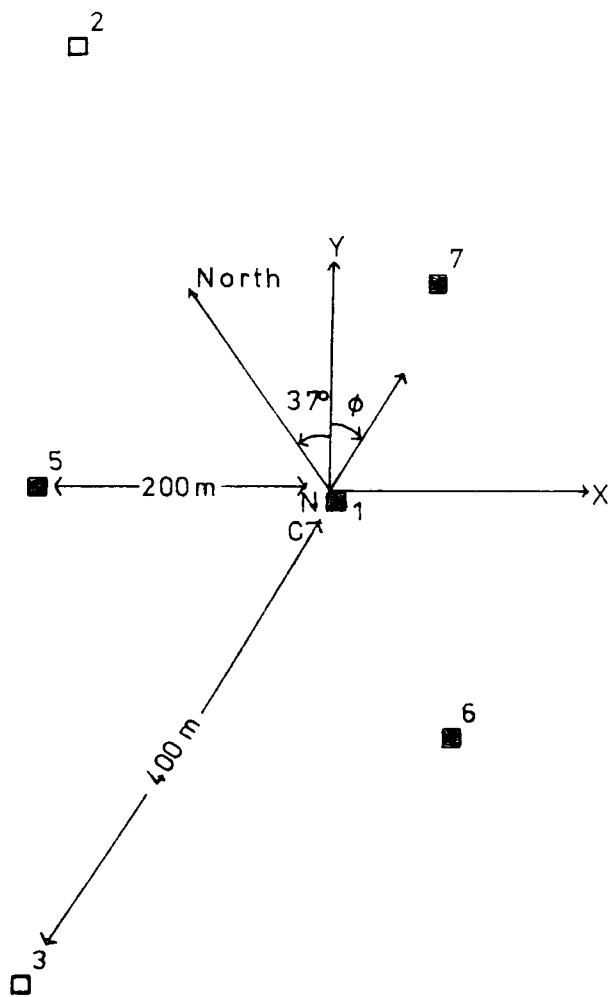
□	Outer) Cerenkov Light
■	Inner) Detectors
N	Night Sky Monitor
C	Central Recording Station

0   100   200
metres
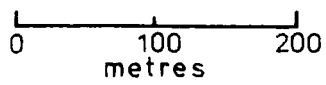
7 fold responses with core distances up to 500 m, Orford (private communication).

3-5   Running Conditions 1977

The array was operated from September to December 1977 – four dark periods when the moon was below the horizon for an appreciable portion of the astronomical night. During this period approximately 100 hours of clear moonless operation were achieved. Half of the period, September and October, was spent commissioning the array, ensuring that each detector was operating according to specification. After this time about 1500 events were recorded.

The weather conditions and the sky clarity were monitored by comparing the counting rate of the array and of individual detectors. This count rate was compared to the current from a 2" diameter photomultiplier viewing the night sky directly. It was found that when clouds were present the count rate dropped significantly and in general the sky became darker. Only those events recorded during a period of stable high counting rate were later analysed. Further developments in accurately determining the weather conditions will be found in the next chapter.

3-6   Results

In this section it is intended to analyse in detail one large shower recorded in the initial period of operation by the Dugway array to demonstrate the various stages of the analysis and then to show the main conclusion from a set of showers. During the first season of observation, the main purpose of the array was to establish that the array recorded showers which analysed to indicate similar characteristics for cascade development to those measured

earlier at Haverah Park, when allowance is made for the different altitudes of the two experiments.

3-6-1 Analysis of an Individual Shower

Figure 3-7 shows the output from the equipment when the pulse histograms in an individual large shower have been decalibrated. First, the arrival direction could be accurately determined by fitting a sphere through the observed times. Second, the location of the core of the shower in the array plane could be established by considering the distribution of the photon densities in the plane of the shower front. Figure 3-8 shows the lateral distribution fitted to the photon densities. The function used for the variation of the photon density, $\emptyset$, with core distance, r, was:-

$$\emptyset \, (r) = A(r + r_0)^{\eta}$$

and $r_0 = 50$ metres. Also shown in figure 3-8 are the variations of rise time and FWHM for each pulse with core distance, according to the analysis.

An alternative view of the timing information is to use it to image the shower as described in Chapter 2. Spherical fronts were fitted through the percentage levels in pulses recorded at core distances beyond 150m. Figure 3-9 shows the centres of the spherical fronts plotted through the atmosphere as a function of the intensity of the light distribution. The average of many near vertical showers from measurements at Haverah Park, Orford and Turver (1976), is also shown. Although the two arrays were situated at different vertical depths into the atmosphere, $862g$ cm^{-2} for Dugway and 1016 g cm^{-2} for Haverah Park, the two images in the atmosphere agree indicating that an extensive air shower appears to be consistent in Cerenkov light, independent

FIGURE 3-7

The information recorded in a large shower during
the season October - December 1977.
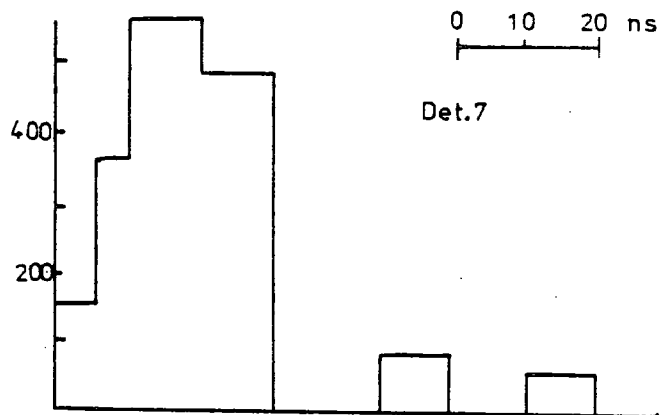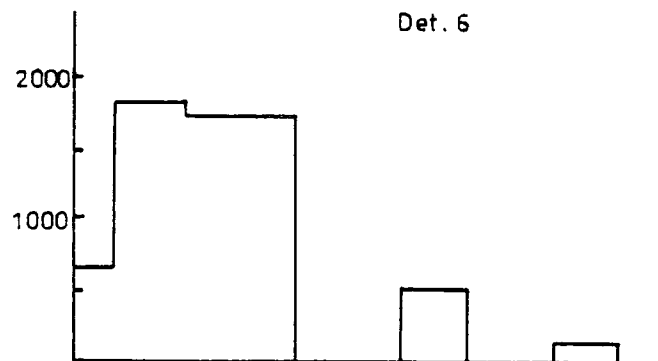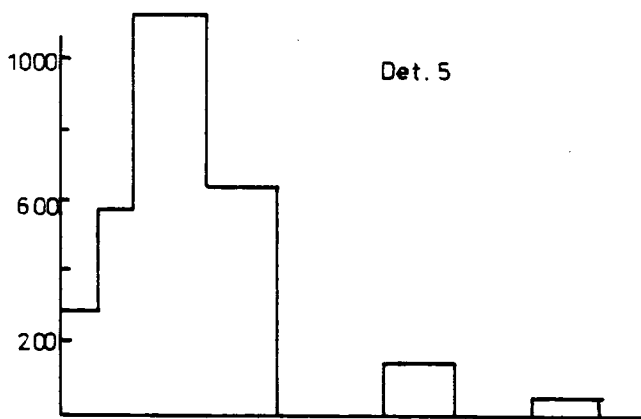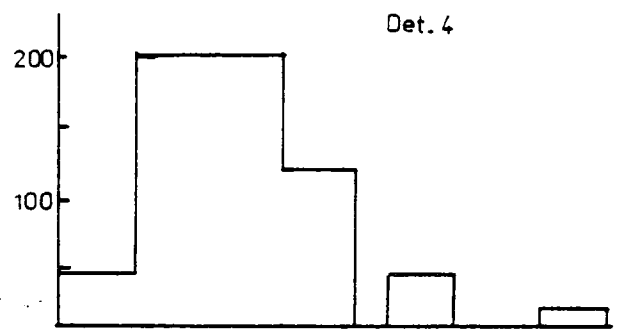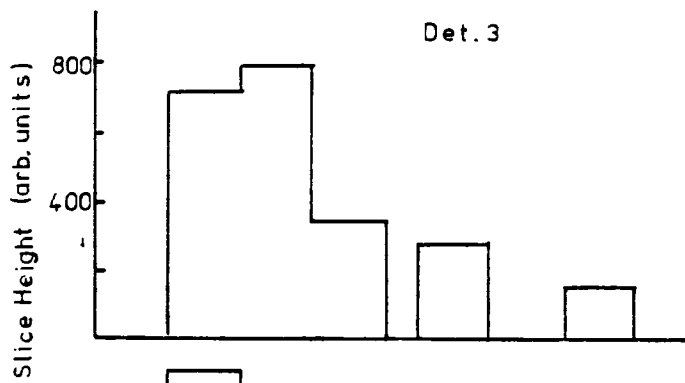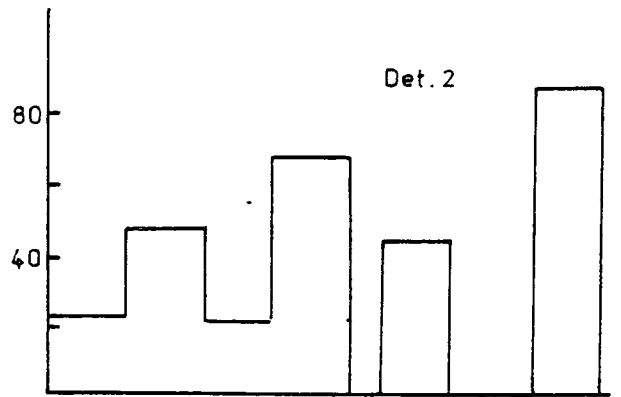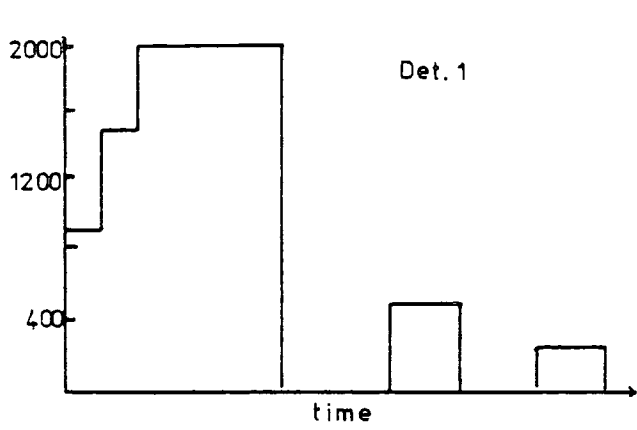
FIGURE 3-8

The derived lateral distributions of pulse area,

rise time and FWHM for a large event recorded during

the season October - December, 1977.

Event 186/2224/77
Date 10/11/77 Time 22:24 MST
θ=29·5° Φ=255·2°
X=-34 Y=-141 Λ=-245
Φ(200m)=2·3×10⁷ photons m⁻²

$\theta=29\cdot5° \quad \phi=255\cdot2°$

$X=-34 \quad Y=-141 \quad \Lambda=-245$

$\Phi(200m)=2\cdot3\times10^{7}$ photons m^{-2}

Photon Density (arb. units)

10^5

10^4

Core Distance (m)

200   500   1000

FWHM (ns)

40

20

5×10^3 10^4 5×10^4

R^2 (m^2)

Rise Time (ns)

20

10

$5\ 10^3$ 10^4 $5\ 10^4$

R^2 (m^2)
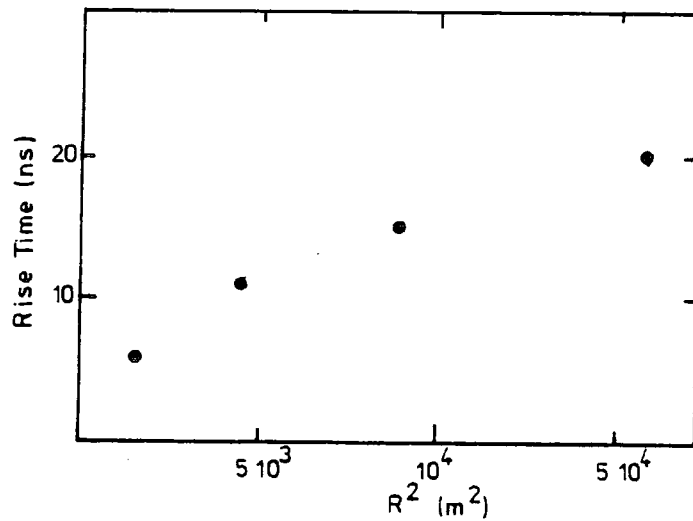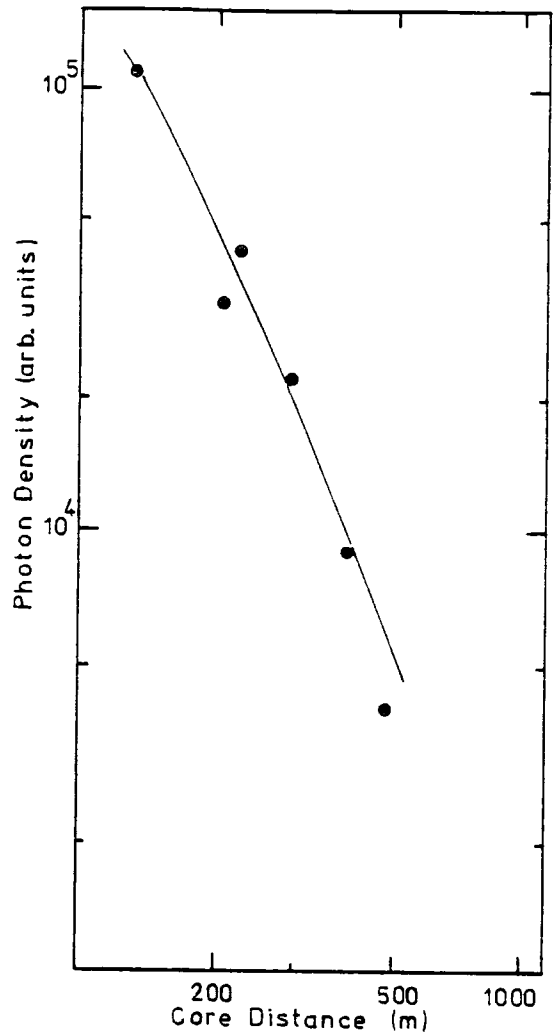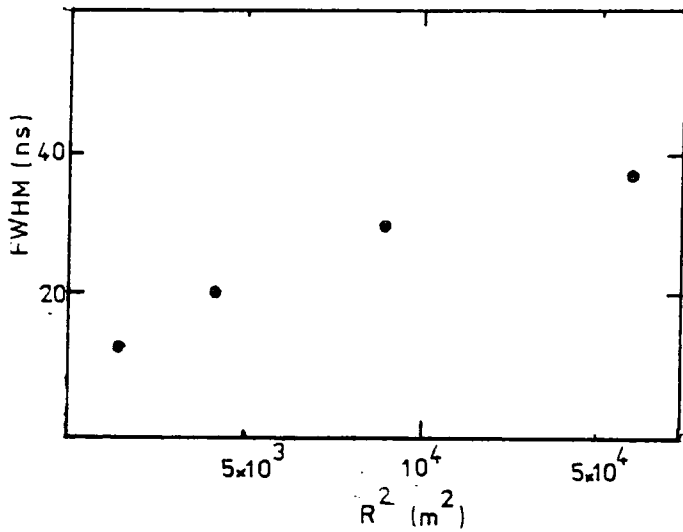
FIGURE 3-9

The Inferred Longitudinal Cascade of Cerenkov
Light.
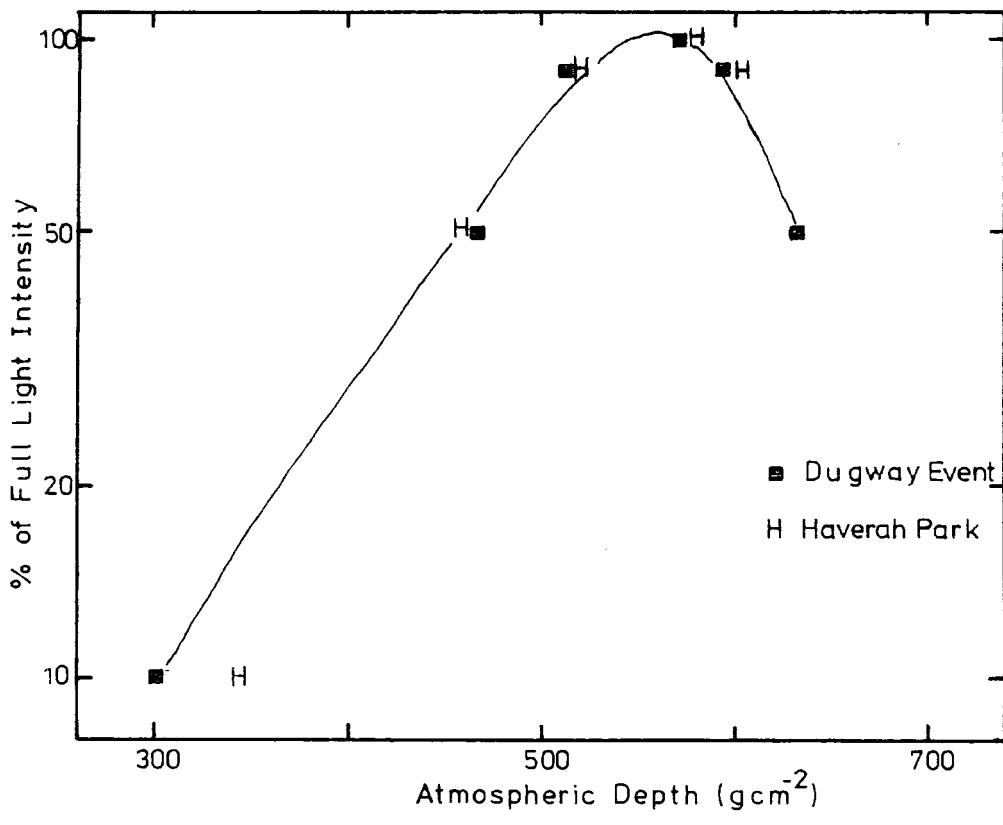
of moderate changes in the observation depth.

3-6-2   Average Characteristics of Cerenkov Radiation

It was found at Haverah Park that the exponent of the
structure function of the lateral distribution for the pulse
area varied with zenith angle. This was to be expected as an
increase in zenith angle increased the distance of the depth of
electron maximum away from the ground. It would be expected that
the breadth of the light pool observed on the ground would increase
with a consequent flattening of the function fitted. At Dugway the
same effect was noted and by overlaying the results of the two
experiments the change in exponent could be plotted from an
equivalent atmospheric thickness of 1500 g cm^{-2} to 862 g cm^{-2}.
Figure 3-10 shows the dependence of structure function exponent
on depth for the two experiments. The region where the two ex-
periments were observing under the same atmospheric thickness,
near vertical showers at Havarah Park and those at about 35°
at Dugway indicated that the two experiments were making similar
measurement of showers of energies about 10^{17}eV.

3-7   Improvements Prior to the 1978/79 Season

Following the four months of observation during August-
December 1977, described above, various minor improvements were
made to the equipment.

The amplifier was replaced by a device containing 2 VV100's
(rather than the VV100 and a discrete 100 MHz a.c. amplifier)
which improved the frequency response of the system. In conjunction
with this modification the method of determining the pulse area
was altered. The QTC was used directly as an integrator, the
signal from the photomultiplier was amplified by a factor of 10
(the first stage VV100) and then split, one channel going for a

FIGURE 3-10

The variation of structure function exponent with
atmospheric thickness.

Figure: Structure Function Exponent versus Atmospheric Thickness (g cm^{-2}). Data points show Dugway data Oct–Dec 1977 and Haverah Park. The arrow marks the Equivalent HP Vertical Thickness. X-axis values: 948, 1034, 1121, 1207, 1293. Y-axis values: −3, −2.
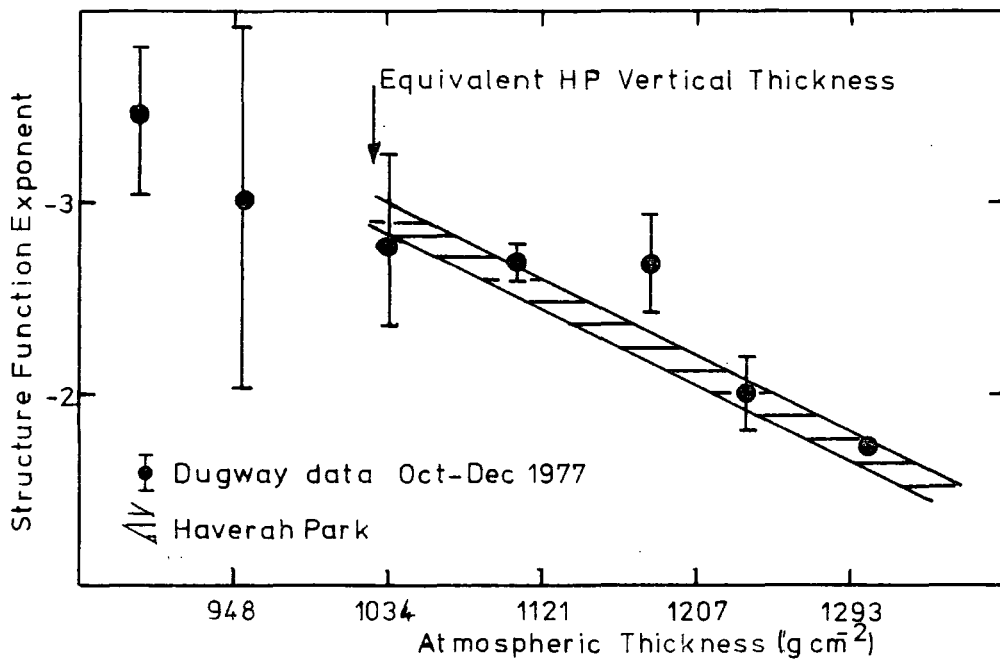
further stage of amplification, the second channel being taken

to the input of the QTC. This channel was gated by a wide

(approximately 250ns) pulse produced from the discriminator module.

The resulting system had an imp roved sensitivity and linearity.

The slicing arrangements for the inner detectors (1,5,6,

and 7, see figure 3-6) were inappropriate, as the pulses at the

core distances at which the detectors normally responded

(approximately 200m) were narrow, consequently the 6th slice

(at 50ns) was rarely above the noise level. It was thought that

this slice could be discarded and and the 5th slice kept in the same

position but enhanced to 8-bit accuracy, so increasing its use-

fulness. For the outer detectors the pulses were often small

and consequently the 20mV level of discrimination was often greater

than 50% of the pulses true height - valuable information of the

rising edge was thus lost. The 6th slice was therefore moved so

that it sampled the 10ns preceding the discriminator threshold

being exceeded. Figure 3-11 shows the arrangement of slices

for season 1978/79.

The output interface buffer was modified to improve the time

stretcher stop process, the calibration pulse generation and to

improve the sensitivity of the temperature sensors. In the array

centre a microprocessor (Fairchild F8) was introduced to replace

some of the hard wired triggering units used previously. The use

of the microprocessor allowed for an easier and more versatile

control of the experiment by the 4051 computer. An 8th detector

was installed between detectors 1 and 2, thus allowing for an

improved sample of the light in individual showers. Figure 3-12

shows the layout for the season 1978/79.

In addition to the measurements of the sky brightness by the

FIGURE 3-11a

The slice arrangement for an inner ring detector.

FIGURE 3-11b

The slice arrangement for an outer ring detector.

inner ring

discrimination
time

Amplitude (mV)

200

100

20 mV

0   10 ns

outer ring

discrimination
time

Amplitude (mV)

40

20

0   10 ns
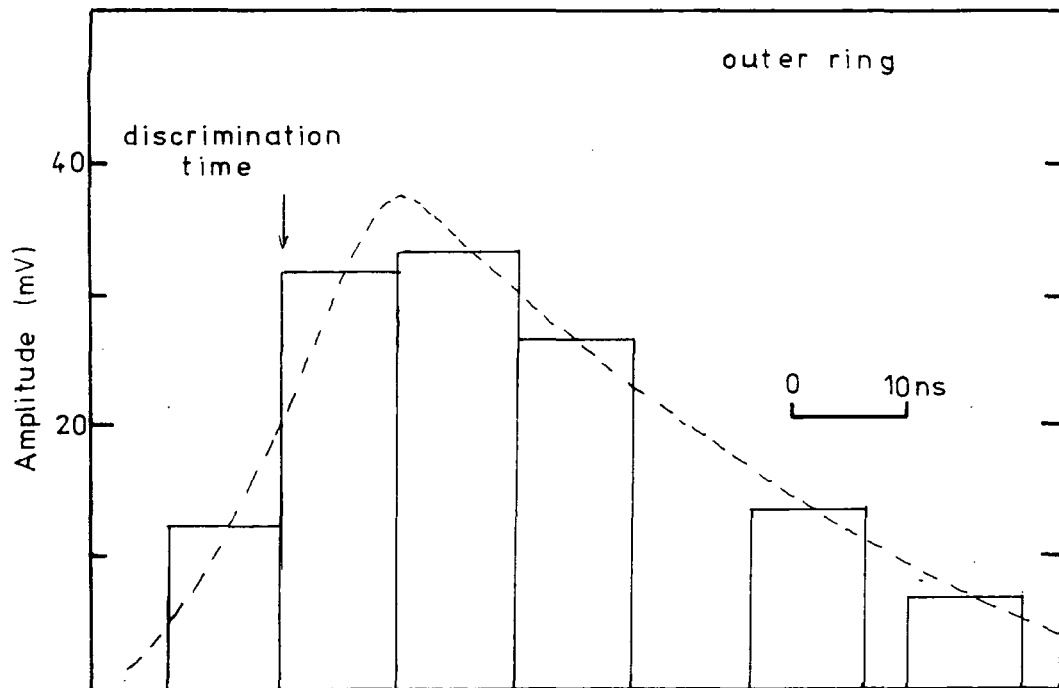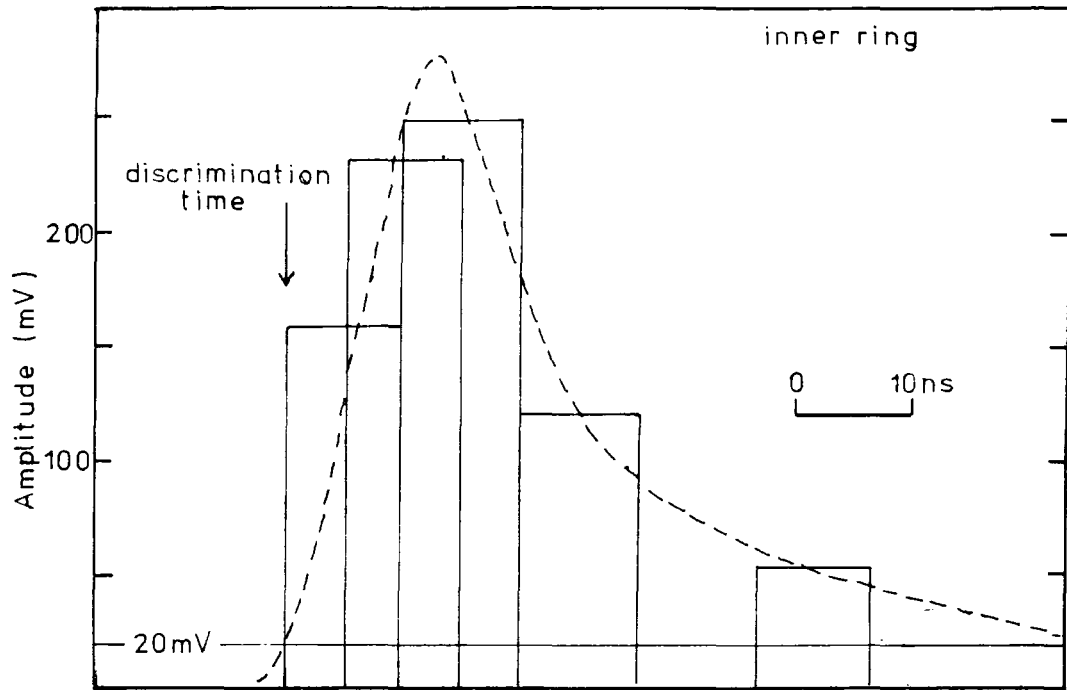
2" photomultiplier and the recording of detectors and array counting rates additional apparatus was installed which could improve the determination of night sky clarity. A time lapse camera was used to photograph the star trails at the zenith; a pressure transducer and 5 independent measures of temperature were all incorporated into the experiment to give more detail of weather conditions.

The array triggering requirements were changed so that a trigger would be made if any 3 of detectors 2, 3, 4, 5, 6 and 7 made a coincidence (window 3.6 μs). This increased the rate of events from about 10/hour to 22/hour. Essentially a trigger was made by the impact of a shower in any of the 4 triangles, defined by detectors 2, 5, 7; 3, 5, 6; 4, 6, 7 and 5, 6, 7; about 5% of the triggers were edge triggers from e.g. detectors 2, 3, 5. To minimise dead-time during each event a calibration and housekeeping record was made every 13 events rather than at each event. The dead-time of the recording system during an EAS was 10 seconds, giving a loss due to dead time of about 6%.

Finally, to further studies of the separation of the particle and light fronts in EAS, see Shearer (1978), $1m^2$ thick plastic scintillators were deployed at locations 0, 1 and 6. From these the time of arrival of the particle front with respect to the light front and the particle density were recorded, thus allowing for firstly, a measure to be taken of the separation of the light and particle fronts and secondly, a measure of the electron lateral distribution.

FIGURE 3-12

The Dugway Cerenkov Light Array for the season 1979/80.

$\square$ ^{2}

$+\blacksquare$ ^{0}

Y

7
$\blacksquare$

North

W

$37°$ ϕ

$\square$ ^{5}

X

+
$\blacksquare$
C

$\square$ ^{4}

$+\blacksquare$ ^{6}

$\square$ ^{3}
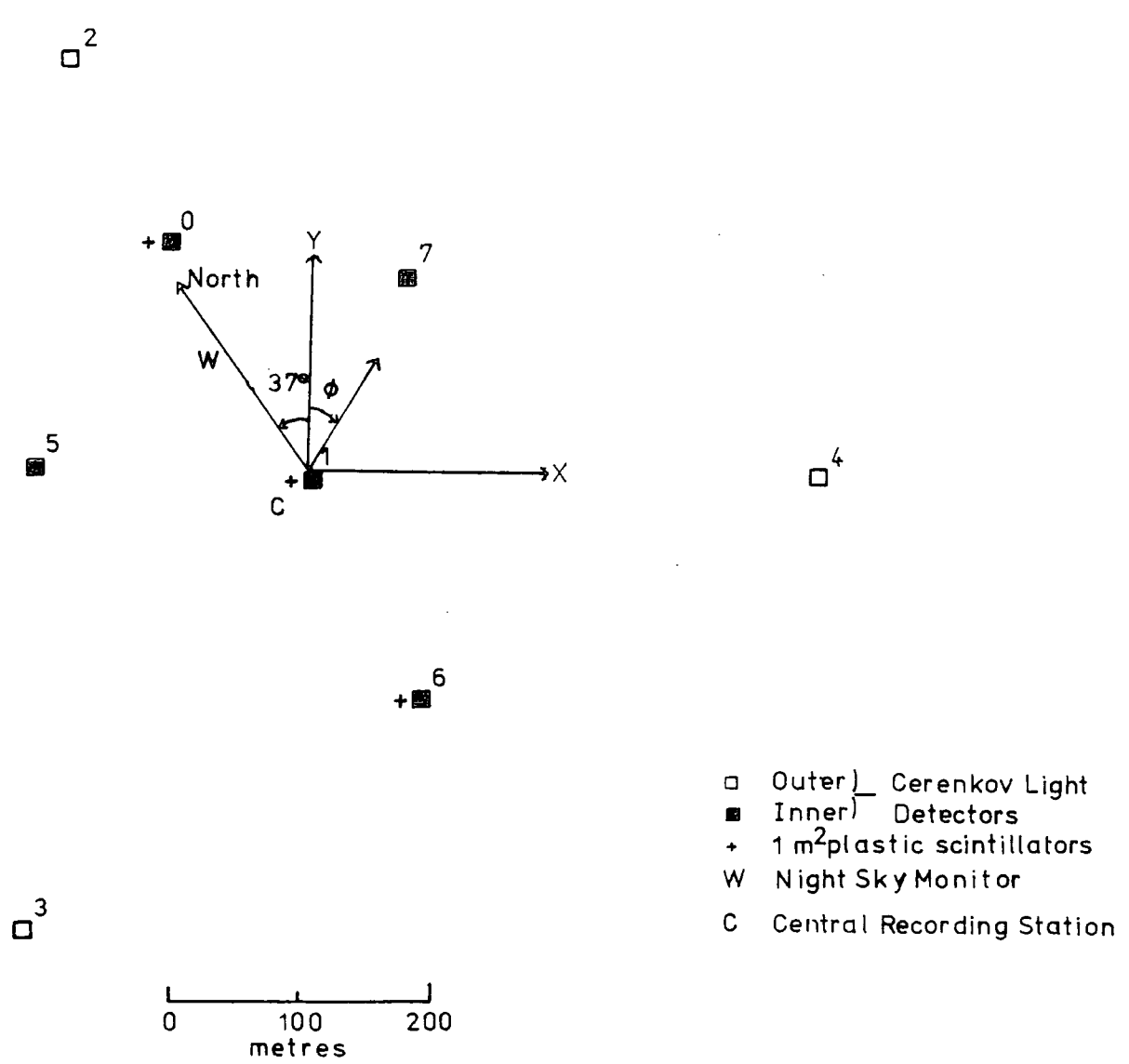
$\square$ Outer) Cerenkov Light
$\blacksquare$ Inner)   Detectors
+ 1 m^{2}plastic scintillators
W Night Sky Monitor
C Central Recording Station

0   100   200
metres

CHAPTER FOUR

Calibration and Data Reduction Procedures

4-1   Introduction

The recording system was calibrated at frequent intervals during the periods of operation of the experiment. This chapter describes the calibration technique. The data reduction procedures implemented in Durham are also described. The calibration may be conveniently divided into 3 sections:-

(1)   The calibrations of the timing systems, including synchronising the response of each detector;

(2)   The measurement of the photomultiplier and amplifier gain,

and (3)   The gain of the digitizing electronics.

The next 2 sections describe the calibration routines giving the estimated error in each parameter.

4-2   Time Calibration

It was necessary to devise a calibration system which would synchronise the detectors' responses to better than 1ns over a period of several μs. Figure 4-1 shows the various times it was necessary to measure in order to accurately synchronise the detectors. These can be summarised as:

(1)   Photomultiplier transit (D1)

(2)   Delays in the electronic circuits (D2) and (D3)

and (3)   The time of the master EAS coincidence pulse to reach the detector (D4).

In addition the time stretcher had to be calibrated to determine its linearity and consistency of stretching.

FIGURE 4-1

Schema of the various timing elements within the

detectors.

Photomultiplier
and Amplifier
Delay

D1

Discriminator
Delay

time stretcher

output interface

Output
Interface
Delay

D2

D3

D4   Trigger
Cable
Delay
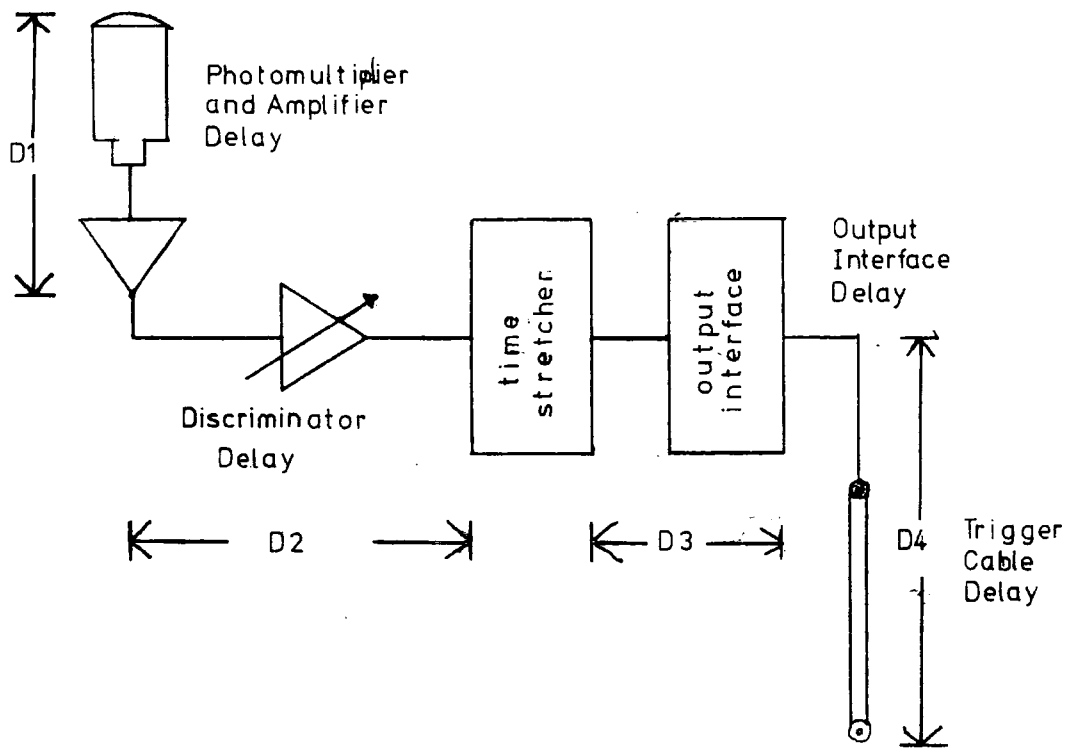
4-2-2 <u>Photomultiplier Transit Time</u>

The gains of the photomultiplier were set to be almost equal, resulting in each photomultiplier operating at a slightly different cathode potential. It would be expected that the transit time of the signal through the photomultiplier should vary (a decrease of approximately 3ns for each additional 100 volts of total photomultiplier potential has been measured by Orford and Stubbs (private communication)).

To measure the relative transit time of each detector a green L.E.D. was illuminated in the field of view of the photomultiplier. By avalanche pulsing the L.E.D. it was possible to produce a very fast rising edge to the light signal; the rise time after passing through the system was less than 6ns. The signal through the photomultiplier was compared to a reference signal which was delayed by approx- imately 100ns with respect to the pulsing of the L.E.D. Figure 4-2 shows the procedure schematically. Figure 4-3 shows a photo- graph of the signal from the photomultiplier and the reference signal. The estimated accuracy of this procedure (the error coming from measuring the Polaroid photographs of the oscilloscope traces) was 0.5ns.

4-2-3 <u>Time Stretcher Calibration</u>

To calibrate the time stretcher module, a method was needed whereby the interval between the start and stopping of the unit could be successively increased by accurately known amounts. To achieve this a crystal controlled 20MHz oscillator was used to generate start-stop intervals at 400ns separation from 400ns to 2.8 μs. To minimise the effects of spurious electronic noise and temperature the two

FIGURE 4-2

The Photomultiplier Transit Time Calibration.

Avalanche
Pulse
Generator

Reversed
Biassed
L.E.D.

NIM
Pulser

Photomultiplier

50 ns

Delay Cable (≈100 ns)

Oscilloscope
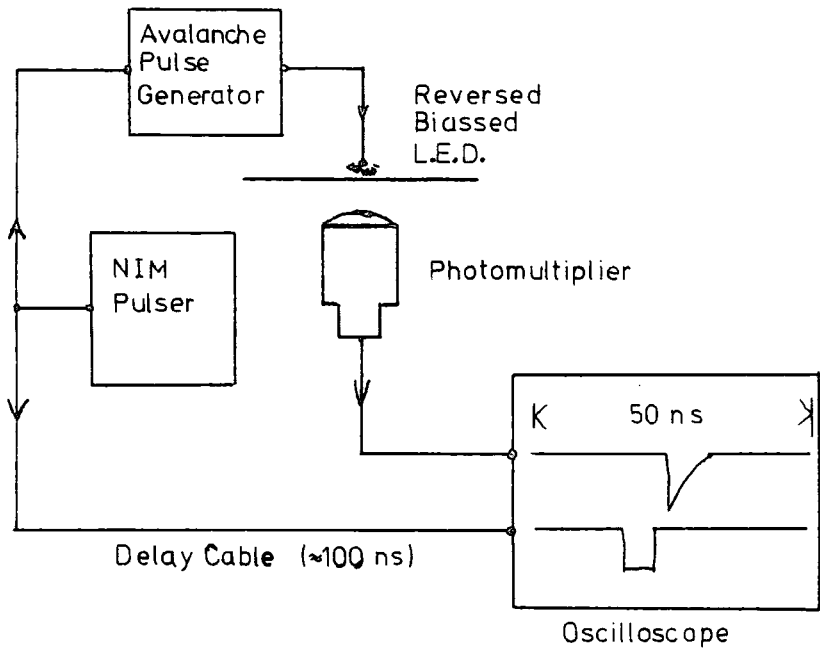
FIGURE 4-3

A photograph of the two signals used to determine the
transit time of the photomultipliers; the graticules
represent 5ns and 10mV per division, for the signal
from the photomultiplier, and 5ns and 100mV per division
for the reference signal. The first pulse on the trace
was the photomultiplier signal.
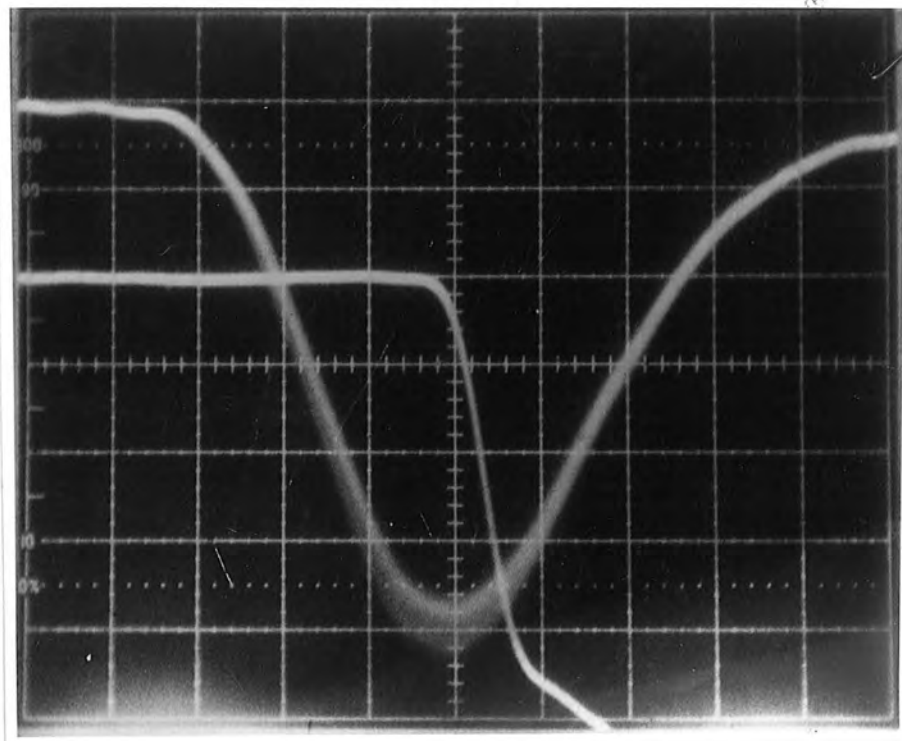
outputs (to start and stop the time stretcher) were matched,
of identical construction (using Schotky TTL components) and
were colocated.

The calibration of the rest of the system was achieved by
using the time interval generator to both trigger the detector,
at the input to the discriminator module, and to trigger the
central coincidence unit, which would then send a pulse to the
detector to stop the time stretcher. The cable used to pass the
start signal from the time interval generator was the same for
all detectors; its length being checked between calibrations.
The size of the pulse at the discriminator module was about 3
volts (about 150 times the discrimination level) thus minimising
any inaccuracies due to changes in rise time.

By increasing the interval between triggering the dis-
criminator and the coincidence unit it was possible to
calibrate the complete timing system over its expected
dynamic range. Also by using the night time calibration system
it was possible to further delay the stop pulse by approximately
1 μs. The two calibrations could not be combined to produce
a universal calibration, but by comparing the two slopes from
each calibration the linearity of the unit over a large
dynamic range could be checked. Figure 4-4 shows the deviation
from the regression line for two calibrations for a particular
detector. The slopes from each regression were 1.4656 and 1.4661
with standard errors of 0.93 and 0.46 bits (0.7 and 0.4 ns).
The change in slope corresponds to an error of about 0.5ns
over 2500ns, the dynamic range of the experiment.

4-2-4   Timing Calibrations-Conclusion

The above calibrations indicated that the detector

FIGURE 4-4

The deviation of a typical time stretcher calibration
data from the regression line, indicating the excellent
linearity of the device over a wide time span.
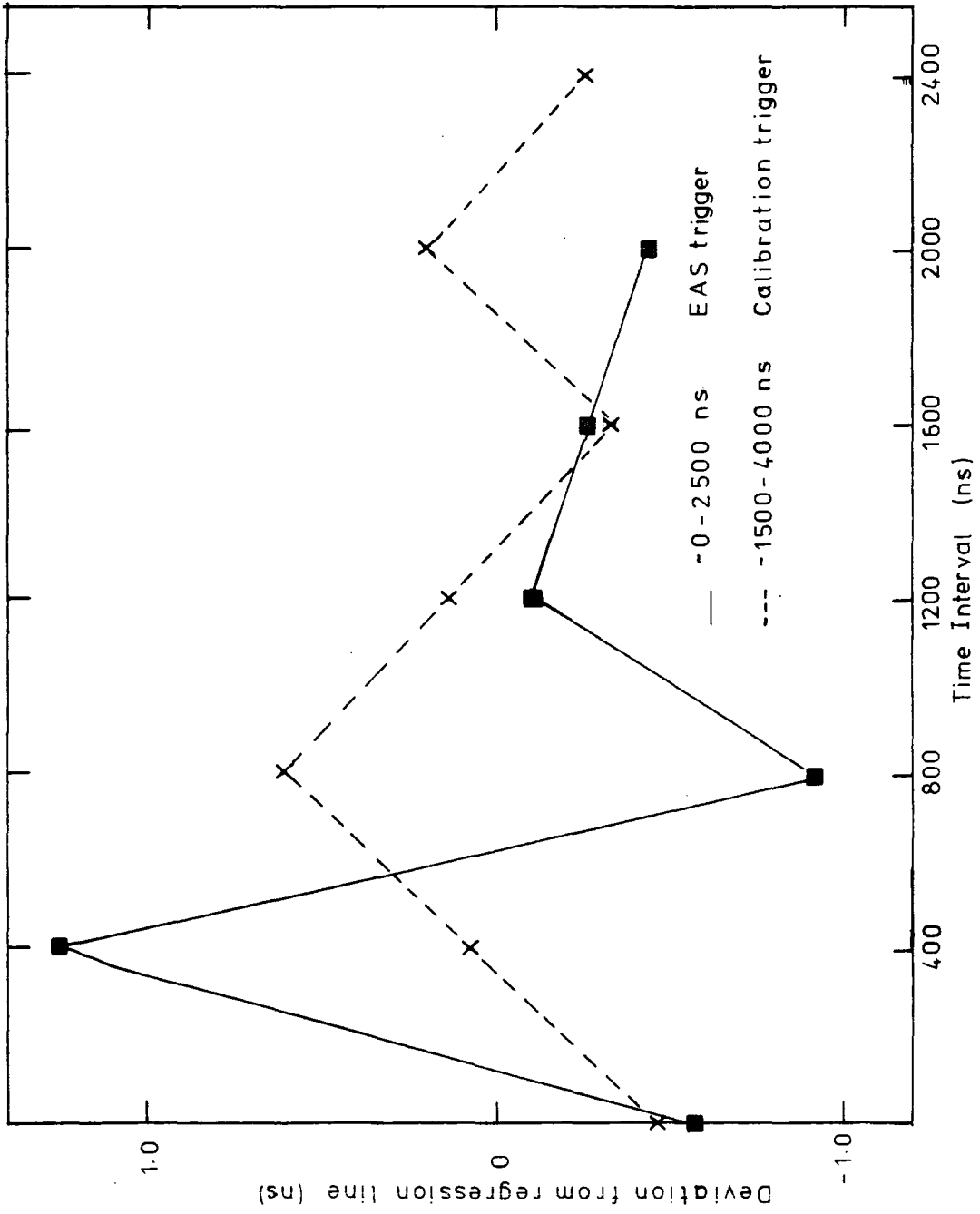
responses could be synchronised to better than 1ns, (0.5ns

from both the determination of photomultiplier transit time

and the linearity of the time stretcher system). It was also

important to accurately determine the detector positions; (any

inaccuracy in the determined position is equivalent to an

error in synchronising the detectors' responses). These were

established using an infra-red tellurometer and theodolite to

better than 5cms, (0.5ns), Chantler (private communication).

4-3   Amplitude Calibrations

4-3-1   Introduction

The amplitude calibration can be divided into two sections:-

(1)   The determination of the relative photomultiplier and
       amplifier gains.

(2)   The measurement of the relative internal gains of the
       digitizing electronics.

To determine the pulse shape the relative gains of the

electronics used to measure the charge sequentially through the

pulse had to be known to about 1%. To determine the lateral

distribution of the light the relative response of the

detectors had to be known to better than 10%.

4-3-2 Photomultiplier Gain

Three techniques were used to establish the relative

gain of the photomultiplier:-

(1)   A portable constant current-driven L.E.D. pulser was
       used to measure relative gains of the detectors;

(2)   A radio-active light pulser, giving a small output, was
       used to give a measure of the absolute response of
       the detectors to a photon flux (as well as indicating
       the frequency response of the detectors).

(3)   A fixed current driven L.E.D. in each detector was

used to indicate the night time gain stability.

The first technique flooded the photomultiplier with light from

a green L.E.D. pulser which produced a flat topped light pulse,

500 ns wide and consisting of about 5×10^5 photons. This

unit was placed on top of the perspex window of each detector

and moved until the signal, observed at the output of the amp-

lifier, was maximised. The heights of the signals from each

detector provided a means of determining the relative gains of

each detector. Figure 4-5 shows a photograph of the output

from one of the detectors. This technique had as its main

source of systamatic error the colour of the L.E.D. which was

green and away from the peak wavelength of the photomultiplier

response, and from the peak of the Cerenkov light distribution.

This source of systematic error could not be alleviated as no

source of the blue light, (e.g. SiC diode) was available which

would illuminate a large proportion of the photomultiplier tube

face. The trace thickness can be seen in figure 4-5 to be app-

roximately 20mV giving an estimated accuracy, for a pulse of

80mV height, of about 10% (the trace centre being established to

within 5mV).

The second technique, that of using a radio-active light

pulser, allowed for the relative response of the array to a known

photon flux, generated by non-electronic (and thus stable)

techniques, to be estimated. The pulser (NE130) consisted

of Am^{241} dispersed through type NE102a plastic scintillator

and the number of photons per flash has been measured to be

1835 ± 300 (Hartman, 1977, private communication). The light

flash has been stated by the pulsers manufacturers to have

FIGURE 4-5

A photograph of the L.E.D. pulser signal as viewed

by the calibration system, the graticules represent

200ns and 100mV per division.
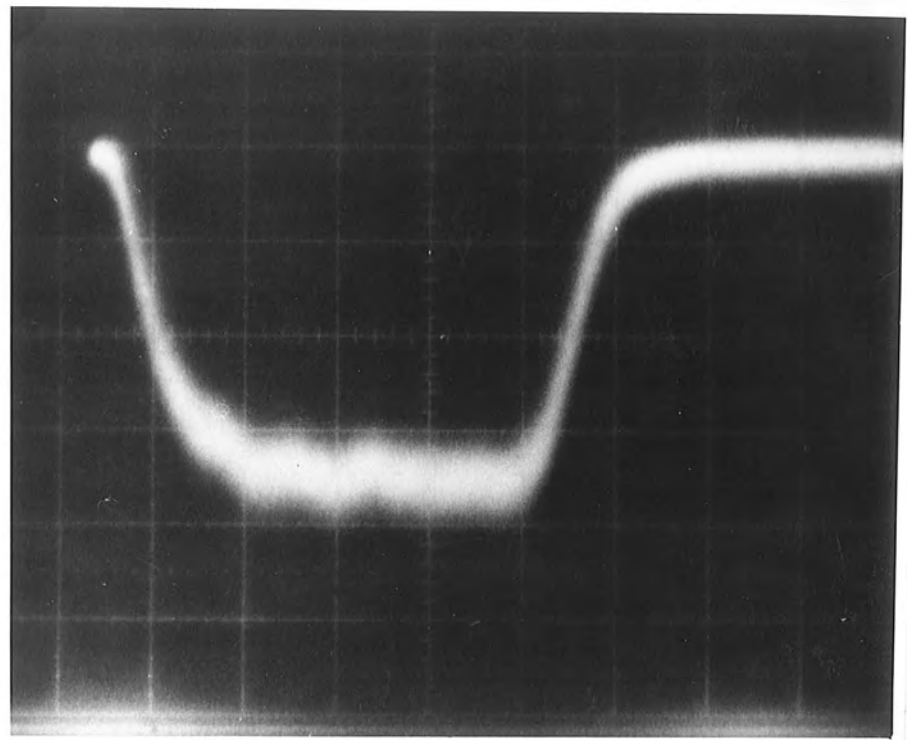
a characteristic decay time of 2ns, it could therefore be used to measure the system's response to a delta function. Figure 4-6 shows a photograph of the light flash observed at the output of the amplifier. This gave the response of the system to a delta function input as a rise time of 6.7ns with a FWHM of 6.2ns. The mean size of the observed pulse was 300mV ns at the output of the amplifier. Considering the number of photons within each pulse the system can be said to give an instantaneous output of 1mV for 6 photons ns^{-1} incident on the tube face.

Of the two techniques the former was considered to be the most reliable, having errors in measurement of about 10%. It would have been preferable to have used a more intense radio-active pulser, which would have allowed comparison to be made over the expected wavelength distribution of Cerenkov radiation, and which would have illuminated the complete photomultiplier face. A device of this sort was not available during the operation of the array. Whilst the gains were being measured it was determined that the brightness of the night sky did not effect the gains of any of the photomultipliers in the experiment, due to the low photomultiplier currents employed.

The third gain check was an insitu current driven L.E.D. which was flashed after every 13 EAS events. This determined any changes in a detectors response during a nights operation.

During the calibrations of the system no significant wanderings in the gain of the detectors was noted. The gains were set at the start of the observing season to be nearly identical. The rate of triggering of each detector was then set to be about 60Hz, causing minor changes in the set gain.

FIGURE 4-6

The response of a photomultiplier to a radio-active

light pulser signal, after being amplified, the graticules

represent 10ns and 5mV per division.

FIGURE 4-6

The response of a photomultiplier to a radio-active

light pulser signal, after being amplified, the graticules

represent 10ns and 5mV per division.
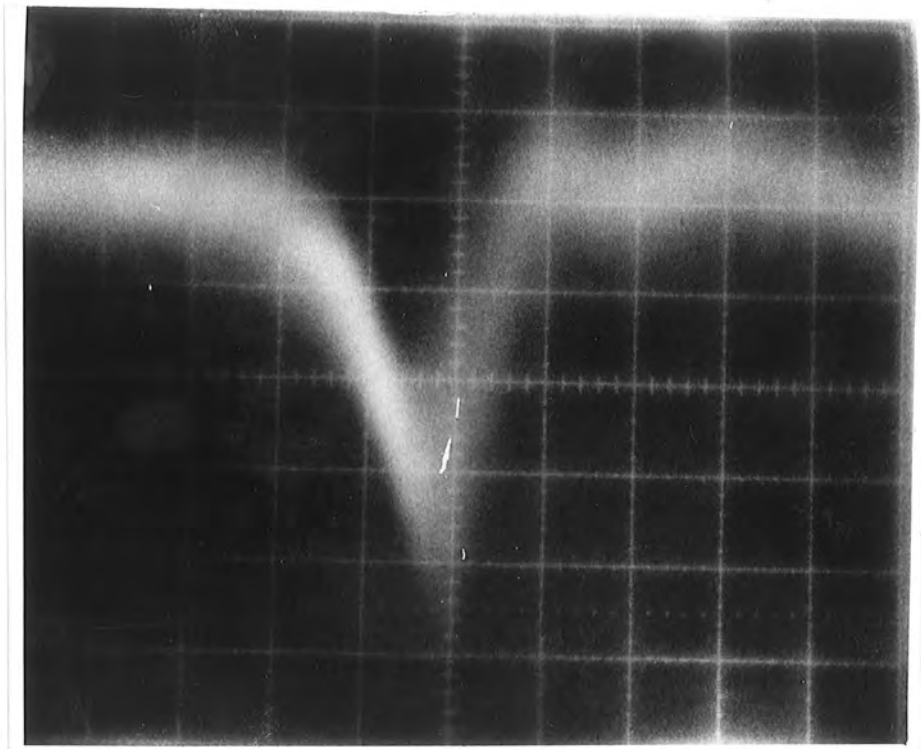
4-3-3 Digitiser Gain

The final stage in the calibration was to determine the response of the amplifier/QTC network to various input charges. This calibration was carried out at least once in every dark period when observations were made. This ensured that any changes in any detectors performance could be identified; the procedure also provided a very good means of checking a detector's overall performance. The procedure is shown schematically in figure 4-7 and consisted of varying the height of a 200ns wide flat-topped pulse before it was injected into the input of the amplifier. All aspects of the digitizing electronics could therefore be calibrated over the systems entire dynamic range. Figure 4-8a shows the calibration data for one of the slices; figure 4-8b shows the data for one of the integrators. These indicate the systems slight non-linearity for small signals.

Throughout the whole season no significant deviations were noticed in the response of the slices; however the integrator pedestal, that is the output for zero input charge, was subject to minor changes, ± 5 bits over the complete winter. These variations could be allowed for and were removed before any of the data was analysed; a description of this procedure is given in section 4-4-3.

In conclusion the pulse slices could be determined to an accuracy of 50mVns (300 photons at the photomultiplier face), the total pulse area to an accuracy of 200 mVns (1200 photons). The dynamic range was 50-15000 mVns for the slices and 250-100000 mVns for the determination of the pulse area.

4-4 Data Reduction

4-4-1 Introduction

FIGURE 4-7

The Digital Electronics Calibration Procedure.

```
                    ┌──────────────┐
                    │   Portable   │
                    │    Pulse     │
                    │  Generator   │
                    └──────────────┘
                       │        │
                       ▼        │
      Delayed     ┌──────────────┐          p/g  Trigger
   Discriminator  │   Switched   │
      Trigger     │1GHz Attenuator│
                  └──────────────┘
                          │
                       Variable
                       ▼Height
                       Calibration
                       Pulse
   ┌──────┐     ┌──────┐        ┌──────────┐
   │      │     │      │        │  Output  │
   │      │     │ PMT  │        │  Inter-  │
   │Disc. │     │ Amp. │        │   face   │◄───── Calibration
   │      │     │      │        │          │       Trigger from
   └──────┘     └──────┘        └──────────┘       Centre
        │    to Delay
        └──►Shaper
           to
         Fanout◄──
```

Portable Pulse Generator

Switched 1GHz Attenuator

Delayed Discriminator Trigger

p/g Trigger

Variable Height Calibration Pulse

Disc.

PMT Amp.

Output Interface

Calibration Trigger from Centre

to Delay Shaper

to Fanout

FIGURE 4-8(a)

Typical Slice calibration profile

FIGURE 4-8(b)

Typical Integrator calibration profile.

Data recorded during periods of bad weather were discarded and the remaining records were divided into manageable blocks for analysis. First, the events were blocked into sets of approximately 150-200 events with each block corresponding to at most one night's data. Each block was then studied before decalibration of the raw data to establish any errors in the response of the detectors. Finally, each event was de-calibrated and subjected to a rigorous preliminary analysis to determine both shower arrival direction and core location. Finally, events recorded under clear sky conditions were stored in a particular format so as to facilitate a future detailed analysis.

4-4-2 Sky/Weather Conditions

The array was fully operational for a total of about 300 hours during about 40 nights of operation. During this period about 140 hours of 'good' weather occurred. Good weather periods were established using three criteria. First, the star trails from the time lapse camera had to be clear and unbroken; second, the current from a 2" photomultiplier was monitored, and finally, the array counting rate was studied. The weather monitoring has been studied in detail by Chantler et al (1979); figure 4-9 from this shows the data from all the weather monitors for the night of 23/24 February, 1979. The period chosen shows the response of the equipment to a night when the sky cloud cover was not stable. A correlation can be seen between the maximum visible stellar magnitude and the array triggering rate. Also the sky brightness measured with a 2" photomultiplier is seen to vary with the array triggering rate although not as clearly as the maximum detectable stellar magnitude. A
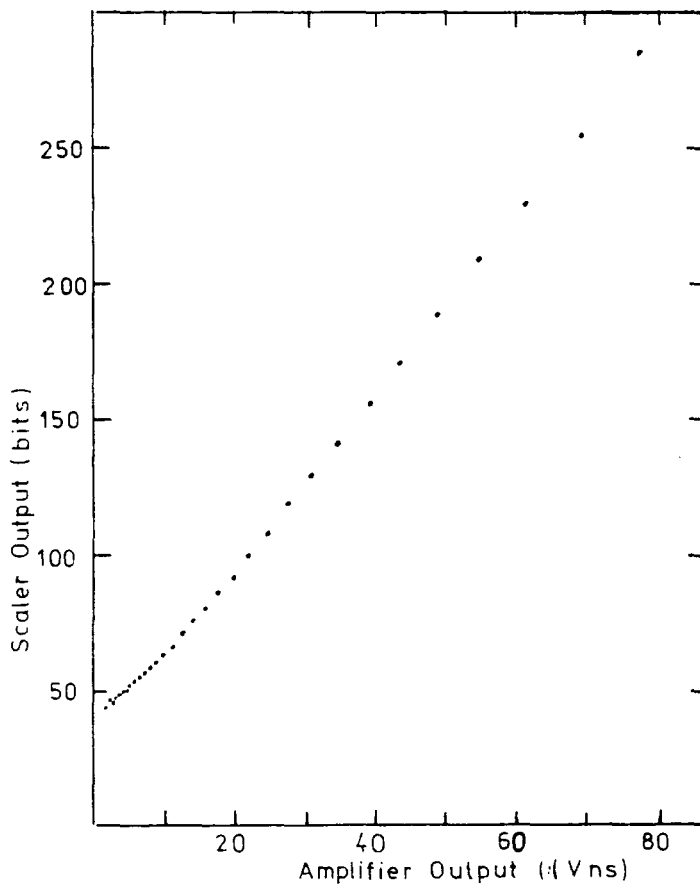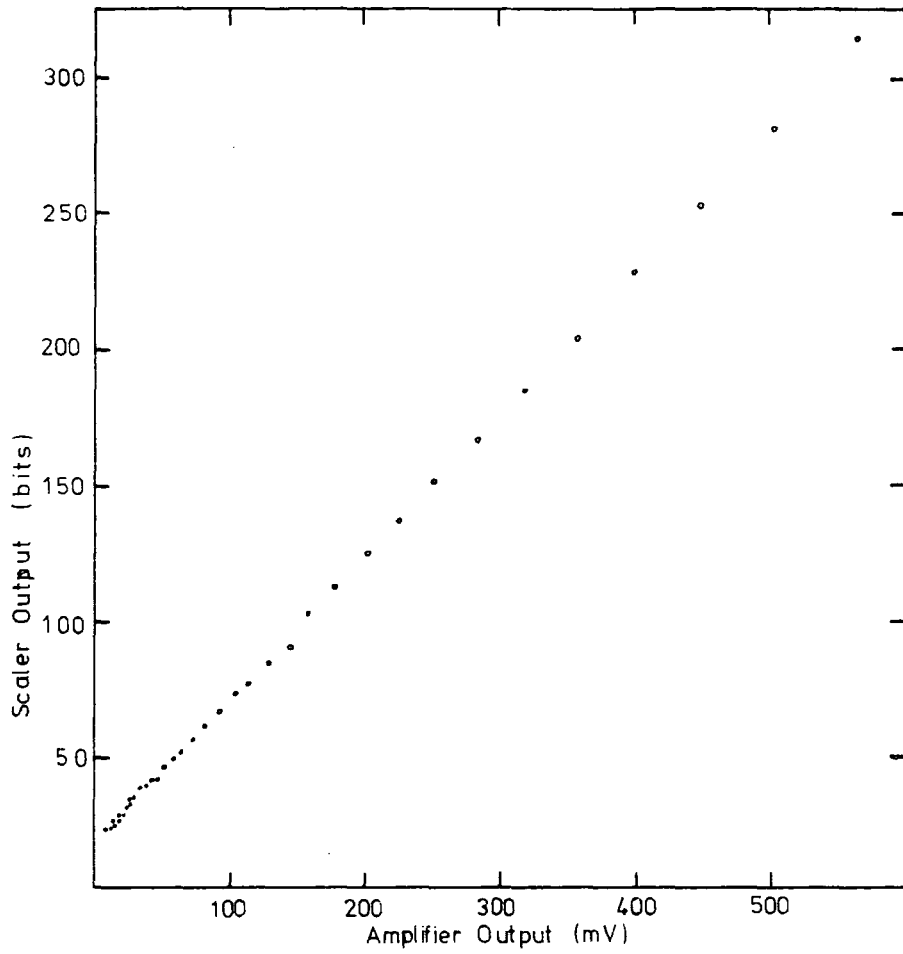
FIGURE 4-9

Some of the detector and atmospheric monitoring

information available for each night. This sample

is for 23/24 February, 1979.

Atmospheric Pressure (mb) — 840, 835, 830, 825

PMT# 1 Temp (°C) — 25, 20, 15

Detector Triggers in 30 minute Period ($\times 10^4$) — 4, 2, 0

Maximum Detectable Stellar Magnitude — 8, 6, 4, 2, 0

PMT Current (μA) — 6, 5, 4

Array Trigger Rate (Hr^{-1}) — 30, 20, 10, 0

2000 2200 0000 0200 0400 0600 0800

GMT −7 Hrs
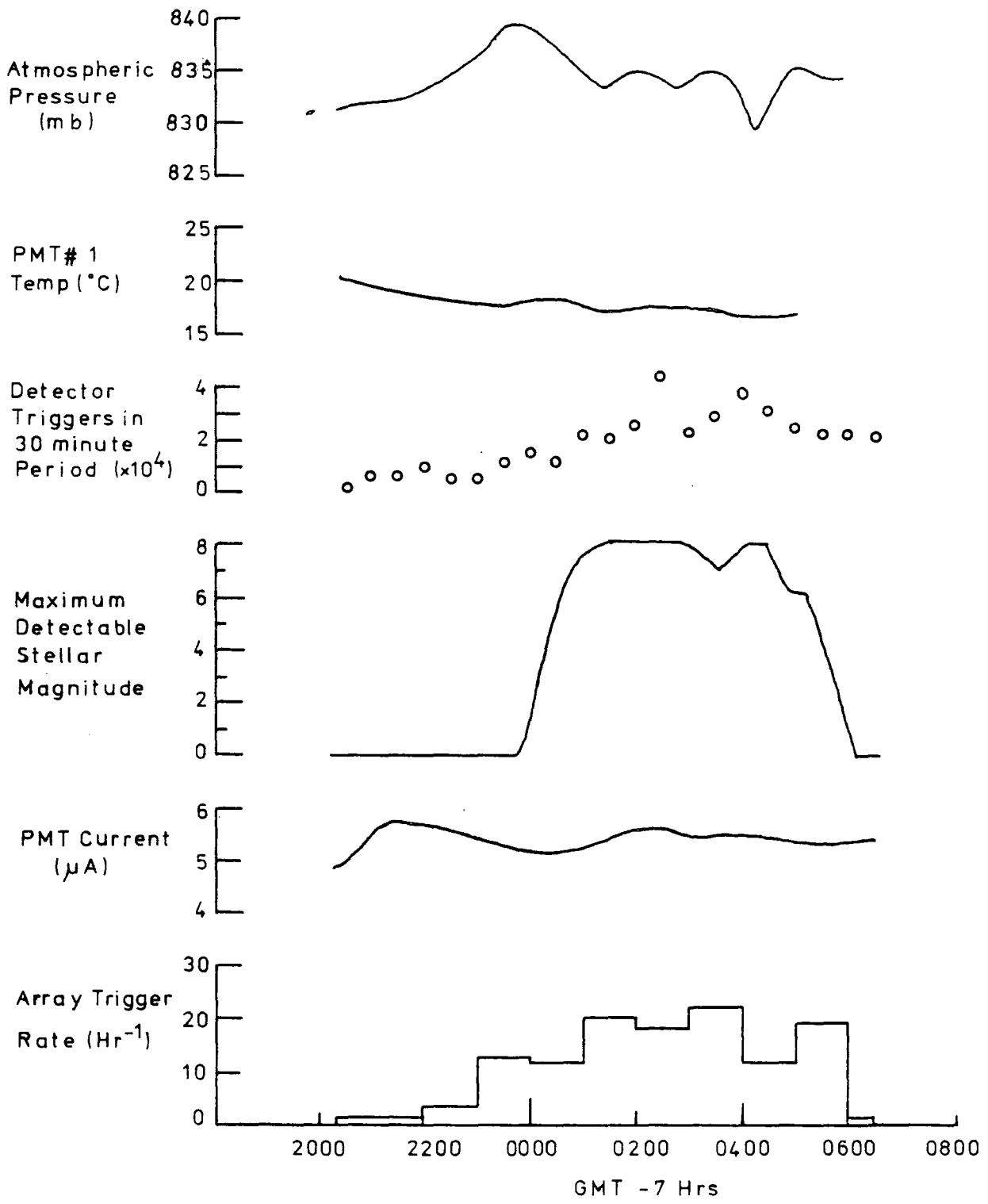
total of 25 blocks of 'good' weather periods was finally
established for the season 1978/79.

4-4-3 Decalibration of the Data

Having established the data blocks which were recorded
during periods of stable sky conditions, the events were
passed through a series of computer programs which decalibrated
the raw data and then analysed the shower for arrival direction
and core location. Before the events were decalibrated two
conditions had to be established:-

(1) that all the decalibration constants were accurately
known,

(2) that any scaler overflows had been accounted for.
The first item was primarily to account for the variation in
the integrator response discussed in section 4-3-3. It was
possible to determine the pulse area in two manners; from the
response of the integrator and from the summation of the slices
through the pulse. The latter method was most accurate for
determining small pulse areas. The integrator was used to
check the summation of the slices in smaller pulses and to
measure the large pulse area.

As no variation in the response of the slices was noted
during the entire season of observation, it was possible to
compare the two methods of determining pulse area from each
data block. By this means the small variations in the integrator
response could be determined.

The second item was to determine whether the scalers in
the detectors had overflowed. The system was designed to
overflow so as to increase the dynamic range of the experiment.
The scalers had a dynamic range of 0-255 bits, which if used

to digitised the complete dynamic range of the analogue system
would have given a sensitivity of 60mVns per bit (400 photons).
It was possible to recover such scaler overflows, the computer
program was designed to flag the need for overflows, action on
these flags could then be taken in an ancillary program for
implementation during subsequent passes of an event through
the program. The need for overflows could be identified by
comparing the pulse area determined by a summation of the slices
and the integrator response. If the two measures of pulse area
were significantly different the distribution of slices was
examined; and particular slices were overflowed until the two
measures of pulse area were similar. The dynamic range of the
integrator was such that only in the rarest of incidences would
its scaler overflow. By allowing scaler overflows the
sensitivity of the slice measurements was increased to 20mVns
per bit. No more than 4 overflows per detector were permitted,
as for more than this it was not possible to ensure a unique
pattern of overflows.

4-4-4 Data Analysis

During this stage of the data reduction each event was
analysed for shower arrival direction and core location; the
detailed analysis of the pulse structure was carried out after
this preliminary analysis. Both the core location and arrival
direction was determined using the optimisation package MINUIT,
James and Roos (1975).

The arrival direction of each shower was determined by
fitting a spherical front to the detector triggering times.
The line joining the centre of the sphere to the array centre
was the arrival direction. The justification for assuming a

spherical front, can be seen from the mean RMS deviation away

from sphericity, 2.8ns for showers having 5 or more responses.

Simulations also indicate that the front defined by the

20mV level, the discrimination level in the detectors, was

in fact, more closely spherical than say, the front defined by

the 10% level in each pulse, Chantler (private communication).

This procedure also provided the depth into the atmosphere of

the centre of the 20mV front.

Having established the arrival direction of the shower, it

was possible to determine the centre of symmetry of the

Cerenkov light pool at ground level in the plane of the shower.

For small pulses ($<$ 5000mVns, about 2.5 x 10^6 photons m^{-2})

the pulse area used in the core location was that determined

by the summation of the slices. Beyond this the integrator was

employed. The purpose of this was to ensure that the density

used in the analysis was the most accurate available. Each

density was normalised to account for the projection of the

photomultiplier face in the plane of the shower. The

relationship between the photon density, $\emptyset$, and core distance, r,

was detemined using a function of the form:-

$$\emptyset (r) \propto (r + r_0)^{\wedge}$$

This was fitted to the observed densities to produce the

core location and the shape of the lateral distribution of the

radiation.

Having established the shape of the lateral distribution,

the primary energy of the showers could be determined. Two

estimates of the primary energy were calculated; $\emptyset$(200m) the

light density at 200 metres from the axis of the shower, and

C_{50}^{250} the integral of the lateral distribution between 50 and

250 metres. The choice of primary energy estimator will be described in detail in the next chapter.

During the analysis, detectors which had misfired could be removed from the analysis, or if part of a detector's response, e.g. one slice, was in error, then this could be corrected.

To summarise, the preliminary analysis described in this section produced the following information:-

(1) The arrival direction of the shower

(2) The depth of the 20mV light front

(3) The core location of the showers

(4) The shape of the lateral distribution of the light density

(5) Two estimates of the primary energy.

4-4-5 Reduced Data Store

Once an event had passed through the main analysis program a few times, the number of passes depending on the degree of action required, the event was stored. The criteria for data storage to provide a set of showers for preliminary interpretation were, first, that all decalibration parameters for the events data block were finalised. Second, that all slices which required overflowing had been; pulses which could not be overflowed were flagged as such. Third, the core location and arrival direction fits were of 'good' quality - the criteria being that the R.M.S. deviation on the arrival direction fit was $<$ 10ns, and on the core location $<$ 1500 mVns or the ratio of the RMS and $\emptyset$ (200) was $<$ 0.20. These very loose selection criteria allowed for a large number of events to be stored, thus allowing for more rigid selection criteria to be introduced

at a later time. The information stored allowed for a

complete reconstruction of all information derived from the main

analysis program. The analysis procedure described above was

of sufficient quality to become the basis of understanding

the nature of Cerenkov radiation from large E.A.S.

4-5   Pulse Shape Reconstruction

It was necessary, having accurately decalibrated all

the information about a detector's response to a light flash,

to deduce the pulse profiles from the distribution of slice

sizes. No simple alogarithm could be found from studies of

simulations which would convert a distribution of slices into

a profile of a pulse, and one which would remain stable for most

configurations of slices, Orford (private communication).

Although at the time of writing a solution to this problem has

not been fully determined, the technique of spline fitting (Cox

(1972)), has been developed which should, in the future, provide

a means of accurately determining the structure of light

profiles. The development of spline-fitting will be described

by Chantler (Ph.D. thesis, in preparation).

In the interim, for the purpose of this work, a

technique was evolved which although using a spline function,

also employed manual pulse reconstruction. Essentially a

quartic-spline was fitted to the slice areas, and all re-

constructed pulses were checked by eye; any deviation from a

smooth monotonic function fit passing through all data points

was corrected. After this analysis the shape of each pulse

was described by:-

(1)   Rise-time, 10% - 90% levels on the leading edge.

(2)   Top-time, 90% - 90% levels

(3) Fall-time, 90% - 50% levels on the falling edge.

(4) FWHM, 50% - 50% levels.

As the FWHM spanned more slices (normally 4) than the other parameters (normally 2), this quantity should be considered to be measured with more accuracy than other measures of the pulse shape.

4-6   Data Reduction Conclusion

This chapter has shown that the calibration procedures could determine the response of the detectors to a high degree of accuracy. Further,an analysis procedure had been developed which could produce accurate arrival directions and core locations. The next chapter describes the average characteristics of Cerenkov radiation from EAS based on the analysis procedure described in this chapter.

CHAPTER FIVE

The Average Characteristics of Cerenkov

Radiation from EAS

5-1   Introduction

A small number of showers recorded in 1978/79 were
selected for a preliminary determination of the average
characteristics of Cerenkov radiation from EAS at 1451m
above sea level. Each shower selected was analysed and
scrutinized to ensure it fulfilled the following criteria:-

(1)   Each shower must be sampled by at least five
detectors, to ensure some redundancy of data.

(2)   Each shower arrived at a zenith angle within 50°
of the vertical.

(3)   The derived core location for each shower was within
the sensitive area of the array.

(4)   The R.M.S. error on the fits to determine core location
and arrival direction to be $<$ 1000mVns and $<$ 5ns
respectively. This arbitrary condition removed from
the sample any events which had corrupt data.

and (5)   The 5 or more detectors must have sampled the shower
with at least one measure within 100m and at least
one measure outside 250m from the shower core.

In all, approximately 130 showers satisfied these criteria
representing a small sample of the total number of showers
and thus providing a first analysis, which will be extended
to a larger sample in future work. It should be noted that the
size of the preliminary sample compares favourably with the
data available to other groups; 64 measured showers for the

previous work by the Durham group (Hammond et al 1978)), 500

showers (1 measurement per shower) for the Adelaide group;

(Thornton et al 1979)) and 82 measured showers from the

Yakutsk array (Grigor'ev et al (1978)).

The above selection criteria were chosen to reduce the effects

of triggering biases in the experiment. It is well known that

all EAS arrays are prone to recording those showers which fulfil

the threshold requirements most readily. We expect our array

to show such biases. Further, showers satisfying the criteria

outlined above had no significant correlations existing between

supposedly independent variable, e.g. no correlation existed

between shower size and typical core distance. Figure 5-1

shows the distribution of the impact points of cores in the

observation plane for the showers in this preliminary sample.

The present interpretation aims to establish the variation

with core distance, zenith angle and primary energy of the shower

for the following quantities:-

   (1)   The lateral distribution of the photon density.

   (2)   The shape of the light pulse at 300m from the shower

         axis.

and (3)   The radius of curvature of the extreme light front.

5-2   Primary Energy Estimator

A necessary prerequisite of any shower analysis is to

determine a shower parameter which can be related uniquely to

the energy of the primary. According to the results of computer

simulations (Smith & Turver (1973)) ϕ(200m), the photon density

at 200m may be a measure of primary energy. Figures 5-2 and

5-3, from Smith and Turver (1973), show the average lateral

distribution predicted for proton initiated showers of various

FIGURE 5-1

The distribution of core locations for showers used

in this preliminary analysis

2

0

7

5 1 4

6

0 m 200

3
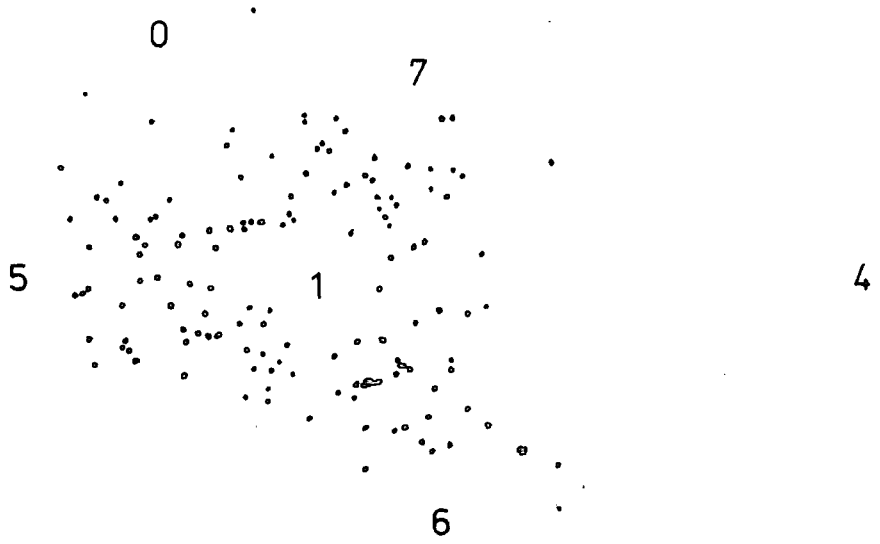
FIGURE 5-2

The lateral distribution of Cerenkov radiation for proton

primaries of different energy, from Smith & Turver (1973)

FIGURE 5-3

The lateral distribution of Cerenkov radiation for proton

primaries of energy 10^{17}eV showing the effect of fluc-

tuations in shower development, from Smith & Turver (1973)

Photon Density (m^{-2}) vs Core Distance (m)

E_p (eV)
■ 10^{15}
○ 10^{16}
● 10^{17}
× 10^{18}
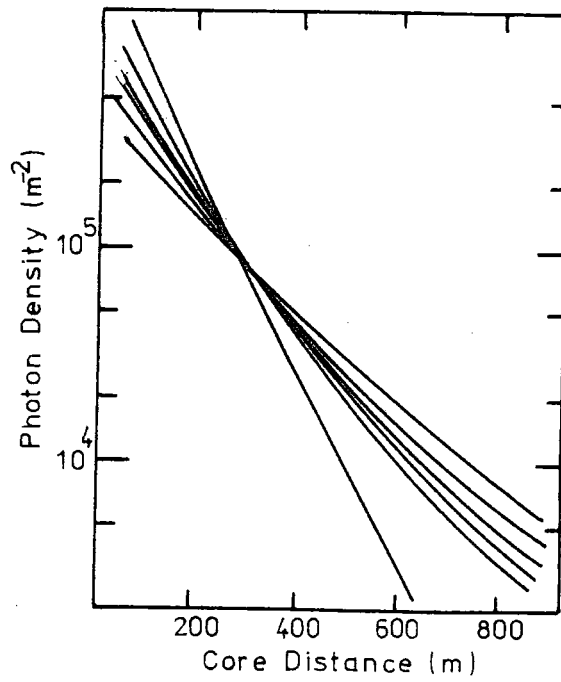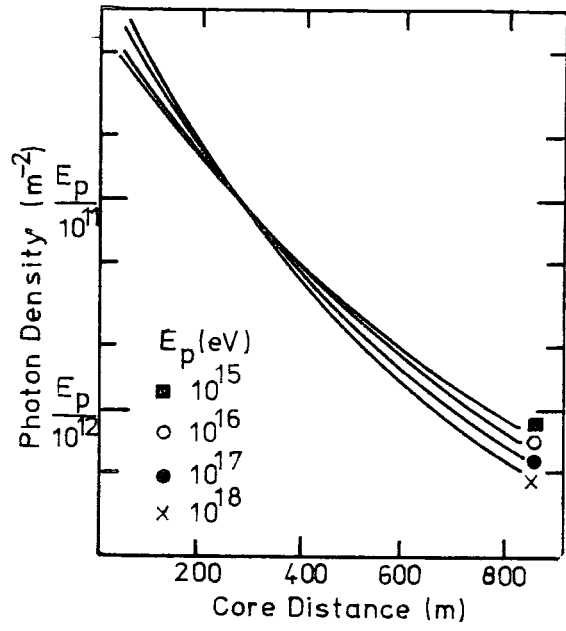
energies, and those for fluctuating showers at fixed primary energy. At a core distance of about 200m the photon density can be seen to be independent of shower development and only depends on the shower's energy. This calculation employed the CKP model for the pion momentum distribution (Cocconi et al (1963)), which has been subsequently found to give an inaccurate description of particle interactions and momentum distributions at accelerator energies. The CKP model has therefore been replaced in recent simulations by the Feynman hypothesis of scaling, although many aspects of showers are less well represented by the prediction from such a model. Figure 5-4 shows the lateral distribution of Cerenkov photons for a series of average showers (based on the scaling hypothesis) at two depths into the atmosphere. The cross-over at 200m shown in figure 5-2 now occurs at $<$ 50m at sea level, and at the lesser depth of 835g cm^{-2}, more appropriate to the Dugway experiment, the lateral distributions do not show a cross-over distance. From this it can be seen that selecting a primary energy estimator for the Dugway experiment will not be straight-forward. Depending upon the shower model adopted, ϕ(200m) may or may not be a worthwhile energy estimator and the atmospheric depth at which the observation is made may also be important. Moreover, the quantity ϕ(200m) was measured in a sea-level ex-periment and was found to correlate well with ρ (500)$_{ve}$, the Haverah Park primary energy estimator (Wellby (1977)).

In another experiment during the testing of the Dugway detectors, Waddoup (unpublished) compared the quantity ϕ(200m) with the electron size measured by the Volcano Ranch array, Linsley (1973). Here ϕ(200m) was found to produce a
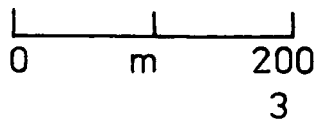
FIGURE 5-4

The lateral distribution of Cerenkov radiation for proton

primaries of different energy, calculated using the scaling

model

more significant correlation than the photon density at any
other distance with the electron size. This result is important
as the Volcano Ranch array is situated at a mean atmospheric
depth of 835g cm^{-2}, at which the showers are thought to be
at or near maximum development, Linsley (1973). If we assume
showers at maximum have a size proportional to primary energy
(a usual assumption, but in contrast to the predictions of the
scaling model), then this is a further indication that $\phi(200m)$
reflects primary energy.

In an attempt to obtain an improved primary energy estimator
the total flux between 50 and 250m was calculated giving the
quantity C_{50}^{250}, defined as:-

$$C_{50}^{250} = 2\pi \int_{50}^{250} r \; \phi(r) \, dr$$

where $\phi(r)$ is the functional form of the lateral distribution
and r the core distance. The quantity was chosen as firstly it
can be assumed that total light flux, if the observational plane
is below the depth of the shower maximum, is closely related to
the energy in the electromagnetic cascade and hence the primary
energy. The total light flux is not measureable without
extrapolation, but the integration of the lateral distribution
between two widely spaced limits (within the measurement
capability of an experiment) provides a first order estimate
of the total light flux. Secondly, the limits of integration
must contain the region of the lateral distribution where the
effects of fluctuations in shower development are minimised.

Figure 5-5 shows the results of recent computer simulations
by McComb (unpublished) for the variation of C_{50}^{250} and $\phi(200m)$

SEA LEVEL 835 g cm^{-2}

$\dfrac{\text{Photon Density}}{\text{Primary Energy}}$ (m^{-2} eV^{-1})

Core Distance (m)
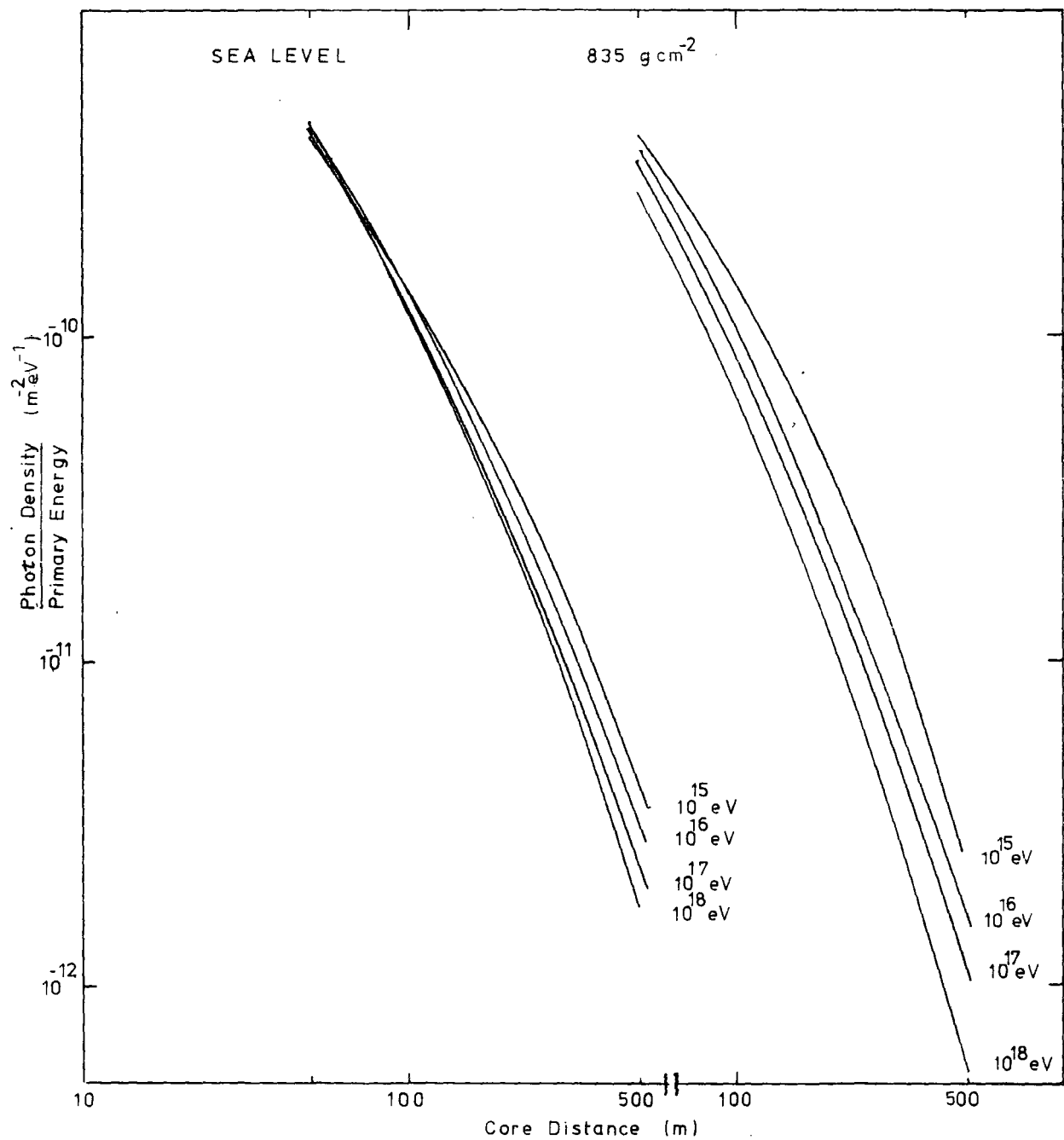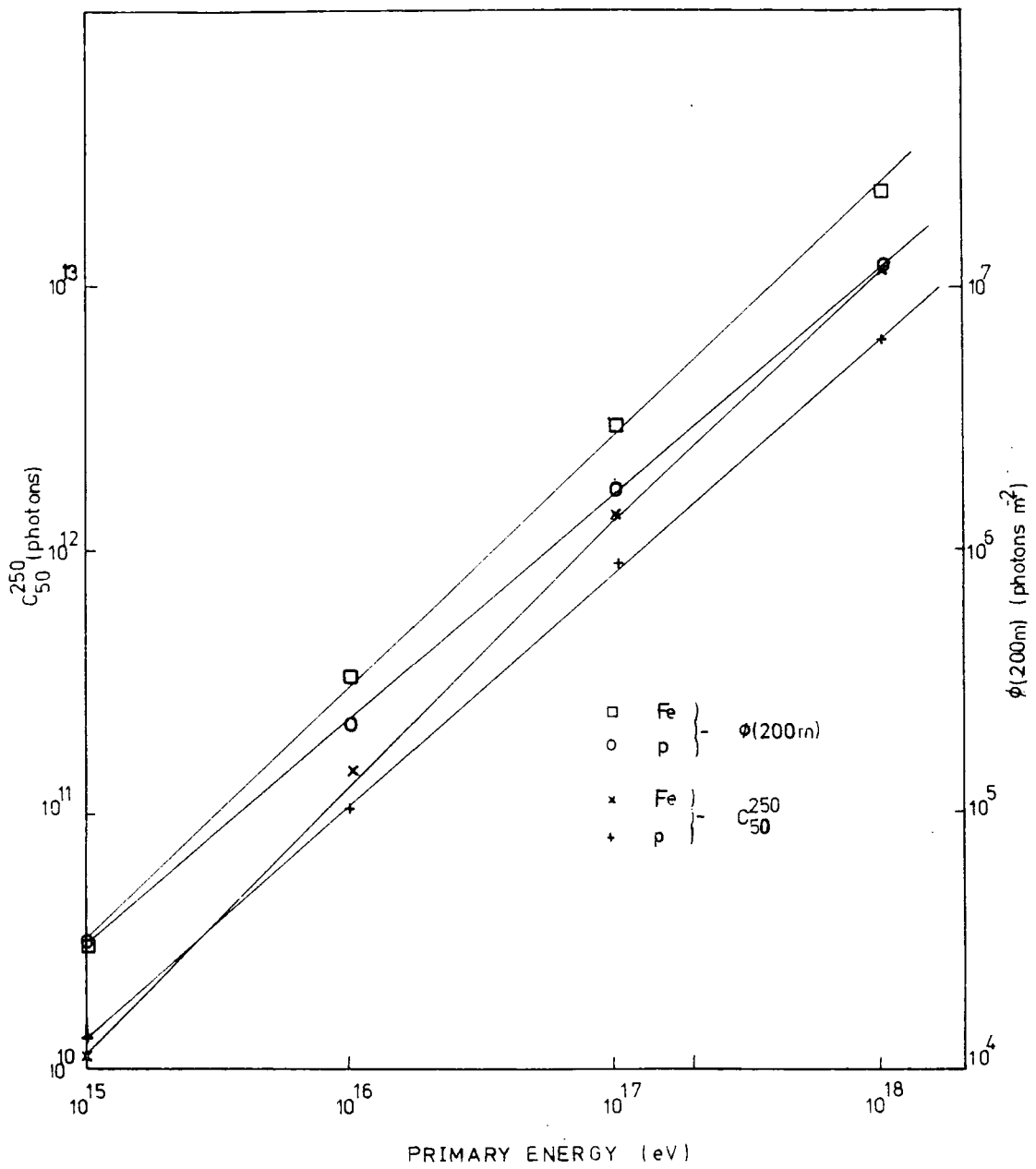
PRIMARY ENERGY (eV)

FIGURE 5-5

The variation of $\emptyset(200m)$ and C_{50}^{250} with primary energy, calculated using the scaling model

with primary energy. For a given mass of the primary, both
quantities vary with primary energy in a similar manner.
Figures 5-6a and 5-6b show the variation of C_{50}^{250} and $\phi(200m)$
with the electron size at maximum (Ne_{max}) for 10 fluctuating
proton showers calculated using a Landau type model. The Landau
type model used in the calculation has been described by
Gaisser et al (1978). The simplified form of the model used
predicts a scaling pion-momentum distribution for the high
energy pions and a $E^{\frac{1}{4}}$ multiplicity distribution for the lower
energy secondaries. This model which has been found by Gaisser
et al to give an adequate description of the measurements of
Cerenkov radiation made at Haverah Park will be used along with
a classical scaling model to interpret the results of this work.
From this it can be seen that both $\phi(200m)$ and C_{50}^{250} are affected
by changes in Ne_{max} for a given primary energy which arise from
such a model. The effect on the energy estimator of variations
in shower development is seen to be less for C_{50}^{250} than for $\phi(200)$.

To summarize, there is evidence to support the choice
of either $\phi(200m)$ (from measurement) or C_{50}^{250} (from calculation)
as a primary energy estimator which is independent of cascade
development. In the following interpretation C_{50}^{250} will be
employed as a primary energy sensitive parameter.

Attempts to interpret the magnitude of measured showers
(expressed in mVns) depends upon the quite difficult gain
calibration of each detector employing a radio-active light
pulser (cf section 4-3-2). It is possible to relate values of
C_{50}^{250} to other measures of primary energy.

FIGURE 5-6 a,b

The variation of C_{50}^{250} and $\emptyset(200m)$ with electron size (Ne_{max}) from simulations of proton primaries of fixed energy, $10^{17}eV$
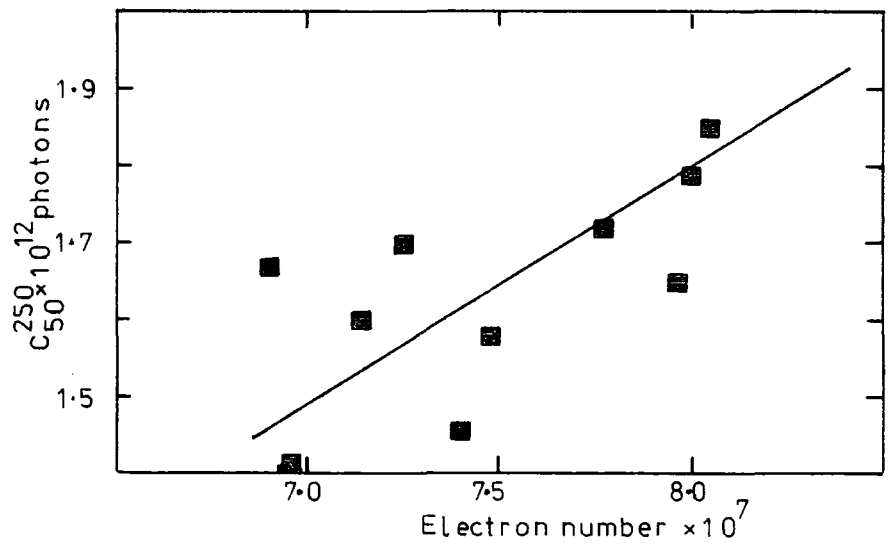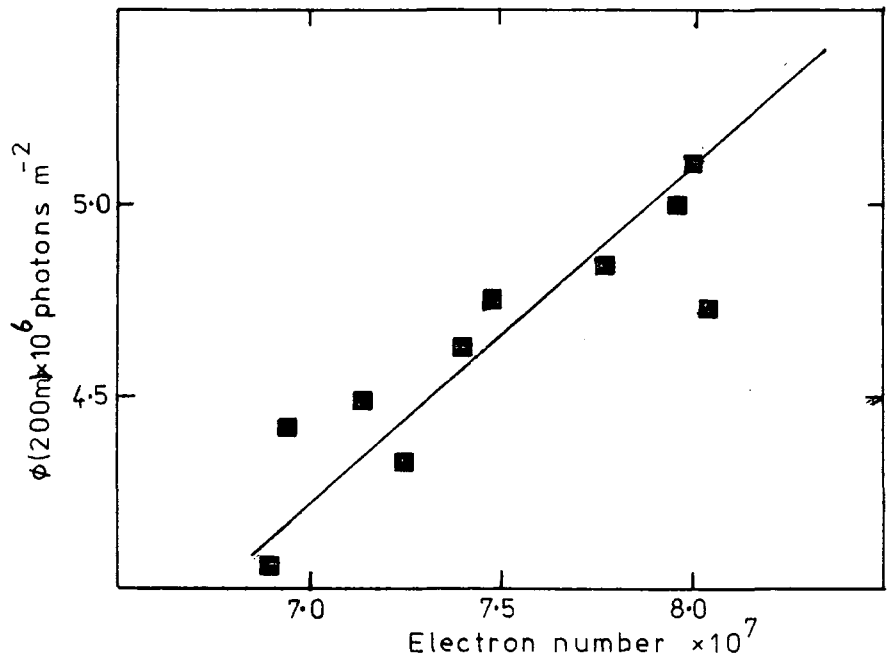
$$C_{50}^{250} = 10^9 \text{ mVns} \approxeq 5 \times 10^{11} \text{ photons}$$

$$\approxeq \phi(200\text{m}) \text{ of } 10^6 \text{ photons/m}^2$$

$$(\approx 5 \cdot 10^{16} \text{eV according to models})$$

$$Ne_{max} \text{ of } 10^7 \text{ particles at Volcano Ranch}$$

$$\rho \ (500)\text{ve of } 0.3\text{m}^{-2} \text{ at Haverah Park}$$

It must be emphasised that some of these interrelationships are model dependent and may not represent a true intercalibration of the response of various arrays. All comparisons of shower energy shown here are made using C_{50}^{250} in mV ns without the uncertain conversion to photons. It should be stressed at this point that C_{50}^{250} is an interim measure of primary energy, and it will probably be developed in the light of future analyses of the complete Dugway data set and from the results of further computer simulations for vertical showers and an important new set of stimulations of showers incident at zenith angles up to 45°.

5-3   The Data Set

To examine the average characteristics of Cerenkov light in EAS the data were divided into a matrix of primary energy and zenith angle intervals. The intervals chosen were:-

$$8.33 < \log_{10} C_{50}^{250} \leqslant 8.67 \qquad\qquad \sec\theta \leqslant 1.1$$

$$8.67 < \log_{10} C_{50}^{250} \leqslant 9.0 \qquad\qquad 1.1 < \sec\theta \leqslant 1.2$$

$$\qquad\qquad\qquad\qquad\qquad\qquad 1.2 < \sec\theta \leqslant 1.3$$

$$9.00 < \log_{10} C_{50}^{250} \leqslant 9.33 \qquad\qquad 1.3 < \sec\theta \leqslant 1.4$$

$$9.33 < \log_{10} C_{50}^{250} \leqslant 9.67 \qquad\qquad 1.4 < \sec\theta \leqslant 1.5$$

$$\qquad\qquad\qquad\qquad\qquad\qquad 1.5 < \sec\theta \leqslant 1.6$$

Table 5-1 shows the number of showers within each interval, indicating a fairly uniform distribution of showers within the matrix.

5-4   The Lateral Distribution of Cerenkov Radiation

A principal aim of the measurement was to determine the lateral distributions of Cerenkov photons in individual showers which reflect the depth of the electromagnetic cascade maximum of the shower. It was previously assumed that the change in the shape of the lateral distribution resulting from the increased distance above the detector plane of the cascade maximum, when larger zenith angles are considered, was similar to the change resulting from variations in the position of cascade maximum above the observation plane resulting from differences in primary energy. Such assumptions form the basis of the elongation rate theorem discussed by Linsley (1977). It was also assumed that the thickness of the atmosphere varied directly with the secant of the zenith angle, for inclinations less than 60°. With these assumptions it was intended to relate average changes in a measured lateral distribution shape with energy to average changes in the depth of cascade maximum in the atmosphere.

The average lateral distributions resulting from sorting all measured densities for showers of specified zenith angle and energy into 50m wide bins are shown in figures 5-7 to 5-9. A power law of the form expressed in equation 4-1 was fitted to these distributions and the values of the exponent, η , fitting the data are shown in table 5-2. The lateral distributions are seen to be broader for increasing zenith angle and for decreasing primary energy, consistent with the

TABLE 5-1

The Distribution of Events in Zenith Angle
and Primary Energy Intervals

PRIMARY ENERGY ESTIMATOR

	$8.33 < \log_{10} c_{50}^{250} \leqslant 8.67$	$8.67 < \log_{10} c_{50}^{250} \leqslant 9.0$	$9.0 < \log_{10} c_{50}^{250} \leqslant 9.33$	$9.33 < \log_{10} c_{50}^{250} \leqslant 9.67$
$\sec\theta \leqslant 1.1$	2	12	14	5
$1.1 < \sec\theta \leqslant 1.2$	5	15	10	5
$1.2 < \sec\theta \leqslant 1.3$	3	8	8	4
$1.3 < \sec\theta \leqslant 1.4$	2	1	6	3
$1.4 < \sec\theta \leqslant 1.5$	3	7	5	3
$1.5 < \sec\theta \leqslant 1.6$	-	5	3	3
	$10^{16} < E_p \leqslant 2.5\times10^{16}$	$2.5\times10^{16} < E_p \leqslant 5\times10^{16}$	$5\times10^{16} < E_p \leqslant 10^{17}$	$10^{17} < E_p \leqslant 2.5\times10^{17}$

APPROXIMATE PRIMARY ENERGY (eV)

FIGURES 5-7 - 5-9

The observed lateral distributions of Cerenkov radiation from showers of differing energy and incident at different zenith angles

$8.67 < \log(C_{250}^{50}) < 9.0$
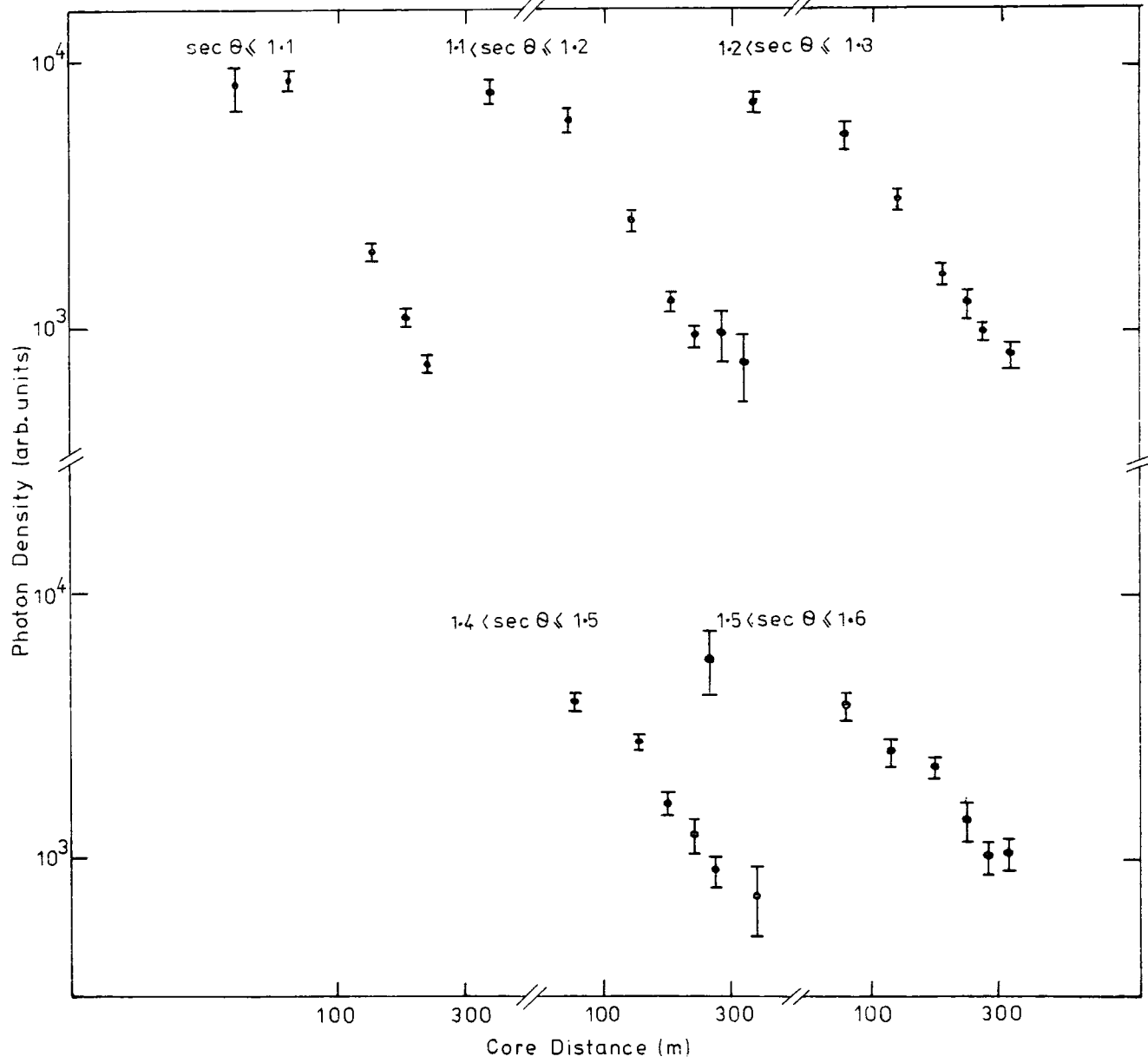
$9\cdot0 < \log(C^{50}_{250}) < 9\cdot33$
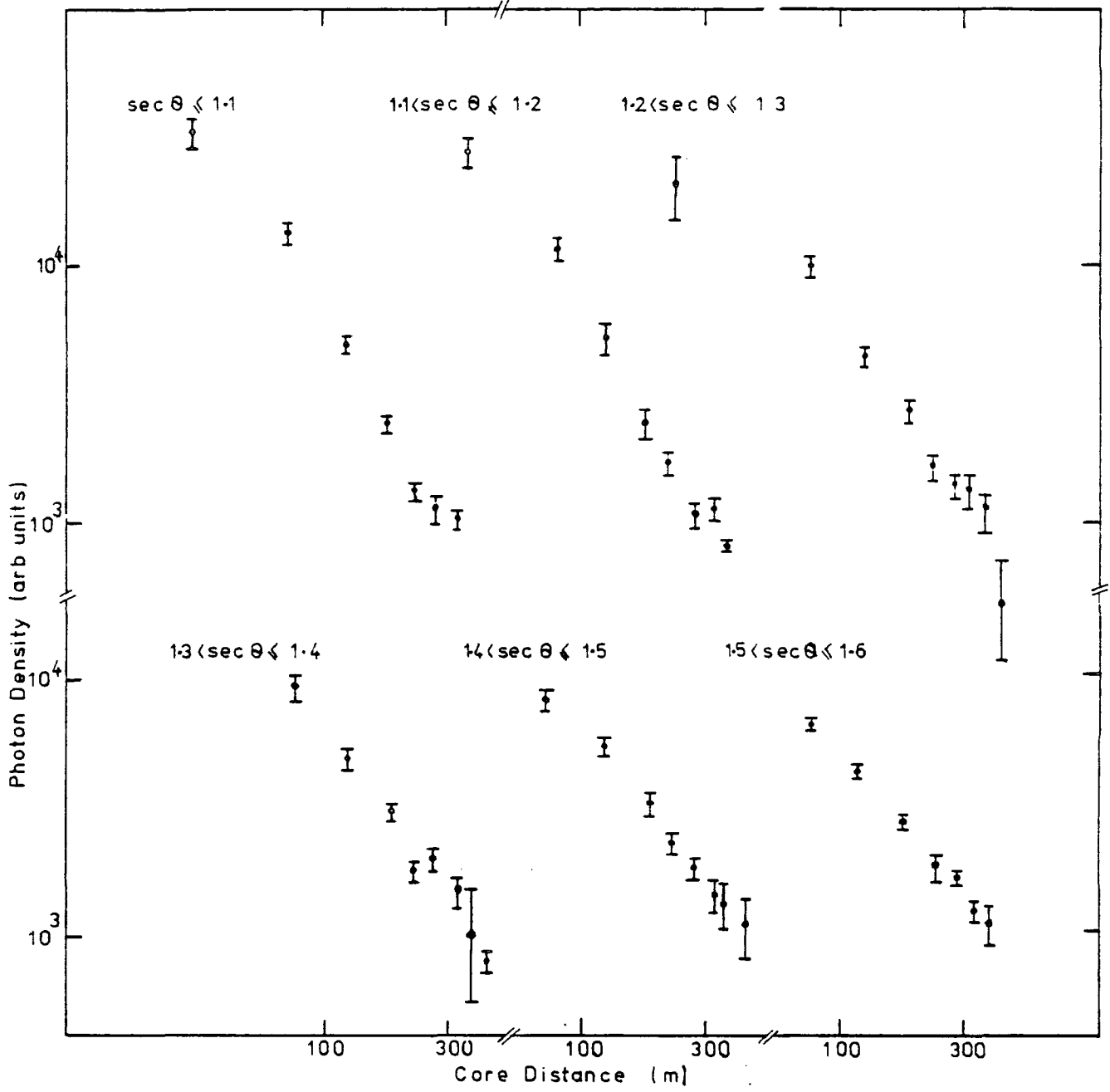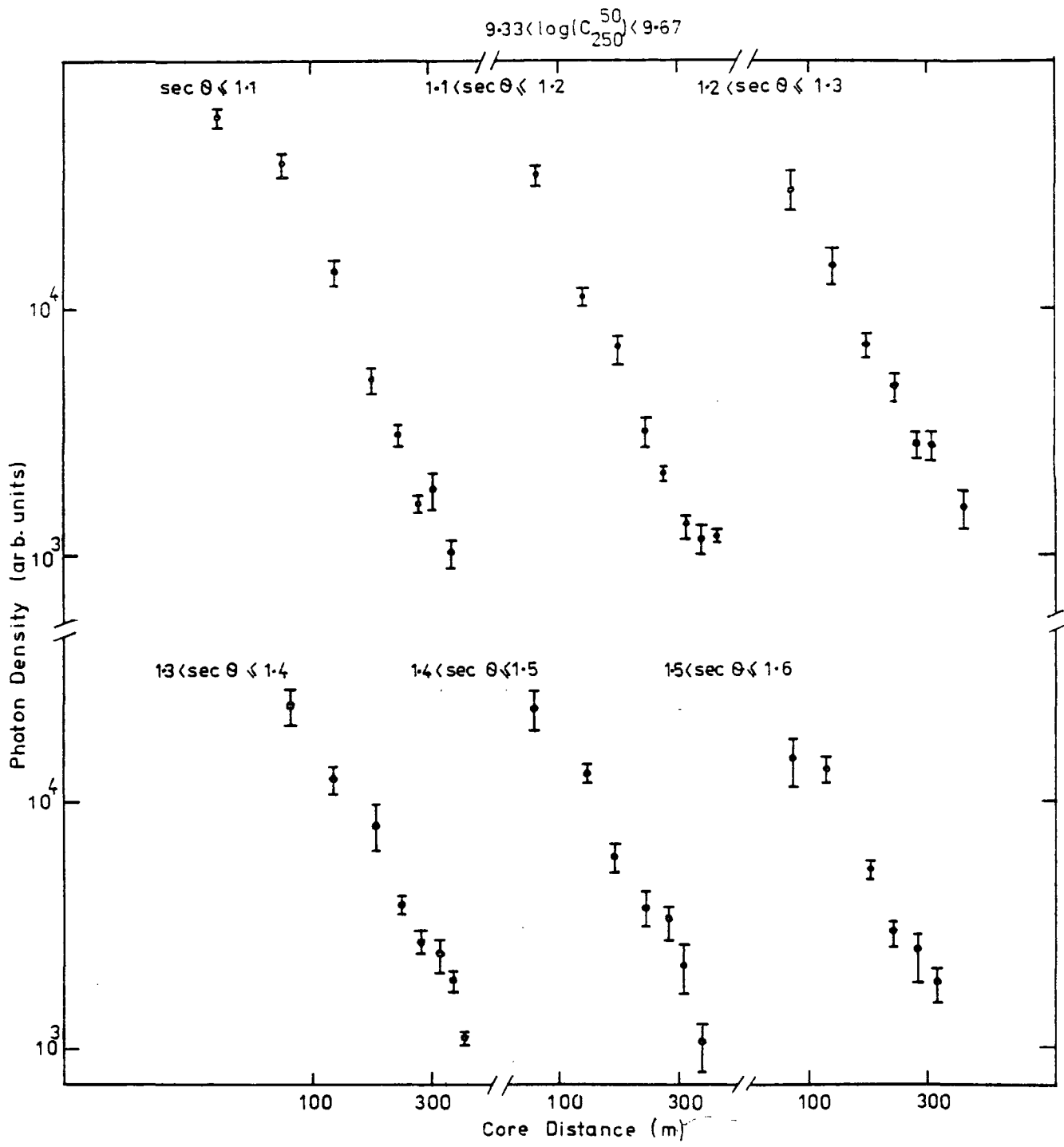
TABLE 5-2

The value of the exponent of the average lateral distribution

Primary Energy Estimator

	$8.67 < \log_{10} C_{50}^{250} \leqslant 9.0$	$9.0 < \log_{10} C_{50}^{250} \leqslant 9.33$	$9.33 < \log_{10} C_{50}^{250} \leqslant 9.67$
$\sec\theta \leqslant 1.1$	-2.65 ± 0.22	-2.19 ± 0.09	-2.92 ± 0.16
$1.1 < \sec\theta \leqslant 1.2$	-1.43 ± 0.22	-2.17 ± 0.12	-2.89 ± 0.14
$1.2 < \sec\theta \leqslant 1.3$	-1.69 ± 0.12	-1.73 ± 0.17	-2.37 ± 0.17
$1.3 < \sec\theta \leqslant 1.4$		-1.52 ± 0.22	-2.25 ± 0.18
$1.4 < \sec\theta \leqslant 1.5$	-2.09 ± 0.19	-1.72 ± 0.13	-2.28 ± 0.16
$1.5 < \sec\theta \leqslant 1.6$	-1.29 ± 0.18	-1.53 ± 0.14	-2.51 ± 0.23
	$2.5 \ 10^{16} < E_p \leqslant 5\times10^{16}$	$5\times10^{16} < E_p \leqslant 10^{17}$	$10^{17} < E_p \leqslant 2.5\times10^{17}$

Approximate Primary Energy (eV)

position of electron cascade maximum moving away from the obser-
vational plane. We find that on average we can, from a multiple

regression, represent Λ by:-

$$\Lambda = a_o + a_1 \ (\sec \ \theta - 1) + a_2 \ \log_{10} \ C_{50}^{250}$$

where $a_o = 9.4 \pm 3.5$

$a_1 = 3.2 \pm 1.0$

$a_2 = -1.3 \pm 0.4$

from these average lateral distributions.

In addition to the lateral distribution averaged over
all showers it was possible to fit a lateral distribution to
each shower. To reduce any possible effects from sampling
different showers over different core distance ranges, a further
data selection was made. In the subsequent analysis only
those showers with at least 3 recorded densities lying between
50 and 350m were used. Any effects from the changing shape
of the distribution over the range of measurements are thus
reduced.

The choice of the functional form of the lateral dis-
tribution was also extended by considering an alternative
lateral distribution of the following form:-

$$\phi(r) \propto \exp(\beta \ r) \qquad \text{Equation 5-1}$$

This was introduced to investigate the effects of using a
different function in determining the shape of the lateral
distribution. This particular function also has the advantage
that, unlike the function used in the preliminary analysis,
equation (4-1), it is integrable over its entire core distance
range for $\beta < \Box$. This allows for an estimate of the total
flux to be determined, so producing another possible primary
energy estimator, C_o^{∞} . It is beyond the scope of this work

to discuss the validity of using C_0^∞ as a stable primary energy estimator. It is more important here to show that a consistent value of C_{50}^{250} can be determined from 2 different forms of the lateral distribution function. Figure 5-10 shows a scatter plot of C_{50}^{250} deduced from the data set using an expontial lateral distribution against the value determined using a powerlaw fit. The relation between the two may be represented by:-

$$C_{50}^{250} \text{ (pow)} = 5\times10^6 (\pm 1.2 \times 10^7) + 0.957 (\pm 0.009) \, C_{50}^{250} \text{ (exp)}$$

$$\text{Equation 5.2}$$

We conclude that little difference in the value of C_{50}^{250} arises from the form of the assumed structure function used in the analysis. The comparable scatter-plot of $\phi(200m)$ derived from the use of the two structure functions is shown in figure 5-11. The derived relationship between the two values for $\phi(200m)$ was

$$\phi(200m) \text{ (pow)} = 219(\pm49) + 0.803(\pm0.012) \, \phi(200m) \text{ (exp)}$$

$$\text{Equation 5-3}$$

Clearly, C_{50}^{250} appears to be the quantity which is less dependent on the form of the structure function used in the analysis procedure. This may be a further reason for the preference of C_{50}^{250} as the primary energy estimator.

The densities in each of the showers within the sample were fitted using the two forms of structure function. The derived measures of shape, η and β, could be compared for showers of various zenith angle and primary energy. Figure 5-12 shows the variation of β with zenith angle and primary energy; figure 5-13 shows similar plots for the variable η. There seems little difference in the sensitivity to cascade development resulting from the choice of fitted function. Showers fitted with both functions showed the expected sensitivity to changes

FIGURE 5-10

The variation of C_{50}^{250} as determined by the two structure functions

functions

FIGURE 5-11

The variation of $\emptyset(200m)$ as determined by the two structure functions
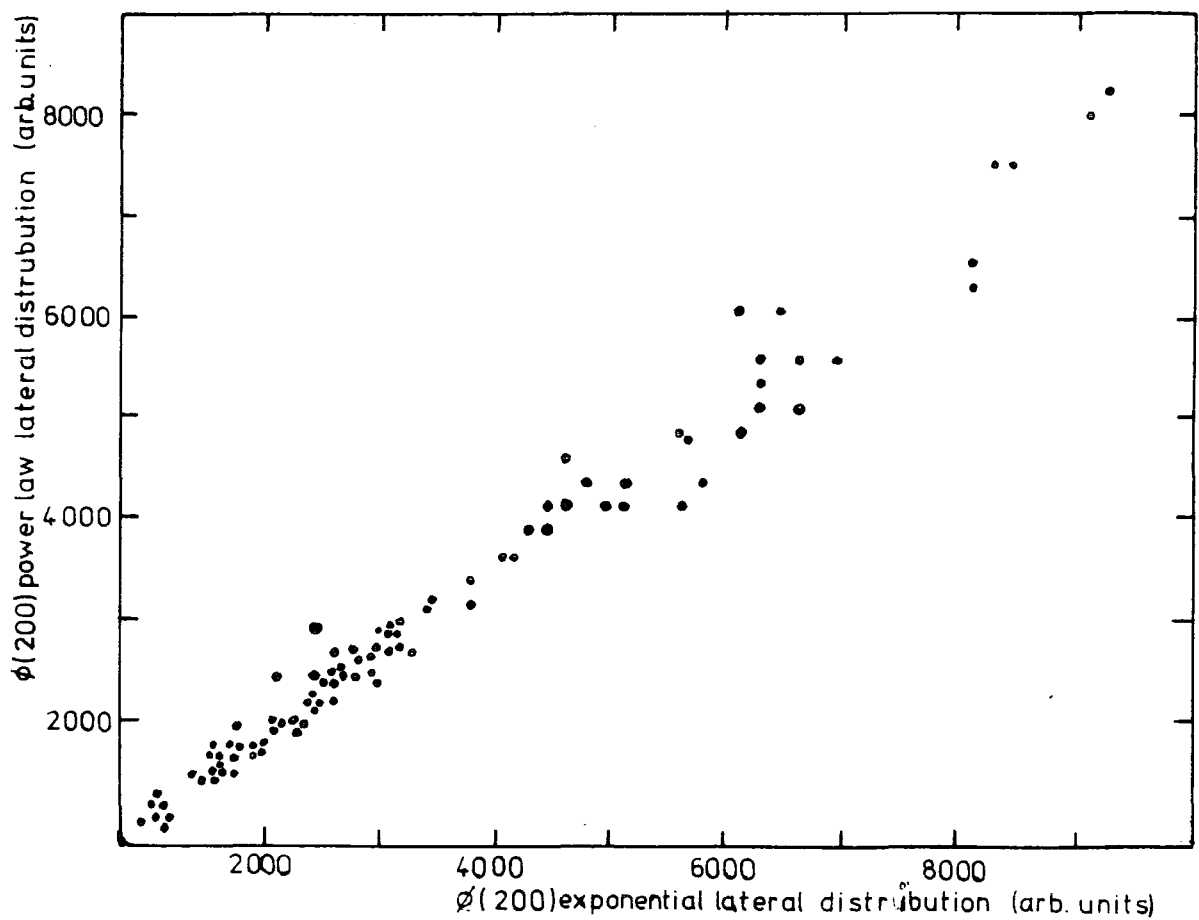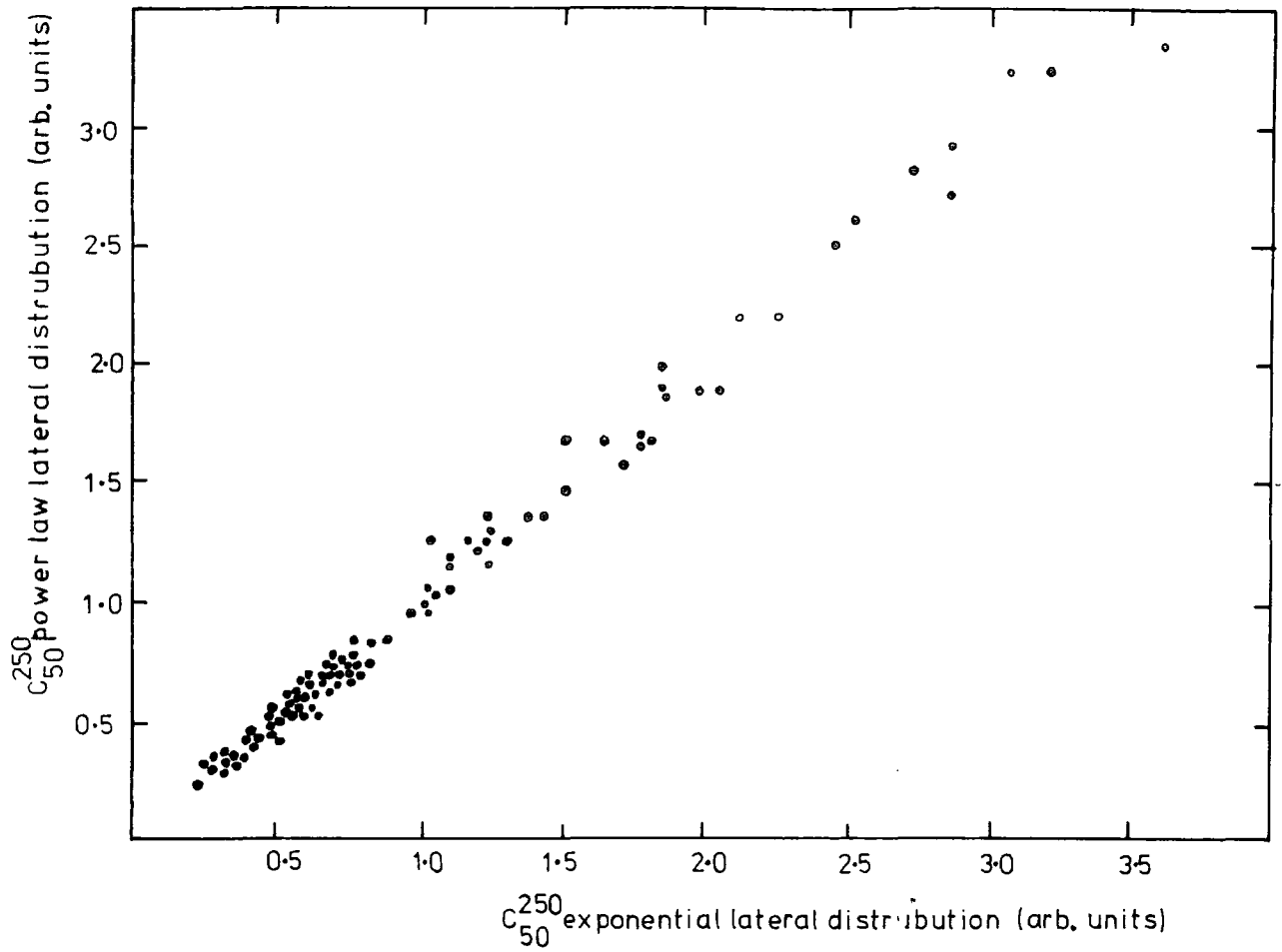
functions

FIGURE 5-12

The variation of the exponent of the exponential structure
function with zenith angle and primary energy

FIGURE 5-13

The variation of the exponent of the power law structure
function with zenith angle and primary energy

in depth of maximum inferred from changes in zenith angle and primary energy.

Finally, to quantify the sensitivity of each of these variables with zenith angle and primary energy, least squares multiple regressions were performed. In order to further minimise array selection biasing, only those larger showers with $C_{50}^{250} > 10^9$mVns (5×10^{16}eV) were considered. The following relationships were found.

$$\eta = 4.55(\pm 2.83) + 3.41(\pm 0.56) \ (\sec \theta -1) - 0.84(\pm 0.30) \ \log_{10}C_{50}^{250}$$

<div align="right">Equation 5-4</div>

$$\beta = 0.0134(\pm 0.0146) + 0.0160(\pm 0.0029) \ (\sec \theta -1) - 0.0031$$
$$(\pm 0.0015) \ \log_{10} \ C_{50}^{250} \qquad \text{Equation 5-5}$$

Both variables show significant sensitivities to zenith angle and primary energy; with the latter being the least sensitive. Such behaviour is observed in other recent EAS experiments (e.g. the Haverah Park in filling experiment, (Craig et al (1979)).

Extreme caution should be exercised in interpreting these changes of variable with primary energy and zenith angle as indicative of the elongation rate of EAS. This is so because:-

(1) It is not yet proven that the detailed changes of variable with zenith angle and primary energy are similar in origin.

(2) The elongation rate determined from this experiment may not be directly comparable with those derived from other types of experiment (see Linsley (1977) and Gaisser et al (1979)).

(3) We have reason to believe that the array triggering biases on this experiment are strong and this

Exponent of Structure Function

Exponential

0·015

0·010

9·33 < log(C_{250}^{50}) < 9·67
9·0 < log(C_{250}^{50}) < 9·33
8·67 < log(C_{250}^{50}) < 9·0

1·1   1·3   1·5

Secant Zenith Angle

Power Law

−3·5

−3·0

−2·5

−2·0

−1·5

9·33 < log(C_{250}^{50}) < 9·67
9·0 < log(C_{250}^{50}) < 9·33
8·67 < log(C_{250}^{50}) < 9·0

1·1   1·3   1·5

Secant Zenith Angle
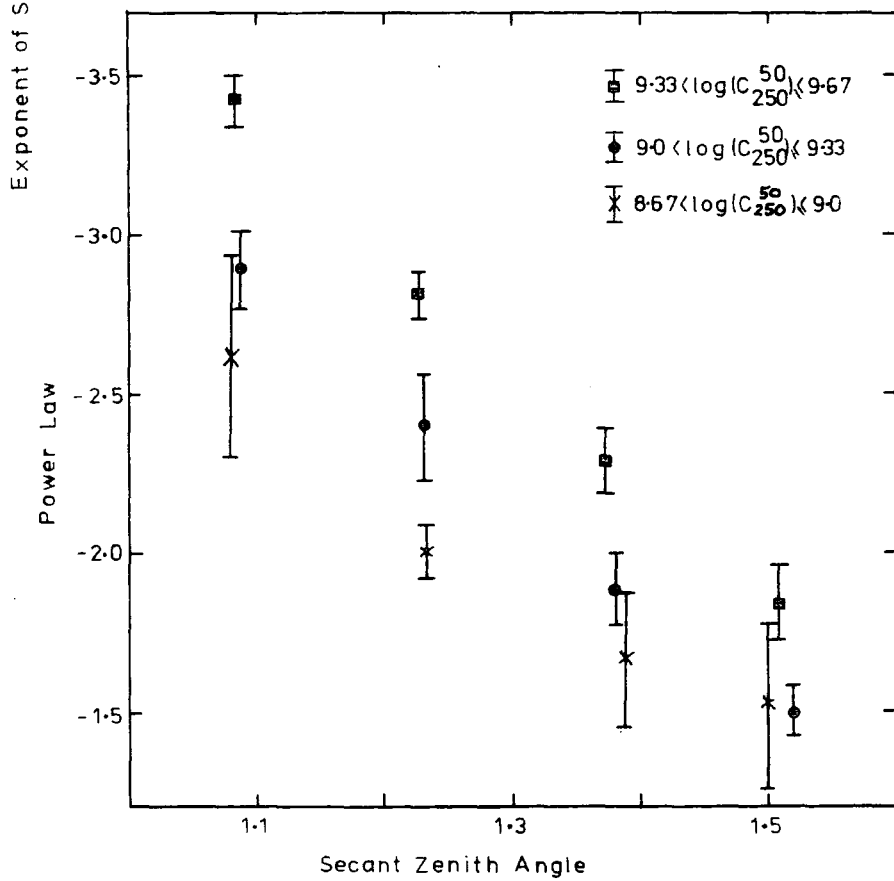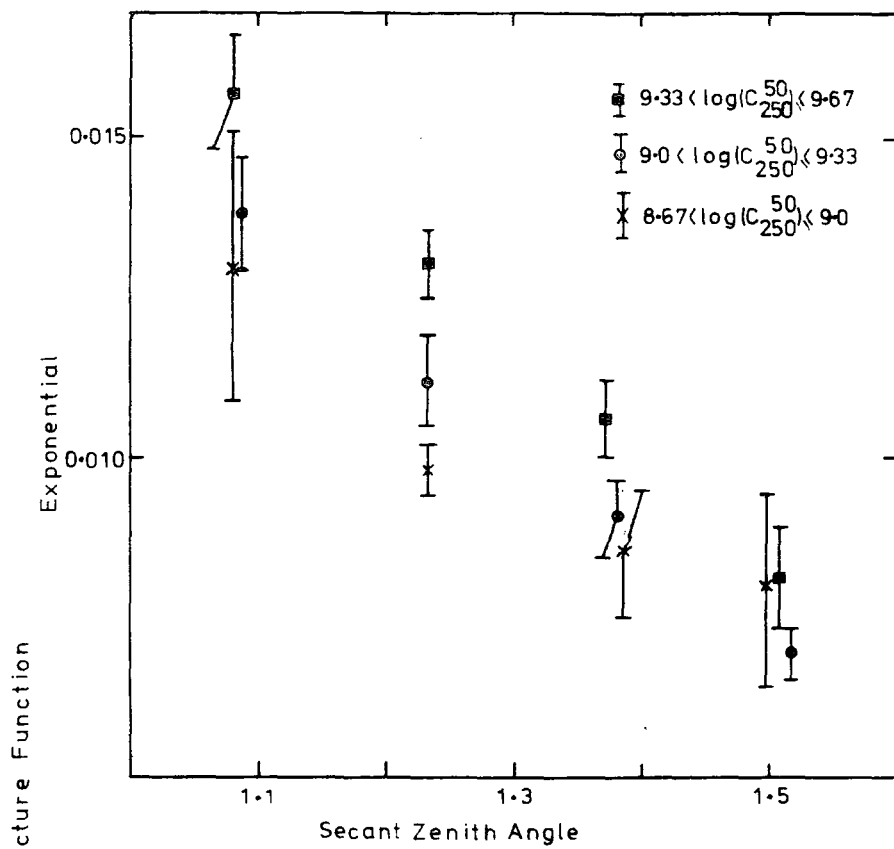
preliminary data set may well still contain the effect

of residual biases.

5-5   The Cerenkov Pulse Shape

In this preliminary analysis only the FWHM of the pulse

will be considered as a measure of the Cerenkov pulse shape.

This will provide consistency with observations made at other

arrays throughout the world; the details of the shape of the

rising and falling edges of the pulse will be considered

later.   It is here assumed that the FWHM had the following

variation with core distance:-

$$FWHM \ (r) = a + br^2 \qquad\qquad Equation\ 5\text{-}6$$

The justification for this is given in the work of Orford and

Turver (1976). These authors, as was discussed in

Chapter 2, showed that the fronts defined by the various

percentage levels through a Cerenkov pulse were closely

spherical.   It would be expected that the difference between

the two levels, e.g. the FWHM, would manifest an approximate

r^2 dependency; this was observed by Hammond et al (1978).

Figure 5-14 shows the average lateral distribution of the

FWHM for showers in a narrow band of primary energy

$(9.33 \langle \log_{10} C_{50}^{250} \langle 9.67)$, recorded at various zenith angles.

Table 5-3 shows the FWHM at 300m from the axis of the showers

deduced from each of the average lateral distributions.

The data were adequately represented by an r^2 dependency and

showed the expected narrowing of the pulses with increasing

zenith angle as the depth of cascade maximum receded further

away from the observation plane.

Figure 5-15 shows the variation of the FWHM (300m) with

zenith angle and primary energy for the complete data set

FIGURE 5-14

The variation of FWHM with core distance for showers incident

at different zenith angles and of energy $9.33 < \log C_{50}^{250} < 9.67$

Shown are the fits to FWHM=$a + br^2$.
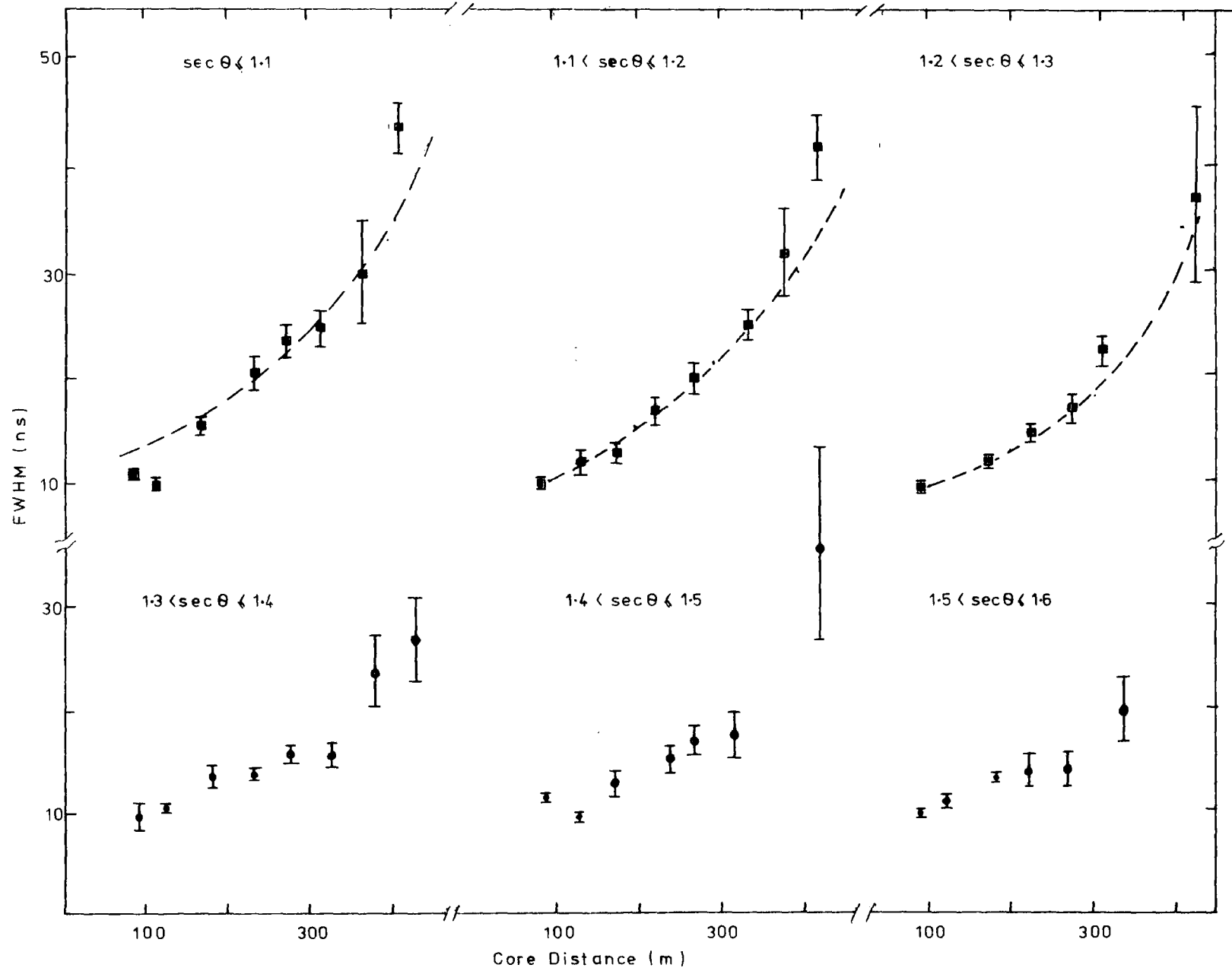
TABLE 5-3

The Average values of FWHM(300m) for showers of various primary
energies at different zenith angle

Primary Energy Estimator

	$8.67 < \log_{10} c_{50}^{250} \leqslant 9.0$	$9.0 \leqslant \log_{10} c_{50}^{250} \leqslant 9.33$	$9.33 < \log_{10} c_{50}^{250} \leqslant 9.67$
$\sec\theta \leqslant 1.1$	23.0 ± 1.3	24.4 ± 2.2	25.4 ± 2.0
$1.1 < \sec\theta \leqslant 1.2$	17.5 ± 1.5	22.2 ± 0.6	21.0 ± 2.9
$1.2 < \sec\theta \leqslant 1.3$	18.0 ± 1.3	19.8 ± 1.4	19.7 ± 2.6
$1.3 < \sec\theta \leqslant 1.4$		15.3 ± 1.3	17.1 ± 2.5
$1.4 < \sec\theta \leqslant 1.5$	16.6 ± 2.3	16.1 ± 1.1	16.1 ± 1.7
$1.5 < \sec\theta \leqslant 1.6$	14.7 ± 1.1	18.8 ± 3.2	17.1 ± 0.9

FIGURE 5-15

The variation of FWHM (300m) with zenith angle and primary energy
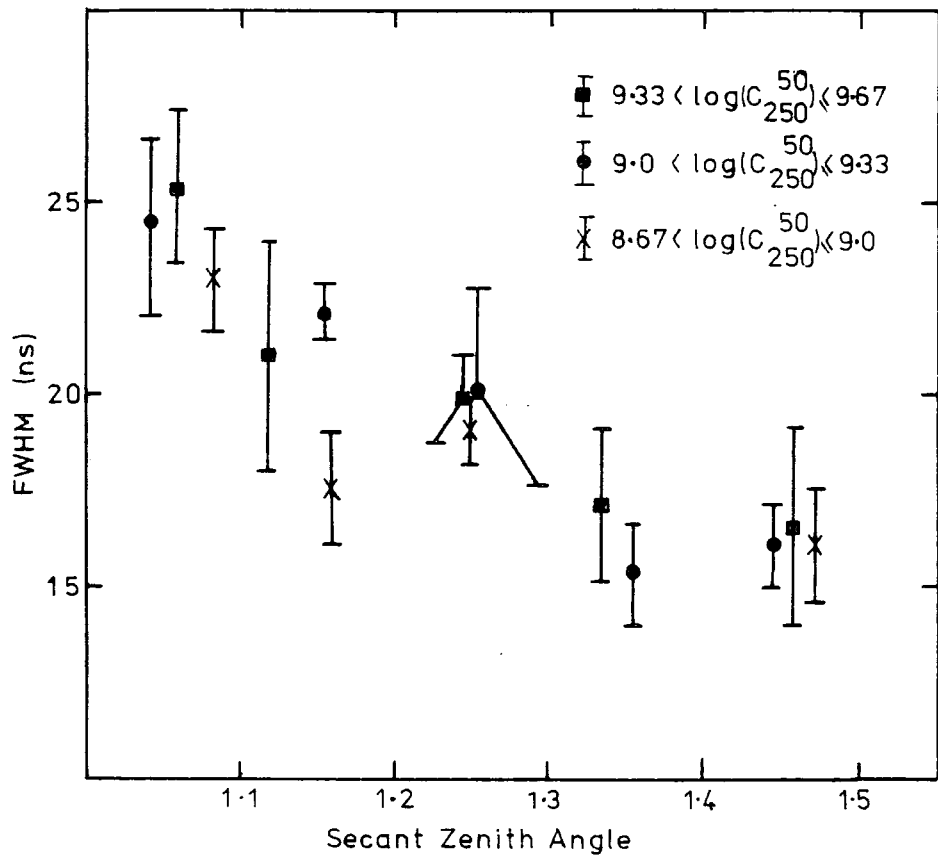
(spanning a greater primary energy range than used in figure 5-14). The zenith angle dependence of FWHM (300m) is clear from these data and the less significant sensitivity to primary energy is noted. A multiple regression of FWHM (300m) against $\sec\theta - 1$ and $\log_{10}C_{50}^{250}$ for this sample gave the following relationship.

$$FWHM(300m) = -10(\pm 24) - 27.2(\pm 5.3) (\sec\theta - 1) + 3.9(\pm 2.6) \log C_{50}^{250}$$

This regression quantifies the trends shown in figure 5-15. It should be noted that this preliminary data set might contain certain residual biases (as was suggested at the end of section 5-4); the existence of such a bias would have the effect of narrowing the mean recorded pulses. This narrowing may be evident in the data of figure 5-15 and will be discussed later.

5-6   The Peak Height of the Cerenkov Pulse

During the derivation of the shape of the Cerenkov pulses, the peak height of each pulse was determined. This quantity provides an alternative measure of Cerenkov pulse shape. In common with conventional analyses, the pulse height of a pulse is affected by the system bandwidth. In the simplest representation, the area of a pulse is the product of pulse height and the FWHM. Thus a study of any 2 of the 3 quantities, area, height and FWHM represent a complete investigation. It has been customary to study area and FWHM; the equipment at Dugway was appropriate for a measurement of pulse height and an alternative approach may be found to be worthwhile. It would be expected that the peak height will be directly proportional to the light density at small core distances, where all pulses are limited by the system response,

and to relate more to the shape of the pulse at larger core distances. Figure 5-16 shows the average lateral distributions of the peak height of showers of fixed primary energy incident at various zenith angles. To parameterise these distributions a relation of the form:-

$$\text{Peak Height } (r) \propto (r + ro)^{\delta} \qquad \text{Equation 5-8}$$

was fitted to the observed distributions. It is expected that the functional form of the peak height lateral distribution may be changed after a more detailed analysis of the complete Dugway data set. Table 5-4 shows the derived values of δ from the lateral distributions averaged over all showers in the preliminary data set. Figure 5-17 shows the variations of the mean values of δ with zenith angle and primary energy. It can be seen that the lateral distributions are, as expected, broader for more inclined showers and for those showers of lower primary energy. The height of the Cerenkov signal therefore represents a further measure of cascade development which is substantially independent of the pulse area measurement.

5-7   The Radius of Curvature of the Cerenkov Light Front

Measurement of the pulse shapes provided information on the time of arrival at the peak height for each detector. These times were found to be well represented by a spherical front. The position of the centre of curvature of this front should, according to the work of Orford & Turver (1976), indicate the position of Cerenkov light maximum in the atmosphere. Andam et al (1979) have derived the depth of cascade maximum for near vertical showers observed with the Dugway array to be 609 ± 45 gcm^{2}. This compares favourably with

FIGURE 5-16

The average lateral distributions of peak height

for showers of energy $9.33 < \log C_{50}^{250} < 9.67$ at

incident at various zenith angles.

Figure showing Peak Height (arb. units) versus Core Distance (m) for various ranges of sec θ.

Labels on plot:
- $\sec\theta \leqslant 1\cdot1$
- $1\cdot1 < \sec\theta \leqslant 1\cdot2$
- $1\cdot2 < \sec\theta \leqslant 1\cdot3$
- $1\cdot3 < \sec\theta \leqslant 1\cdot4$
- $1\cdot4 < \sec\theta \leqslant 1\cdot5$

Y-axis: Peak Height (arb. units), with values 10^3, 10^2, 10^3, 10^2

X-axis: Core Distance (m), with values 100, 200, 500, 100, 200, 500, 100, 200, 500
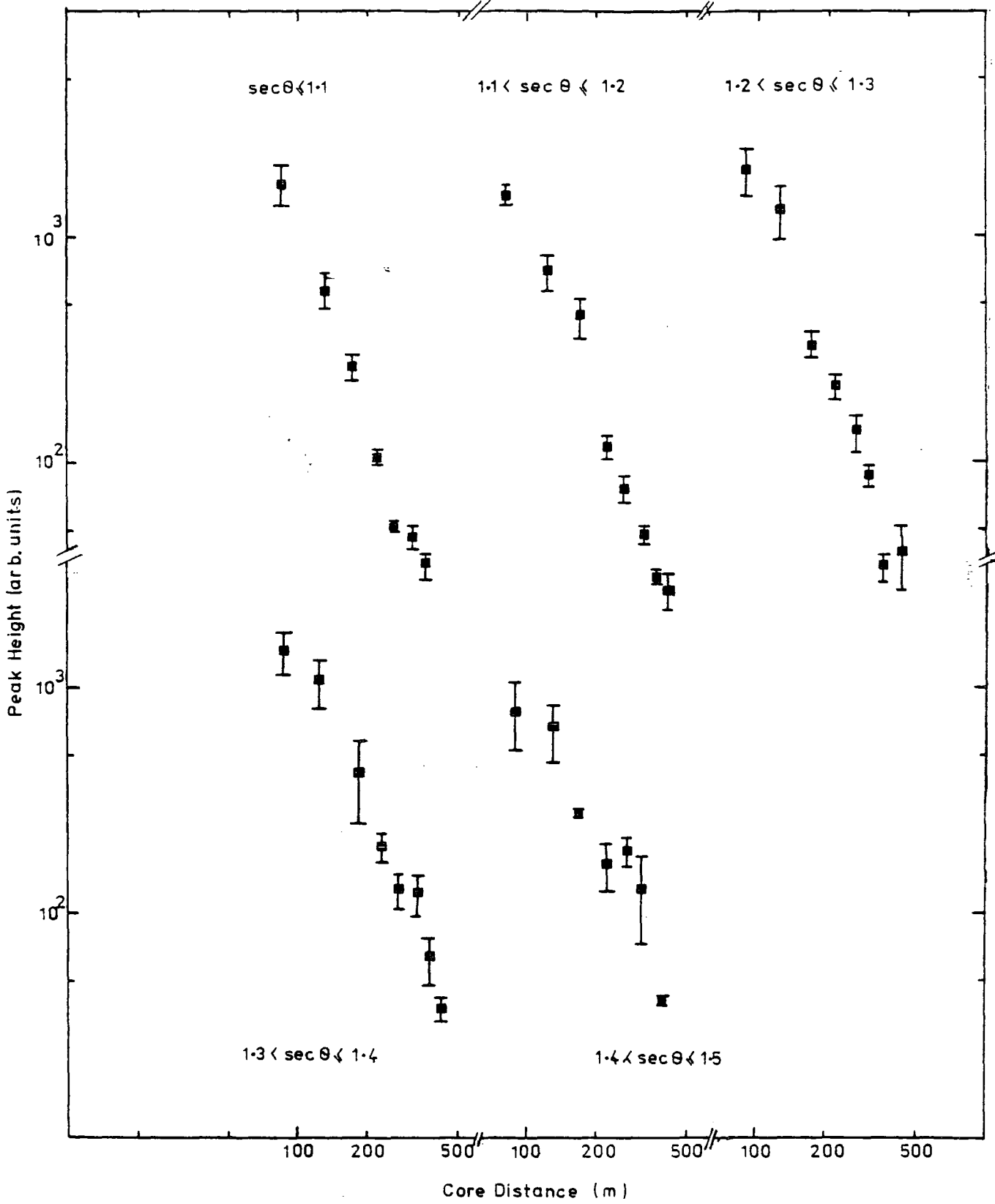
TABLE 5-4

Peak Height structure function exponent for showers
recorded at different zenith angle and primary energy

	$8.67 < \log_{10} c_{50}^{250} \leqslant 9.0$	$9.0 < \log_{10} c_{50}^{250} \leqslant 9.33$	$9.33 < \log_{10} c_{50}^{250} \leqslant 9.67$
$\sec\theta \leqslant 1.1$	-3.45 ± 0.10	-2.74 ± 0.15	-3.93 ± 0.11
$1.1 < \sec\theta \leqslant 1.2$	-2.29 ± 0.12	-2.93 ± 0.09	-3.81 ± 0.12
$1.2 < \sec\theta \leqslant 1.3$	-2.08 ± 0.17	-2.63 ± 0.19	-3.57 ± 0.17
$1.3 < \sec\theta \leqslant 1.4$		-2.67 ± 0.19	-2.96 ± 0.24
$1.4 < \sec\theta \leqslant 1.5$	-2.17 ± 0.21	-1.98 ± 0.25	-3.17 ± 0.32
$1.5 < \sec\theta \leqslant 1.6$	-1.75 ± 0.13	-1.40 ± 0.28	

FIGURE 5-17

The variation of the exponent of the peak height
structure function with zenith angle and primary
energy.
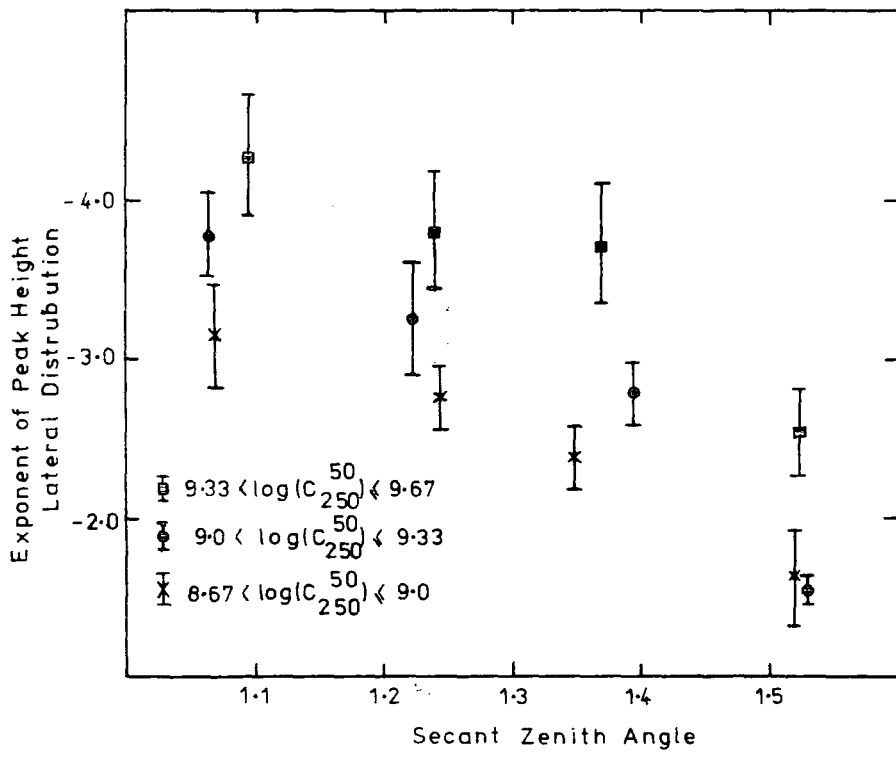
the value of 607 ± 19 gcm^2 obtained at Haverah Park for near

vertical showers. The detailed analysis of the synchronised

time information of the detectors, one of the major topics of

the analysis programme, is still continuing and will be

reported by Chantler (Ph.D thesis, in preparation).

5-8   Average Shower Characteristics - Conclusions

The results described in the previous sections showed

that the following measured quantities were sensitive to

changes in cascade development which may be induced by

studying showers incident at different zenith angles:-

(1)   The exponents of the lateral distribution of

pulse area; η , when represented by a power law and β

when represented by an exponential function.

(2)   The exponent, δ , of the lateral distribution of peak

height.

and (3)   The FWHM at 300m from the axis of the showers.

Furthermore, although comparisons were made over a range of

only ½ decade in primary energy, these quantities were also found

to be sensitive to changes in primary energy. Further discussion

of these results will be given in the next chapter.

CHAPTER SIX

Comparison With Computer Simulations and Other Work

6-1   Introduction

In this chapter comparisons will be made with the average characteristics of EAS as observed with the experiment at Dugway, and the results from other experiments. First a comparison will be made between these results and those obtained in 1973-1976 by the Durham Group at Haverah Park. The fundamental difference between the two experiments - the different bandwidth used in the recording systems and the different mean vertical atmospheric depths posed problems in the comparison. This comparison will involve using a single set of computer simulations for an average cascade development which predicted the expected response for the two experiments. Further, using these simulations, the expected changes in shower parameters resulting from observing showers at two different vertical depths into the atmosphere will be explored. The effect of these considerations on the elongation rate theorem will be discussed. Finally, the average characteristics from the Dugway experiment will be compared to the results from the work of the Yakutsk and Adelaide groups.

6-2   The Comparison between the Results Obtained at Haverah
       Park and Dugway

6-2-1 Introduction

The average response of the Dugway and Haverah Park experiments to EAS resulting from primaries of various masses and energies have been calculated. These simulations, based

upon the Feynman hypothesis of scaling, took into account the
bandwidth of the detectors and have been described by Protheroe
(1977). By investigating how the two arrays responded to the
light produced by the same electromagnetic cascade it was possible
to compare the experimental results from the two arrays.

The difference in the bandwidths of the two systems can
be seen by comparing the response of the two systems to the same
radio-active light pulser. The FWHM of the light pulse, from
a NE130 pulser, after it had passed through the two systems was
19ns for Haverah Park and 6.7ns for Dugway. At Haverah Park
observations were made in the range of core distances 100-
500m, whilst the comparable figures for Dugway were 50-350m.
In addition the functional form of the lateral distribution had
evolved during the time between the two experiments. This
difference in the form of the structure function between the two
experiments arose from a better understanding of the lateral
distribution of Cerenkov radiation. The forms of function
used were:-

(1) $\emptyset(r) \propto r^{\gamma}$ at Haverah Park

and (2) $\emptyset(r) \propto (r + r_o)^{\eta}$ at Dugway

By linking the results of the two experiments via simulations
it was possible to allow for these differences.

6-2-2 The Lateral Distribution of Pulse Area

Both at Haverah Park and at Dugway the exponents γ and η
of the structure function were found to be sensitive to changes
in zenith angle. To make the comparison it was necessary to
determine, via simulations, the relationship between the
exponent of the two different functions. It was found, from
simulations that the relation between η and γ could be well

represented by:-

$$\eta = 1.38 \, \gamma - 0.13$$

Using this equation, the variation of γ with zenith angle,

reported by Hammond et al (1978) could be compared to the

variation of η with zenith angle reported in this work.

Figure 6-1 shows the variation of η and of γ from the

measurements of showers incident at various zenith angles and

thus under different atmospheric thicknesses. The two

measurements are shown to be in substantial agreement, although

the exponents from the Dugway experiment appear to be system-

atically lower by about 0.1. This shift could be due to a small

difference in the energies of the two sets of showers or could

represent a fundamental change due to making observations

150 gcm^{-2} higher into the atmosphere. The results from

simulations for the variation of η due to changes in primary

energy (and hence depth of maximum) and due to changes in

observation depth will be discussed in the next section.

Figure 6-2 compares the lateral distribution of the light

in vertical showers at Haverah Park and Dugway. The mean

energies of the showers were $\rho(500)ve = 0.42m^{-2}$ at Haverah

Park and $c_{50}^{250} = 2 \times 10^9$ mVns at Dugway. The photon densities

were determined by using the same calibration technique for

both experiments (the use of a radioactive light pulser as

described in section 4-3-2). It is expected that showers having

$\rho(500)ve = 0.42m^{-2}$ would have $c_{50}^{250} = 1.0 \times 10^9$ mVns. Also

shown in the figure are the expectations from simulations

based upon a Landau type model for a primary iron nucleus of

energy $10^{17}ev$, and having a depth of maximum of $585gcm^{-2}$.

Firstly, from this figure it can be seen that the shapes

FIGURE 6-1

The variation of the structure function exponent
with atmospheric thickness as measured at Dugway
and at Haverah Park from Hammond et al (1978).

Figure showing Structure Function Exponent versus Atmospheric Thickness (g cm^{-2}).

Legend:
Haverah Park
—— $\rho(500)_{ve} = 0.67\,m^{-2}$
Dugway
$9.3 < \log(C_{250}^{50}) < 9.67$
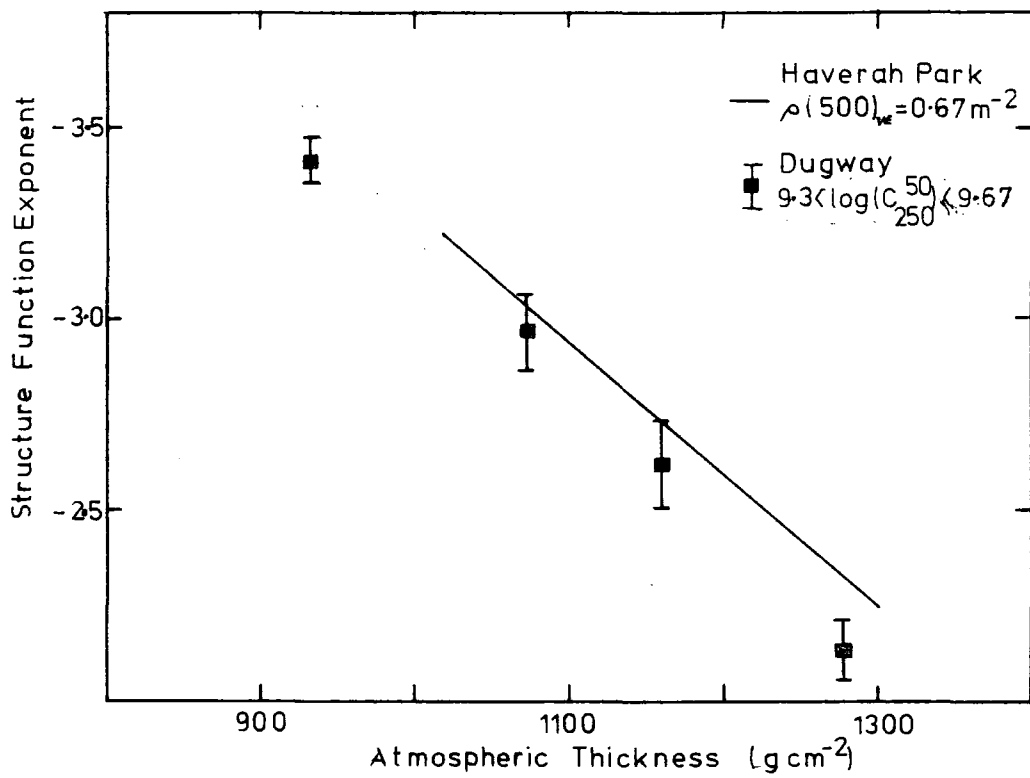
FIGURE 6-2

The average lateral distribution of pulse area as
measured by the Dugway experiment and at Haverah Park.
Also shown are the results of simulations based upon
a Landau type model and having a depth of cascade
maximum of 585g cm^{-2} , the observation depth of the
simulation was 862 g cm^2.

Figure showing Photon Density (m^{-2}) versus Core Distance (m).

Legend:

Dugway, $\theta < 25°$

$C^{50}_{250} = 3 \times 10^{9}$ mV ns

$C^{50}_{250} = 0.7 \times 10^{9}$ mV ns

Haverah Park $\theta < 25°$

$\rho(500)_{vs} = 0.42\,m^{-2}$

— Simulation A=56 $E_p = 10^{17}$ eV
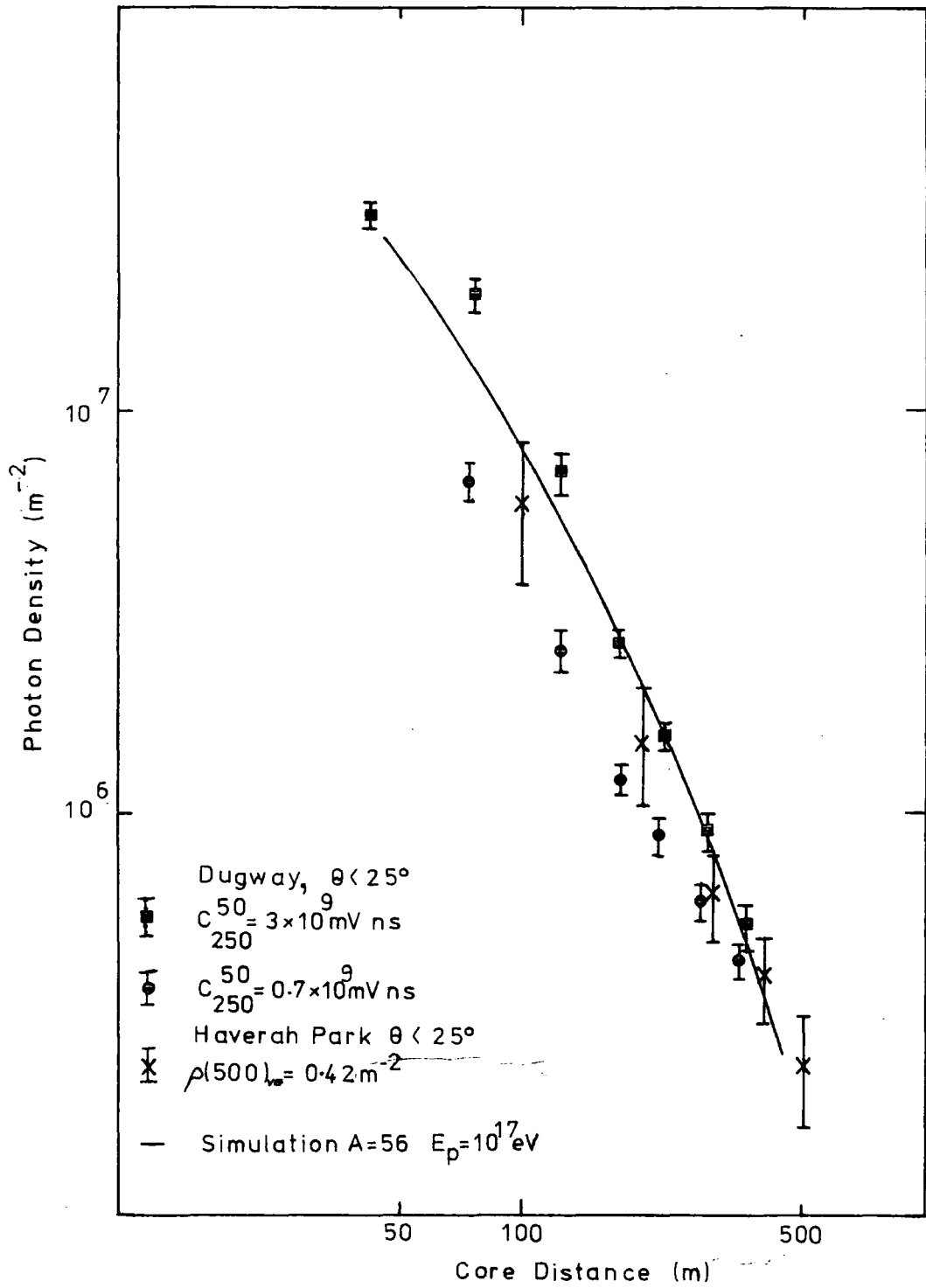
of the distribution are broadly similar at Dugway and Haverah

Park, with the showers recorded at Dugway having slightly steeper

lateral distributions. The error bars (indicating the standard

error in all instances) show that the preliminary Dugway data

set is of sufficient size to produce a more precise estimate

of the average lateral distribution, than was obtainable at

Haverah Park.

6-2-3   The FWHM of the Cerenkov Pulse

Comparison between the pulse shapes measured by the two

experiments was further complicated by the different bandwidth

of the two systems. In order to reduce ambiguities resulting

from removing the effect of the system bandwidth from the

observed pulses from each experiment, comparison will be made

without any attempt at deconvolution. The comparison will be

effected via computer simulations where the bandwidths of the

two systems have been included in the calculation. Figure 6-3

shows the variation of FWHM with atmospheric thickness for

showers of energy $9.0 < \log_{10} c_{50}^{250} < 9.33$ at Dugway and

$\rho(500)ve = 0.42m^{-2}$ at Haverah Park. The results of a simu-

lation for an average iron nucleus initiated shower of primary

energy $10^{17}eV$, with a depth of maximum at $690g\ cm^{-2}$ are

shown for the two experiments. The FWHM measured at Dugway

appears to be less than the results of calculations based upon

the Feynman scaling hypothesis; reasonable agreement can be

obtained with a Landau type model. The change of FWHM (300m)

with atmospheric thickness appears to be consistent throughout

both experiments at approximately $4ns/100g\ cm^{-2}$. This figure is

similar to that derived by Andam et al (1979), since when the

precision of the pulse shape determination has improved and

FIGURE 6-3

The variation of FWHM(300m) with atmospheric thick-
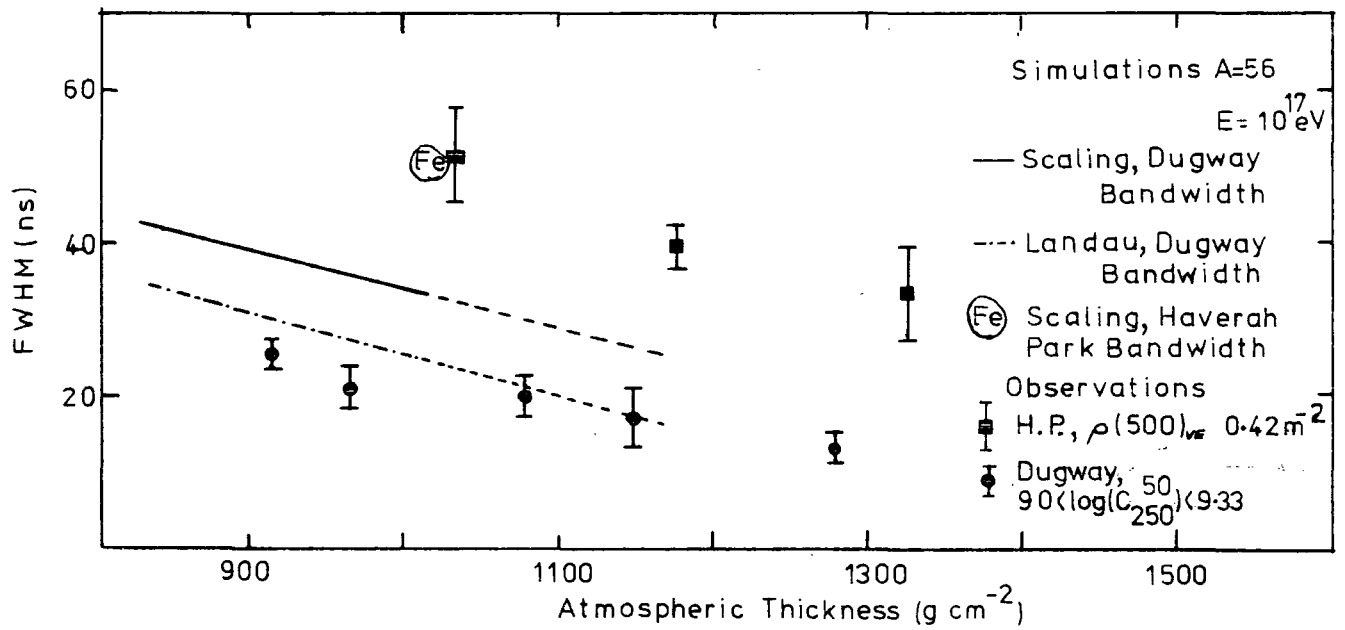ness as measured at Dugway and Haverah Park; also in-
dicated are the results of simulations based upon the
scaling model and a Landau type model.

Simulations A=56
$E = 10^{17} eV$

—— Scaling, Dugway
           Bandwidth

—·· Landau, Dugway
           Bandwidth

(Fe) Scaling, Haverah
       Park Bandwidth

Observations

H.P., $\rho(500)_{VE}$ 0.42 m^{-2}

Dugway, $9.0 < \log(C_{250}^{50}) < 9.33$

the data sample enlarged. The main conclusions of that work are in agreement with this figure, in particular the trend away from the scaling model for inclined showers noted by Andam et al is quantified by the more precise estimate of this work.

The fact that the result is explicable if the Landau type model for the pion-momentum distribution is employed is of great interest. The model predicts a depth of cascade maximum higher than those inferred from cascades based upon the scaling model, having the depth of maximum in this example of 585g cm^{-2}.

Figure 6-4 shows the measured variation of FWHM with core distance for showers incident at zenith angles $<$ 25° at Dugway. The predictions from a Landau type model for two mean vertical observation depths, 862g cm^{-2} and 1016g cm^{-2}, are also indicated on the figure. The expectations from simulations based upon the Landau type model are consistent with these measurements when the mean atmospheric thickness of about 935g cm^{-2} appropriate to the observed sample is considered.

The array triggering bias mentioned previously (cf section 5-4) would have the effect of producing a mean FWHM (300m) lower than expected. From an initial study of simulation results this bias could cause the mean observed FWHM (300m) to be lowered by about 5ns.

6-2-4   <u>The Peak Height of the Cerenkov Light Pulses</u>

The peak heights of the Cerenkov pulses in showers have been demonstrated to be sensitive to changes in the zenith angle of arrival of the showers. Figure 6-5 shows the variation of δ , the exponent of the peak height lateral distribution, with atmospheric thickness. The variation of the quantity according to computer simulations is also shown.

FIGURE 6-4

The lateral distribution of FWHM measured at Dugway

for showers of size 9.33 $\langle$ log $C_{50}^{250} \langle$ 9.67, showing

a comparison between these results and those from

simulations based upon a Landau type model at two
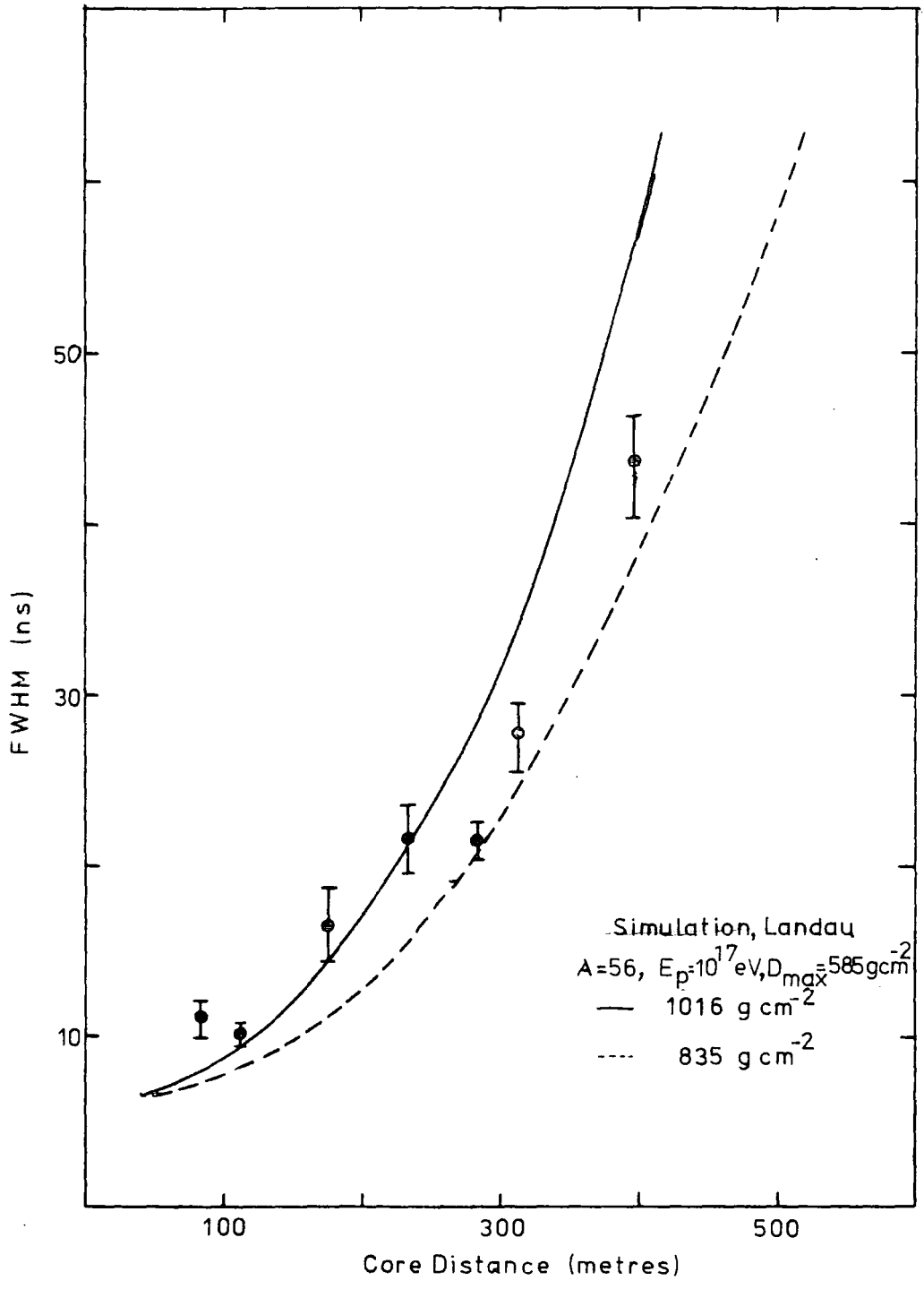
observation depths.

FIGURE 6-5

The variation of the exponent, δ , of the peak height lateral distribution with atmospheric thickness; also showing are the results of simulations based upon the scaling model and a Landau type model.
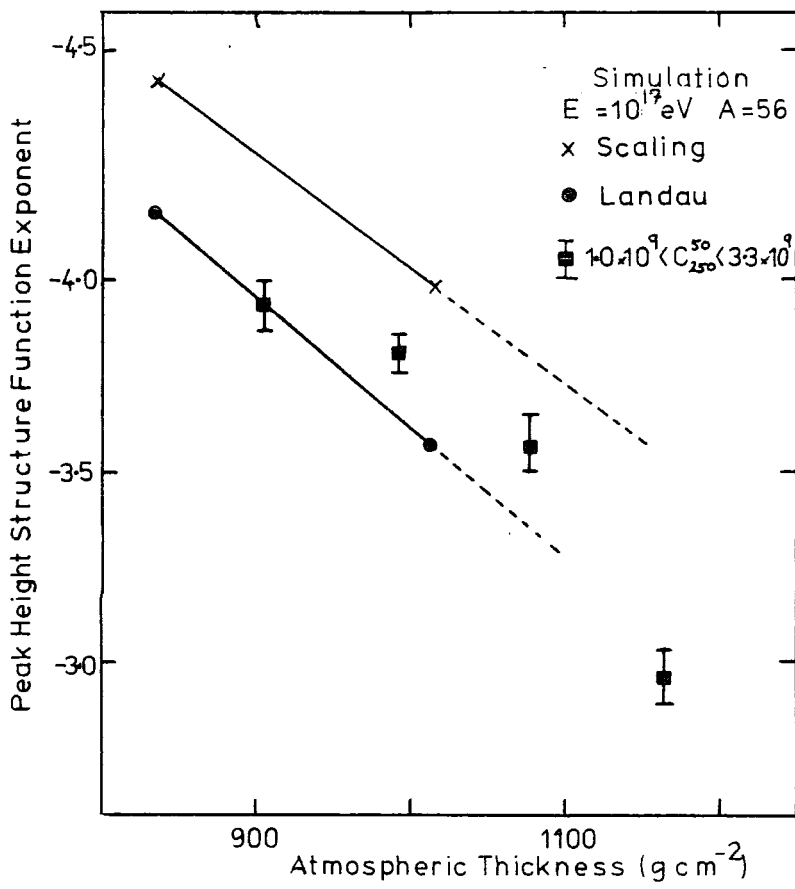
Figure 6-6 shows the peak height lateral distribution at Dugway

for vertical showers of two energies and the predicted lateral

distributions from simulations. These figures indicate that the

lateral distribution for peak height is, at this early stage in

the analysis, also in substantial agreement with simulations

based upon a Landau type model which gives a depth of cascade

maximum of 585g cm^{-2}. No comparable data were available from

the Haverah Park experiment.

6-3   The Elongation Rate Derived from Cerenkov Radiation

The variation of the structure function exponent with

zenith angle and primary energy allows for the elongation rate

to be determined, see Linsley (1977). At Haverah Park, on

the basis of all aspects of the Cerenkov light measurements,

this was determined to be 85$\pm$37g cm^{-2}. At Dugway, although

the present work is preliminary and the sensitivity to primary

energy has not been fully established, the elongation rate from

this work was 212$\pm$41g cm^{-2}. (As will be shown below this number

can be reduced by about 60% to indicate an elongation rate

of 136$\pm$26g cm^{-2}). The latter value is high when considering

conventional shower models and it is confidently expected that

after allowance is made for array triggering biases, this value

will be reduced.

The elongation rate theorem has been described by Linsley

(1977) and discussed by Linsley (1979) and Gaisser et al (1978),

(1979). Essentially the elongation rate (the change in depth

of cascade maximum with primary energy) can be determined

experimentally if a parameter, P, can be considered to vary

independently and in a similar manner with changes in depth of

cascade maximum due to differences in primary energy and to

FIGURE 6-6

The average lateral distribution of peak height for
showers of energy $9.33 < \log C_{50}^{250} \leqslant 9.67$ also shown are
the results of simulations based on a Landau type model,
the vertical scale refers to the simulation, the Z
data sets were normalised at 200m.

Figure axes: Core Distance (m) on horizontal axis (100, 200, 500); Peak Height (photons $m^{-2} ns^{-1}$) on vertical axis (10^5, 10^4).

Legend:
— Simulation $E_p = 10^{17}$ eV Landau model $A = 56$

■ This work $9.33 < \log(C_{250}^{50}) < 9.67$
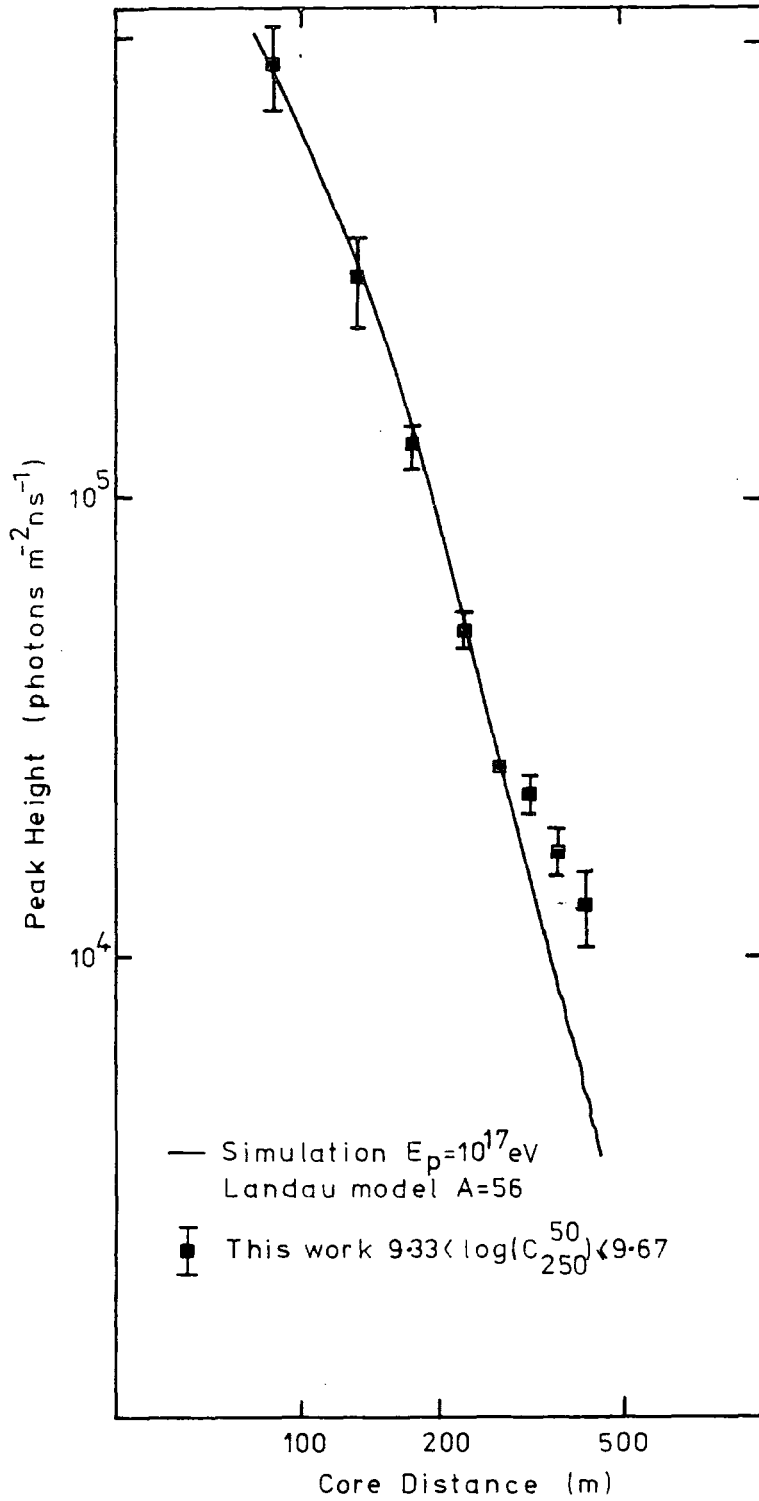
changes in the depth of the observation level. A further

requirement is that the depth of the observation level

increases with the secant of the zenith angle, and that

showers develop in a similar manner regardless of the zenith

angle depending only on the thickness of the atmosphere. The

elongation rate can be deduced from measurements of the parameter

P, as follows:-

$$\Delta P = \frac{\partial P}{\partial \log E_O}\bigg|_T \Delta \log E_O + \frac{\partial P}{\partial T}\bigg|_{E_O} \Delta T = 0$$

where E_O was the primary energy and T the observation depth.

Linsley in his original description considered parameters which

fell into two distinct categories:

(1)   where $\Delta T = \sim \Delta \ T_{max}$

and (2)   where $\Delta T = \frac{-T}{T_{max}} \times \Delta \ T_{max}$

where Tmax was the depth of the electron cascade maximum.

The elongation rate can then be defined as:-

(1) $\dfrac{\partial P/ \ \partial \log E_O\big|_T}{\partial P/ \ \partial \ T \ \big|_{E_o}} \equiv ER(1)$

and (2)   ER(1) x Tmax/T $\equiv$ ER(2)

Essentially penetrating components of EAS, e.g. Cerenkov

radiation, are considered to be described by case 1, and non-

penetrating components, e.g. the electron component, by case 2.

Using the results of recent detailed computer simulations for

the distribution of Cerenkov radiation at two different depths

into the atmosphere, 835g cm^{-2} and 1016g cm^{-2}, it is possible to

test the validity of the assumptions necessary to deduce the

elongation rate.

Figure 6-7 shows the variations from simulations of η ,

the exponent of the lateral distribution expected at the two

FIGURE 6-7

The predicted variation structure function exponent with T-Tmax at two different observation depths from average simulations of primaries of energy 10^{15}-10^{18}eV and mass 1 and 56.
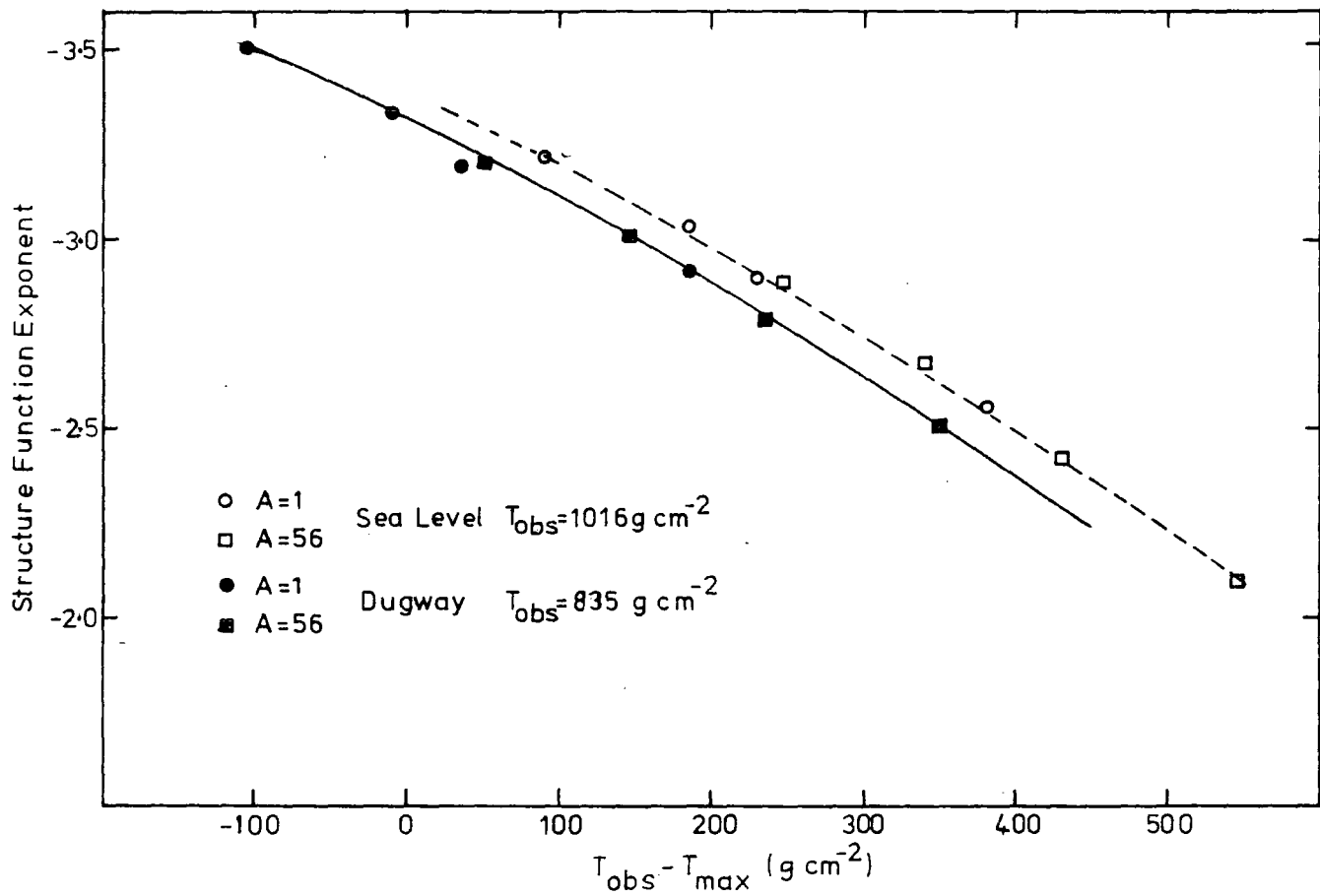
observation depths, with the amount of atmosphere between the

observation level and cascade maximum, T-Tmax. It can be seen

that η is predicted to be systematically smaller at the higher

observation level by about 0.1. These simulation results thus

cast doubt on the elongation theorem for a category (1) parameter

for which changes in depth of maximum are analogous to similar

differences in the depth of the observation plane. It should be

noted at this point that the deviations shown in figures 6-7 are

within the experimental errors of the present work, and were not

noted in earlier simulations. Figure 6-8 shows the simulation

results for the exponent plotted against Tmax/T (appropriate for

a non-penetrating component). Clearly the lateral distribution of

Cerenkov light does not fit into the category (2) either.

In addition to the predictions for η , changes in δ (the

exponent of the peak height lateral distribution) and the FWHM(300m),

with primary energy and the depth of observation were available

from the series of computer simulations. It was also possible, by

considering the results from a series of simulated fluctuating

showers, of fixed primary energy and mass, to determine the change

in the above parameters resulting from changes in depth of maximum,

at fixed primary energy. Table 6-1 summarises the predicted changes

in each of the parameters for changes in depth of maximum of 100g

cm^{-2}. The choice of models is of no consequence as the depth of

maximum and observation levels are the important quantities.

The tendency shown in Figure 6-7 and 6-8 are quantified by

these results. The expected variations in the parameters

are seen to be the same for changes in the average depth of

maximum resulting from changes in depth of maximum (induced by

changes in primary energy) and from direct fluctuations in

the development of individual showers. However, the parameters

FIGURE 6-8

The predicted variation of structure function exponent

with Tmax/T at two different observation depths; from

average simulations of primaries of energy 10^{15}-10^{18} eV

and mass 1 and 56.
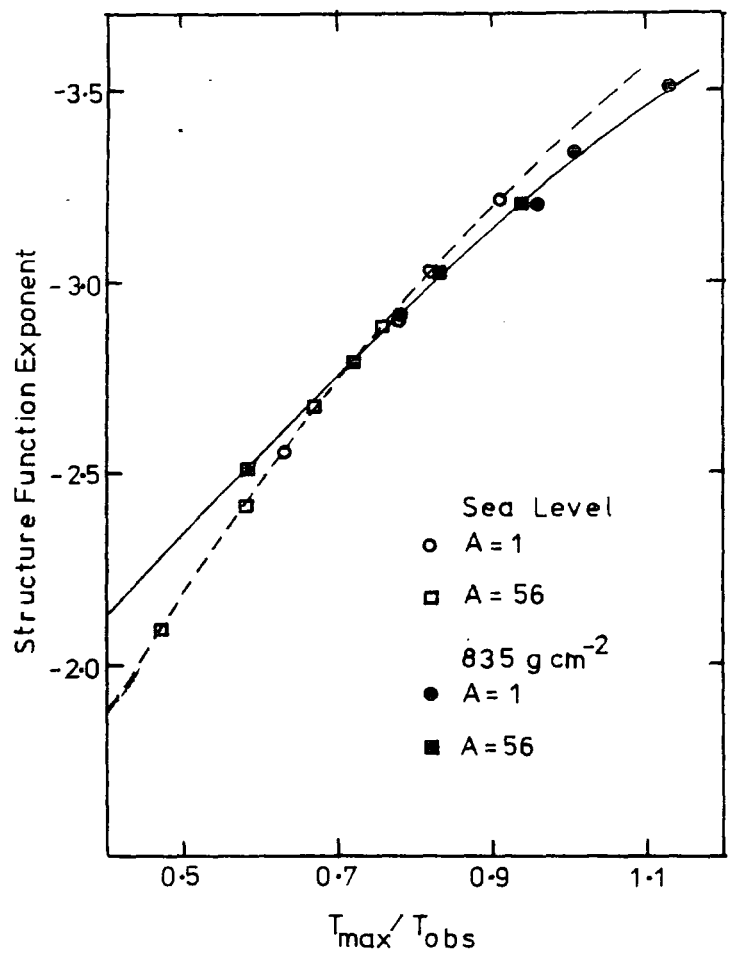
TABLE 6-1

Variation of parameters η, δ, FWHM(300) with changes to $T_{obs} - T_{max}$ of 100 g cm^{-2}

Average showers A = 56 Ep = 10^{15}-10^{18}eV Scaling Model		
CHANGE IN $T_{obs} - T_{max}$ from		
	Change in T_{max} due to Primary energy	Change to observation Depth
η	0.28	0.18
δ	0.40	0.29
FWHM(300m)(ns)	9.7	5.1

Fluctuating showers A = 1   Ep = 10^{17}eV   Landau Model

CHANGE In $T_{obs} - T_{max}$ from		
	Change in Depth of Maximum	Change in observation Depth
η	0.25	0.19
δ	0.36	0.20
FWHM(300m) (ns)	10.7	5.6

are seen to vary at a quite different rate for changes in T-Tmax

due to changes in the observation depth. In general the variations

with observation depth are seen to be about 60% of the changes

with depth of maximum. All these results were for vertical

showers; it would be expected that some parameters in inclined

showers show a further difference as showers develop through

an inclined atmosphere.

To summarise, our simulation results indicate that the

technique of determining elongation rates by comparing changes

in parameters arising from observation of showers of different

energy at different observation depths may be liable to

complications. The problem may be further complicated when

showers incident from a range of zenith angles are considered.

Computer simulations of inclined showers are presently being

calculated and the results may be expected to assist the full

explanation of the results of this and other experiments.

6-4   Comparison with other working

6-4-1 Comparison of the lateral distribution of pulse area

The Soviet group work at Yakutsk pioneered measurements

of Cerenkov light in large EAS and have presented measurements

of the FWHM together with the density lateral distribution of

Cerenkov radiation. Figure 6-9 shows the comparison between

the lateral density distribution measured at the Yakutsk (sea-

level) and Dugway arrays. The Yakutsk measurements were made

in showers of mean sea-level size $\overline{N} = 1.4 \times 10^7$ and $\overline{N} = 1.7 \times 10^8$

particles, incident at a mean angle of 16°. The comparison was

made with showers recorded at Dugway with energy estimators in

the regions $8.67 < \log C_{50}^{250} \lesssim 9.0$ and $9.33 < \log C_{50}^{250} \lesssim 9.67$

and the two sets of data were normalised at 200m for the low

FIGURE 6-9

A comparison of the lateral distribution of photon

density as measured by the Dugway experiment and by

Diminstein et al (1973). The photon density scale

refers to the Soviet work.

Photon Density (m^{-2}) vs Core Distance (m)

Dimenstein et al

■ $\bar{N} = 1.7 \times 10^8$

□ $\bar{N} = 1.4 \times 10^7$

This work

● $8.67 < \log(C_{250}^{50}) \leqslant 9.0$

○ $9.33 < \log(C_{250}^{50}) \leqslant 9.67$
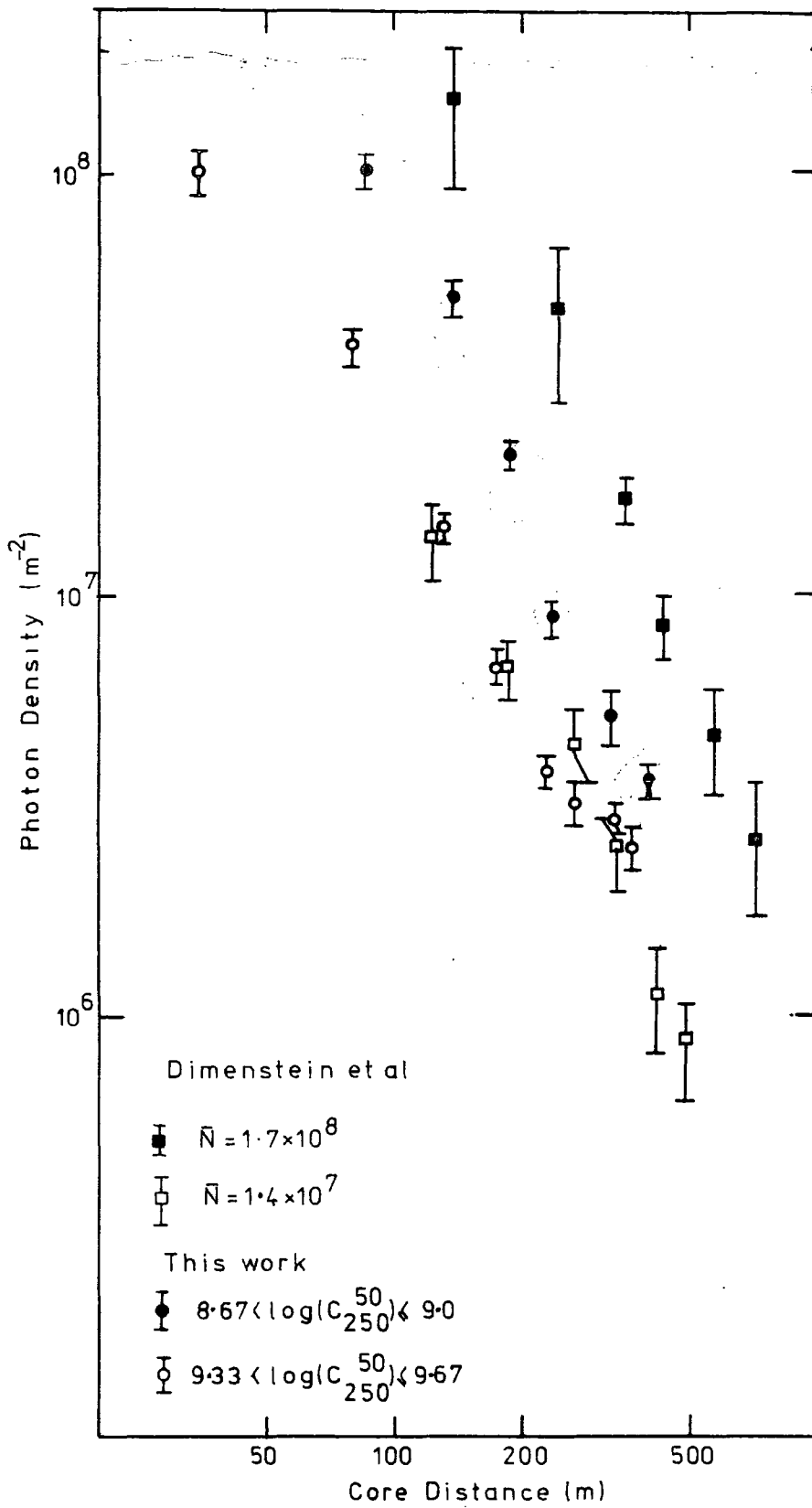
energy showers measured at Yakutsk and the high energy showers measured at Dugway. (The very different photomultipliers used in the two systems would not allow for a meaningful comparison based upon the absolute calibration of the two systems). It can be seen that the showers at Dugway have a steeper lateral distribution than at Yakutsk, in agreement with expectations, as the Dugway array is situated higher into the atmosphere.
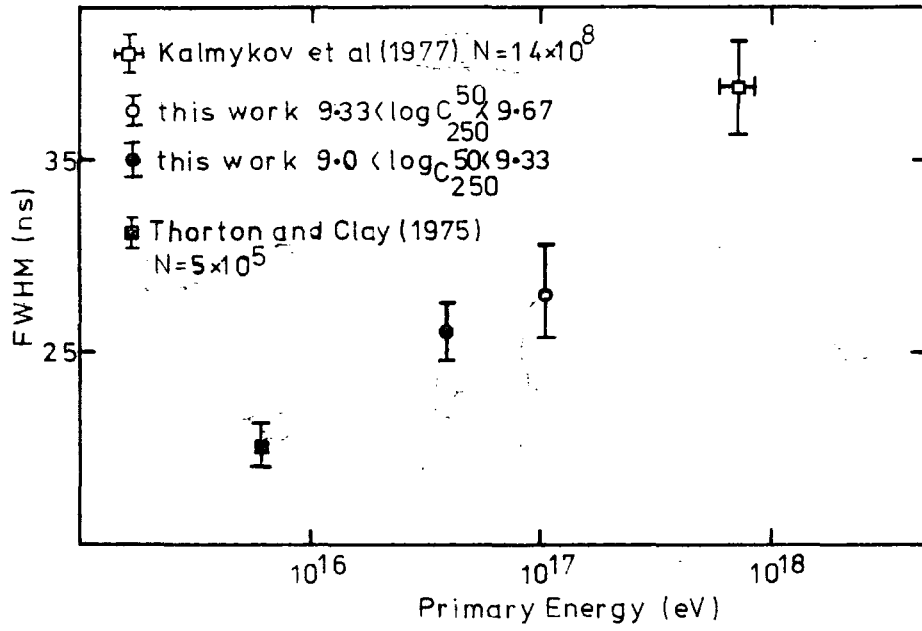
6-4-2 Comparisons of the shape of Cerenkov Pulses

Making comparison of pulse shape measurements is complicated by the very different system responses of the various arrays through the world. The pulse shape measurements at Yakutsk were made using a system where response to 2ns wide pulse from a scintillator was 15ns, Grigor'ev et al (1978). The measurements made at Adelaide were made with equipment with a system FWHM of 5.3ns, Thornton et al (1979). The results from these two experiments have been presented with the system response removed by the authors; in the present work no attempt was made to remove instrumental broadening, although the comparable system FWHM was 6.7ns. The two experiments mentioned above made measurements over a wide range of primary energy, about 10^{15}eV at Adelaide and 5×10^{17}eV at Yakutsk.

Figure 6-10 shows the variation of FWHM (300m) (normalised for system response) from vertical showers with primary energy from $10^{15} - 10^{18}$eV. This plot indicates an approximate 6ns change in FWHM (300m) per decade change in primary energy. Although the present Dugway set is preliminary and probably contains residual array biases basic agreement can be seen on this universal plot.

FIGURE 6-10

The variation of FWHM (300m) for vertical showers with
primary energy from the results of this work, Thornton
et al (1979), and Grigor'ev et al (1978) and Hammond
et al (1978).

FWHM (ns)

35

25

□ Kalmykov et al (1977) N=1.4×10^8

this work 9·33 < logC_{250}^{50} < 9·67

this work 9·0 < logC_{250}^{50} < 9·33

Thorton and Clay (1975)
N=5×10^5

Primary Energy (eV)

10^{16} 10^{17} 10^{18}

CHAPTER SEVEN

Conclusions and Future Work

The Cerenkov light experiment at Dugway was concluded in March 1980. The work reported in this thesis was concerned with the important early stages of the experiment. It has been demonstrated that the experiment at Dugway was able to reliably make measurements of Cerenkov radiation in EAS with a high precision. The measurements included the lateral distribution of the pulse area, the FWHM and the peak height of the Cerenkov signals. Analyses of the variation of the above quantities with zenith angle and primary energy have given confidence in the measurements and have enabled a preliminary investigation of the average longitudinal development of EAS to be carried out.

7-1   Conclusion from the present work

7-1-1   The Digital Recording Array

A novel feature of the Dugway array was the application of digital recording techniques to the measurement of nanosecond signals in a field environment. The construction and calibration of the Atmospheric Cerenkov Detector Array at Dugway have been described in Chapters 3 and 4. The sensitivity of the Dugway equipment to Cerenkov radiation from EAS was demonstrated to be as follows. The time response of the detectors was synchronised to an accuracy of better than 1ns which allowed for measurements of the curvature of the light front to a greater accuracy than in earlier work at Haverah Park. The area of the Cerenkov pulse could be determined to an accuracy of 5×10^{4} photons m^{-2} over the range 3×10^{5} to 5×10^{7} photons m^{-2}. The

pulse structure was determined by measuring narrow segments of
the Cerenkov pulse; such 10ns wide 'slices' could be determined
to a precision of 10^4 photons m^{-2} per slice over the range 5×10^4
to 7×10^6 photons m^{-2} per slice.

The employment of modern microelectronics has provided a
basis for reliable operation of complex equipment over an ex-
tended period. The experiment was operated for three periods,
from October to December 1977, October 1978 to March 1979 and
August 1979 to March 1980. The experiment has yielded a total
of about 7000 showers of energy about 10^{17} eV, 5000 showers of
energy about 10^{16} eV, and 2500 showers of energy about 10^{15} eV
under clear sky conditions. During the first two periods in excess
of 3000 events of primary energy about 10^{17} eV were recorded;
of these 130 were selected from the second period to form a small
sample for a preliminary analysis. The analysis of the full
sample, involving interpretation of about 100000 pulses, based
upon techniques developed for the pilot sample, is now nearing
completion (May 1980).

7-1-2 Data Analysis

The characteristics of Cerenkov light averaged over 130
showers of energies around 5×10^{16} eV have been measured. From
these showers it was possible to establish the following
quantities:-

  (1) A very accurate estimate of the shower arrival direction.
  (2) The shape of the lateral distribution of pulse area.
  (3) The shape of the Cerenkov pulses, defined here by
       their FWHM and peak height.

From the lateral distribution of pulse area it was possible
to estimate the energy of each shower. Two possible energy

estimators have been employed, the photon density at a core

density at a core distance of 200m and the integral of the

lateral structure function between 50-250m core distance (rep-

resenting 25% of the total light flux). The new quantity C_{50}^{250}

was found to be less susceptible to the form of function used to

describe the lateral distribution than the quantity $\phi(200m)$. It

was also noted from simulations that C_{50}^{250} did not fluctuate

with Ne_{max} for showers of fixed primary energy. However, it

should be stressed that C_{50}^{250} has not been compared to other

established primary estimators. This is in contrast to

$\phi(200m)$ which compared favourably to particle array primary energy

estimators; measurements of $\rho(500)_{ve}$ at Haverah Park and

measurements of Ne_{max} at the Volcano Ranch array.

The measured average features of the Cerenkov light from

EAS at Dugway were found to be in broad agreement with the

results of simulations based upon a Landau type model where

enhanced low energy particle production produces a rapid cascade

development and a high depth of cascade maximum. In particular,

close agreement was found between measurements made in showers

of energy $9.33 < \log_{10} C_{50}^{250} < 9.67$ (estimated to correspond to

$10^{17}-2 \times 10^{17} eV$) and a simulated average shower of energy

$10^{17} eV$ initiated by a primary iron nucleus which had a depth

of electron cascade maximum of $585 g\ cm^{-2}$. Again, it must be

stressed that for Cerenkov light measurements, the type of model

used in the calculation is not important; the Cerenkov light

signature is governed by the depth of maximum predicted by the

simulation. In the present instance the preliminary results from

the Dugway experiment were consistent with an electron cascade

maximising at the above depth, but do not necessarily indicate

the validity of a Landau-type model or the primary mass used

in the computer simulation.

It was found that the observations at Dugway (mean vertical

depth 862g cm^{-2}) of the distribution of pulse area compared

favourably with the observations made at Haverah Park (mean

vertical depth 1016g cm^{-2}). The variation of the shape of the

lateral distribution of pulse area with atmospheric thickness

indicated that both experiments were observing a broadly similar

development of Cerenkov light in EAS. This was despite a difference

of about 150g cm^{-2} in the mean vertical atmospheric depth at

which measurements were made.

7-1-3 Computer Simulations

The interpretation of this result was extended by considering

a series of simulations of vertically incident showers. It was

noted from the simulations that the variation of the shape of

the lateral distribution with atmospheric thickness should be

different at the two depths of the two experiments. Typically

the lateral distribution in the same shower represented by a

function of the form $(r + r_0)^{\eta}$, would be well fitted with

values of e.g. 3.0 at 862 g cm^{-2} and 2.6 at 1016 g cm^{-2},

consistent with observations. The simulations indicated that the

value of η for the same thickness of atmosphere between the

depth of cascade maximum and the observation plane was different

by 0.1 at the two observation depths. This later difference,

although apparent in the observed distributions, was not sig-

nificant due to the experimental errors in the initial small

data sample.

It was also noted from the simulations that Cerenkov light

parameters did not vary with changes in the position of T_{max}
in the same way, when the changes arose for alterations in the
observation depth (as arises for measurements at Dugway and Haverah
Park), as they did for direct changes in the depth of cascade
maximum (as arises from between shower fluctuations and changes
in primary energy). From these results the validity of the
elongation rate theorem as applied to Cerenkov light parameters
was called into question. It was confirmed that elongation rates
determined by considering the changes in an EAS parameter, P,
due to changes in primary energy (i.e. depth of maximum) and
zenith angle (i.e. observation depth) must account for P not varying
identically with changes in the depth of cascade maximum and the
observation depth. Specifically the FWHM(300m) was found to change
by 9ns for changes in depth of maximum of $100g \ cm^{-2}$ and by
5 ns for changes in the observation depth of $100g \ cm^{-2}$; the
analogous figures for the lateral distribution shape parameter
were 0.28 and 0.18.

7-1-4   The Shape of the Cerenkov Pulses

The understanding of the shape of the Cerenkov pulses was
not at this stage in the analysis as detailed as the understanding
of the lateral distribution of pulse area. The two measures of
pulse shape, the FWHM and the peak height of the pulses, observed
at Dugway were found to be consistent with a simulated shower
based upon a Landau-type model and having a depth of electron
cascade maximum of 585 $g \ cm^{-2}$. This model has been found to be
consistent with the results from Haverah Park, Gaisser et al
(1978). A direct comparison between the results of the experiments
at Dugway and Haverah Park was not possible due to the different

bandwidths of the two systems. The variation of FWHM(300m)
with atmospheric thickness was observed to be similar, about
5ns decrease in FWHM(300m) for each additional 100g cm^{-2} of
atmospheric thickness. A comparison of the results from the Ad-
elaide and Yakutsk groups, indicated that the FWHM(300m) for vert-
ical showers varies uniformly by 6ns per decade of primary energy
in the region $5.10^{15}-10^{18}$eV.

7-2   Future work

7-2-1 The Dugway Experiment

After 3 seasons of observation the Dugway experiment has
recorded in excess of 15000 EAS under clear sky conditions.
The analysis of these showers is still continuing and the
objective is to provide a detailed understanding of the longi-
tudinal cascades of EAS of energy $10^{15}-5 \times 10^{17}$eV. This large range
of primary energy was achieved by utilisation of the versitility
of the equipment which allowed for the detectors to be readily
rearranged to form arrays of different size and thus responding
to EAS of different energy. This review of the expectations of
the Dugway experiment will discuss the conclusion of the analysis
of the results from the array described in this thesis, in the
configuration which made measurements in the highest energy
showers. Finally, the prospects for the measurements made with
the smaller arrays will be discussed.

The understanding of the lateral distribution of pulse
area of the high energy showers measured at Dugway is now at an
advanced stage. However, two problems remain; the need to
determine the best functional form of the lateral distribution,
and to choose the most appropriate primary energy estimator.
Analysis of the 7000 showers recorded by the large array at

Dugway should then allow for a determination of the fluctuations in the shape of the lateral distribution (and hence cascade development) to be accurately determined.

The process of determining the shape of the Cerenkov pulses from the distribution of slices has already been improved and automated to allow the shape of about 100,000 pulses recorded at Dugway to be studied.

The most probable analysis of the reconstructed pulse will be based upon estimates of the rise-time, top-time and fall-time, so providing three independent measures of pulse shape. The preliminary technique of determining pulse shape described in this work has indicated that the three independent measures of pulse shape are already showing the expected sensitivity to shower development. Figures 7-1 to 7-3 show the variation of rise-time, top-time and fall-time with core distance, for showers in the highest primary energy band ($\approx 3 \times 10^{17}$ eV) recorded at zenith angles in the range 0-50°.

To compliment the study of the pulse shape it will be possible to combine the synchronised time response of the detectors with the pulse shape information to 'image' the longitudinal cascade of Cerenkov radiation (cf section 2-4-3). This study should enable the change in the depth of cascade maximum with changes in primary energy to be determined without the problems inherent in the elongation rate theorem.

Finally, these measurements of Cerenkov light in EAS were complemented by data from up to four 1 m^2 plastic scintillators, deployed to measure the electron component. Earlier measurements at Haverah Park, Shearer (1978), indicated that the separation of the particle and Cerenkov light fronts was a parameter which

FIGURES 7-1 - 7-3

The variation of rise time, top time and fall time

with core distance for the preliminary data sample
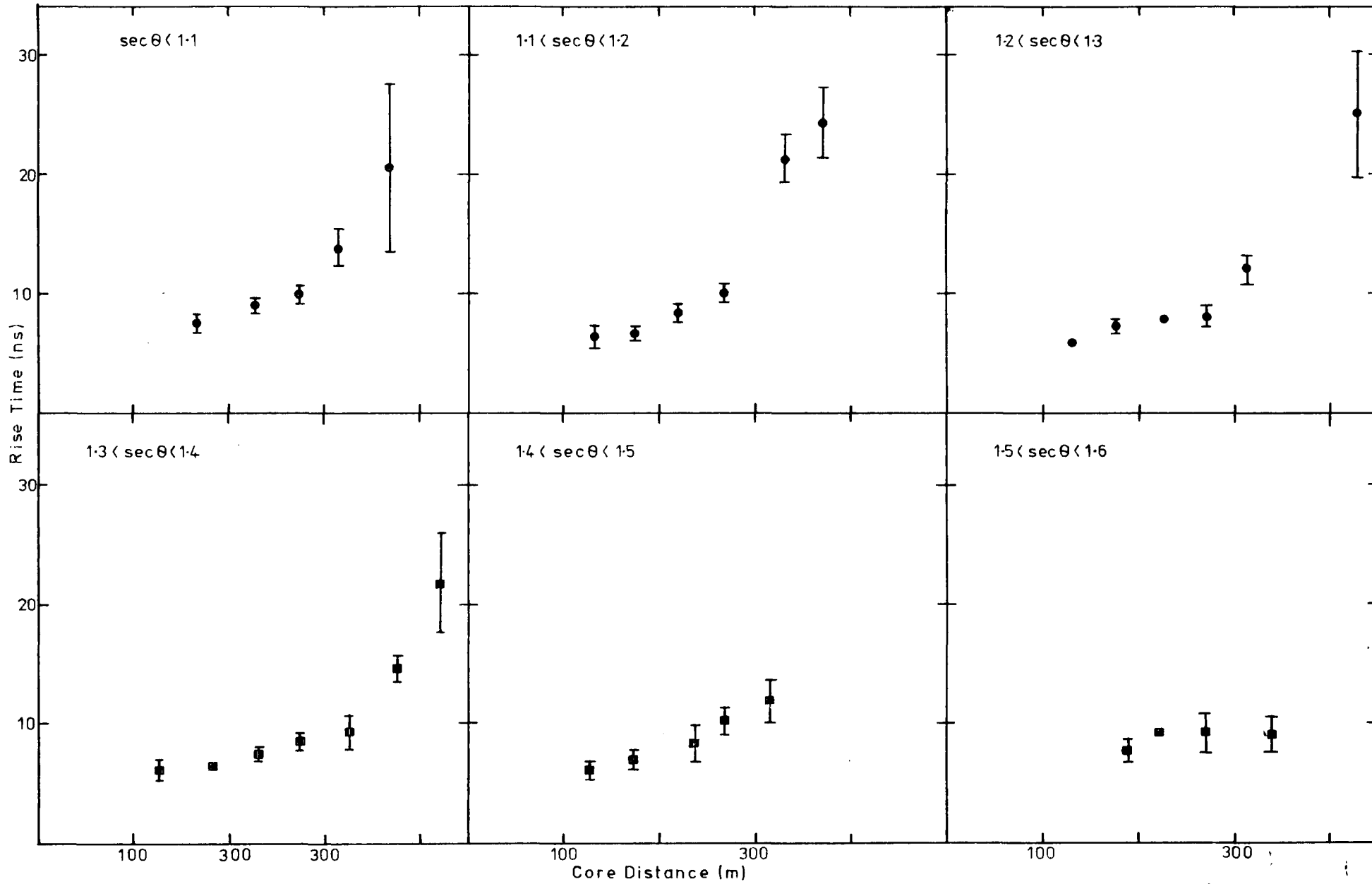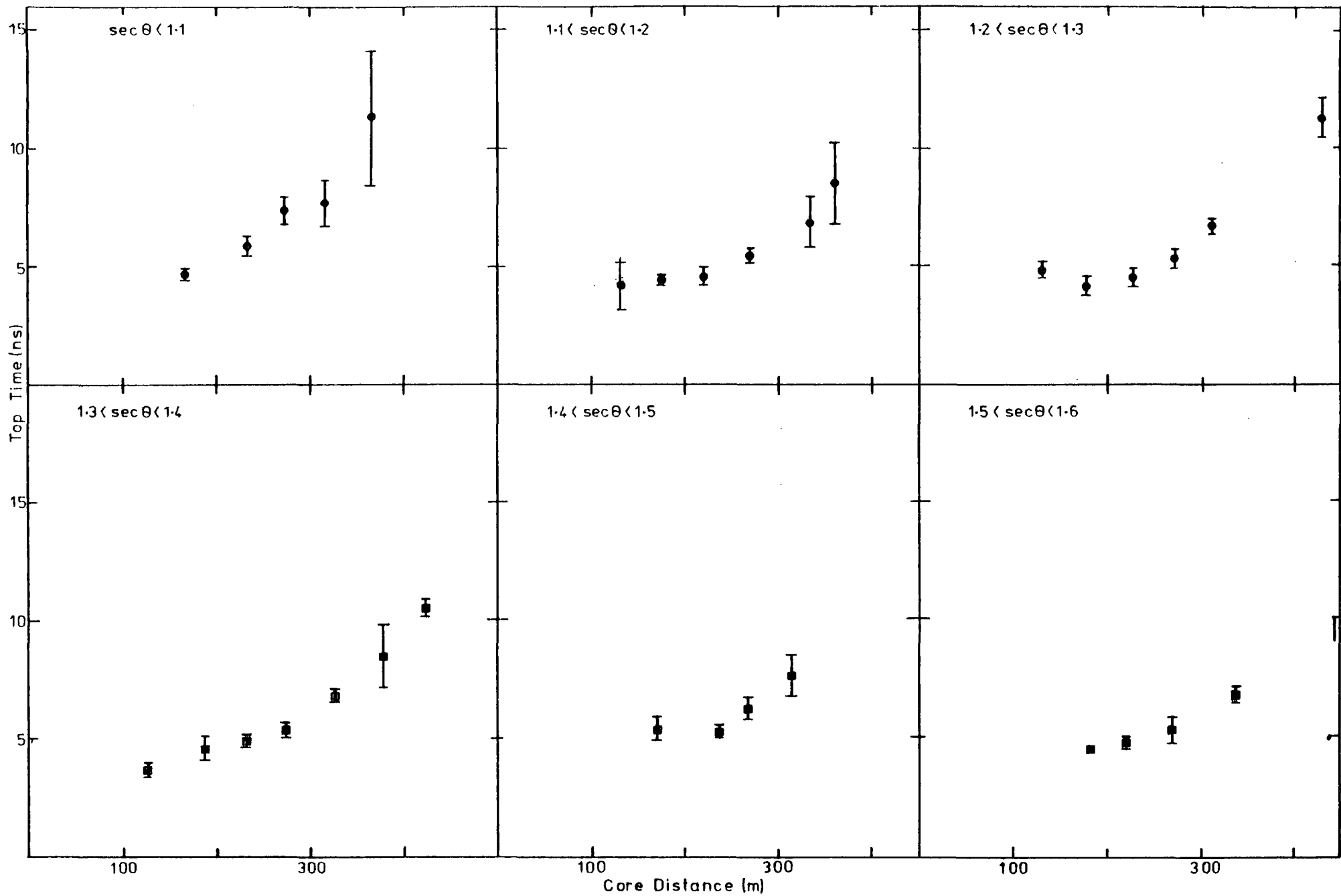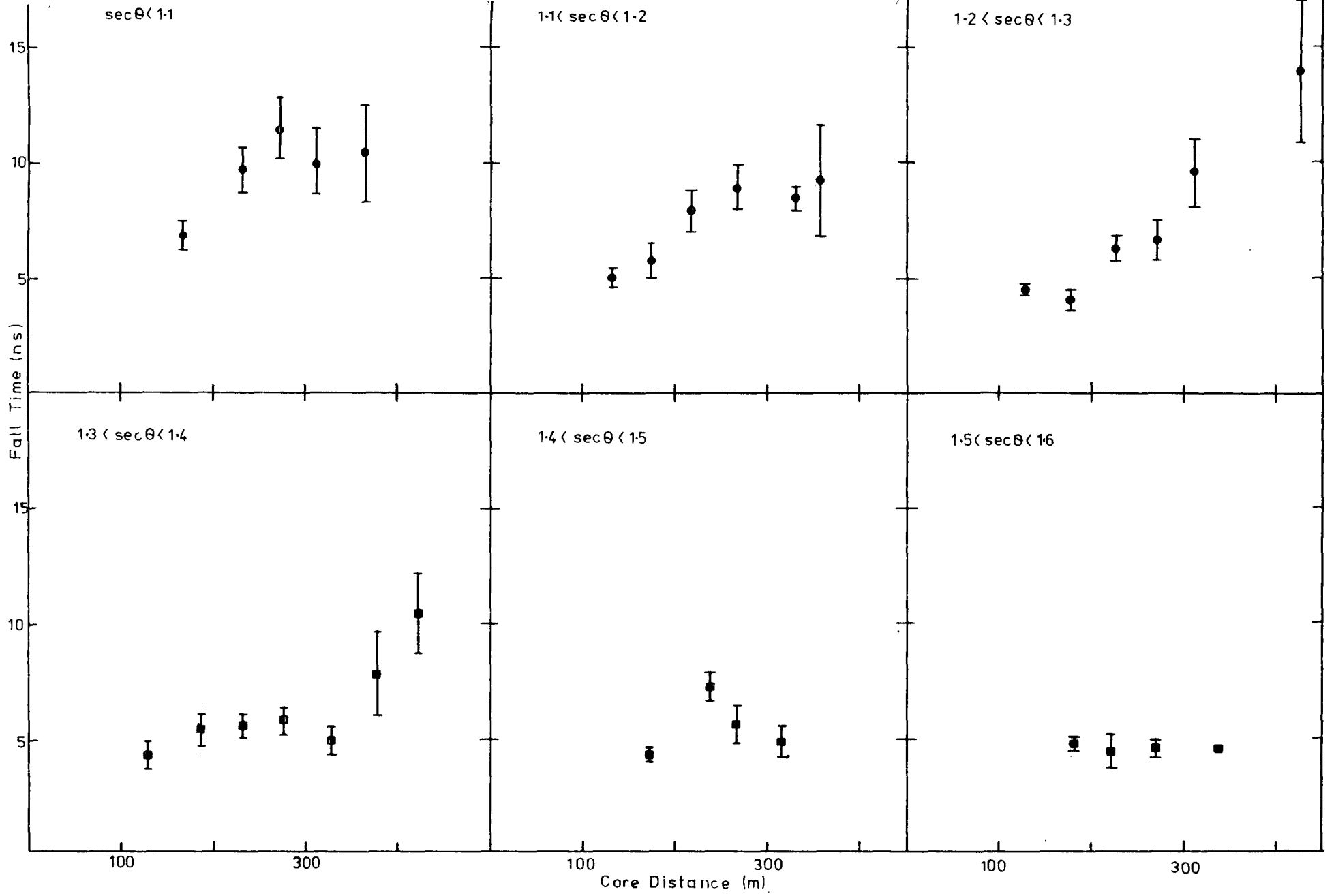
was also showed sensitivity to shower development. It has been

further suggested by Chantler et al (1979)b and Gaisser et al

(1979) that the ratio between the Cerenkov light and particle

denisty, at say 100m, would provide a classic non-fluctuating/

fluctuating parameter measurement and thus a further measure of

shower development. Chantler et al presented the preliminary study

of the time response of 2 of the scintillators recorded during the

second season of observation. The authors demonstrated with a

sample of showers taken from only 30 hours of observation that the

separation of the two fronts was a measureable quantity which

showed sensitivity to shower development. They concluded that

measurements of the separation of the two fronts were also un-

usual in that the front separation increases with increasing at-

mospheric thickness between the observation level and the cascade

maximum (and thus with decreasing primary energy and zenith angle).

This is in contrast with most EAS parameters which lo se sensitivity

to cascade maximum in smaller or more inclined showers.

The conclusion of this analysis of the data from the

Cerenkov light array measuring showers of energy $5x10^{16}$-$5x10^{17}$eV

is that finally there should be measurements of up to seven

independent variable in more than 1000 showers. After a detailed

study of the errors of the experiment it should be possible to

study the true fluctuations in the seven quantities and hence

in the cascade development.

The experiment at Dugway has already been extended to measure

showers of lower primary energy. By rearranging the array so

that the distance of the outer ring of detectors was reduced

from 400m from the array centre to 200m, 100m and finally 50m,

it was possible to observe showers over the range $\simeq 10^{15}$eV to

$\rangle 10^{17}$ eV. Such changes occurred typically during a single day

between consecutive nights observing periods. It was the

original intention with this experiment to study the important

region of the energy spectrum at 3×10^{15} eV after the main work

on high energy showers had been completed. The requirement for

this study was emphasised by the work of Thornton and Clay (1979)

which suggested that the depth of electron maximum changes very

rapidly in the region 5×10^{15}-5×10^{16} eV. It should be possible to

test Thornton and Clay's conclusion with our array of 8 detectors,

thus removing the possible spurious core distance dependence still

remaining in Thornton and Clay's work, see Orford and Turver

(1980). However, some limitations are foreseen. The Dugway

experiment was specifically designed to measure Cerenkov

radiation in large EAS at core distances greater than 200m where

the pulses are not seriously affected by the system bandwidth

and have FWHM $\rangle$ 20ns. The design specification of the equipment

will be exceeded if pulses are to be measured at core distances

less than 100m. Further studies of simulation results indicate

that at core distance less than 100m most Cerenkov light parameters

are insensitive to shower development; the structure function is

broad and less sensitive to cascade development, the Cerenkov

pulse shapes are invariant with cascade development, and the use

of synchronised timing to 'image' the longitudinal cascade becomes

impossible. Despite these inherent problems the results from this

study of the smaller showers may provide exciting insights into

the development of EAS over a wide range of primary energy,

after the sensitivity of such small shower measurements has

been established.

7-2-2 <u>Computer Simulations</u>

Analyses of the preliminary Dugway data have indicated a number of potential problems which it was thought could only be solved after further simulations of showers, especially those incident at a range of zenith angles. The major problem which has been identified concerns the validity of the elongation rate theorem. The theorem and its application is of great importance for the successful analysis of a generation of cascade development measuring experiments. In section 6-3 it was indicated that the inherent assumption in elongation rate theory, that the changes in depth of cascade maximum (arising from changes in primary energy or fluctuations in shower development) are similar to variations in the observation depth (arising in most experiments from changes in zenith angle), was not valid. So far we have shown with the help of simulations for vertically incident showers appropriate to Dugway and Sea-Level, that changes in depth of maximum are not equivalent to changes in observation depth. For example, we expect that the change in structure function exponent or FWHM (300m) per 100g cm^{-2} change in depth of maximum to be about twice that arising from a 100g cm^{-2} change in observation level for showers with the same depth of maximum. It is expected therefore that inclined showers may have significantly different properties to vertical showers and may present further problems to the interpretation of shower parameters.

The difficulties in interpretation are expected to be resolved after studying the results of these computer simulations which at the time of writing are at an advanced stage. In the past observations at Haverah Park and the development of the experiment described in this thesis have benefited from a similar series of simulations for vertically incident showers. The understanding

of Cerenkov radiation in EAS has since developed to the extent
that the Dugway experiment requires these new rigorous simulation
if the full potential of its results is to be exploited. New,
more detailed simulations for the near-core responses in the smaller
showers will have an important role to play in the final inter-
pretation of the small shower measurements.

The present work has clearly shown that the Dugway
experiment has the capability of making measurements of Cerenkov
radiation with a higher precision than was previously attainable.
The limited sample of showers studied in this work have indicated
that the sensitivity of Cerenkov radiation to shower development
suggested by our earlier experiment at Haverah Park was apparent.
There are good indications that the final analysis of the
Dugway data set should make possible, via studies of fluctuations
in the derived independent parameters, a determination of the
validity of particular models of the particle physics. An
assessment of the longitudinal cascade of Cerenkov radiation should
make a useful contribution to the study of the primary mass at
air shower energies.

REFERENCES

Anderson, C.D., 1932, Science, 76, 238.

Andam, A., Chantler, M.C., Craig, M.A.B., Orford, K.J.,
    Shearer, J.A.L., Turver, K.E. and Walley, G.M., 1979,
    Proc. XVIth Int. Conf. Cosmic Rays, Kyoto, 9, 48.

Blackett, P.M.S., 1948, Emission Spectra of the Night Sky and
    Aurora, Physical Society of London Gassiot Committee
    Report, 34.

Boley, F.I., 1964, Rev. Mod. Phys., 36, 792.

Cerenkov, P.A., 1934, Dokl. Akad. Nank., 2, 451.

Cerenkov, P.A., 1937, Phys. Rev., 52, 378.

Chantler, M., Orford, K.J., Shearer, J.A.L., Turver, K.E. and
    Walley, G.M., 1979a, Proc. XVIth Int. Conf. Cosmic Rays,
    Kyoto, 9, 42.

Chantler, M., McComb., T.J.L., Orford, K.J., Shearer, J.A.L.,
    Turver, K.E., and Walley, G.M., 1979b, Proc. XVIth Int.
    Conf. Cosmic Rays, Kyoto, 9, 56.

Chudakov, A.E., Nesterova, N.M., Zatsepin V.I. and Tukish, E.I.,
    1960, Proc. Moscow Conf. Cosmic Rays, 2, 50.

Cocconi, G., Koestler, L.G. and Perkins, D.H., 1961, Lawrence
    Radiation Lab. Seminars, 28, pt. 2, UCID-144, 1.

Cox, M.G., 1972, J. Inst. Maths. Applics., 10, 134.

Craig, M.A.B., McComb, T.J.L. and Turver, K.E., 1979, Proc.
    XVIth Int. Conf. Cosmic Rays, Kyoto, 8, 180.

Diminstein, U.C., Kolosov, V.A., Krasilnikov, D.D., Kusmin, A.I.,
    Kalakovskaya, V.P., Orlov, V.A., Sleptsov, I.Ye.,
    Yefimov., N.N. and Yegorev, T.A., 1972, paper presented to
    the European Symposium on Air Showers, Paris.

Feynman, R.P., 1969, Phys. Rev. Lett., 23, 1415.

Frank, I.M. and Tamm, Ig., 1937, Dokl. Akad. Nauk, 23, 1413.

Gaisser, T.K., McComb, T.J.L. and Turver, K.E., 1978, Rev. Mod. Phys., 50, 859.

Gaisser, T.K., McComb, T.J.L. and Turver, K.E., 1979, Proc. XVIth Int. Conf. Cosmic Rays, Kyoto, 9, 275.

Galbraith, W. and Jelley, J.V., 1953, Nature, 171, 349.

Galbraith, W. and Jelley, J.V., 1955, J. Atmos. and Terrestial Phys., 6, 250, 304.

Grigor'eV, V.M., Efimov, N.N., Kalmykov, N.N., Nechin Yu.A., Prosin, V.V., and Khristiansen, G.V., 1978, Sov. J. Nucl. Phys., 27(2), 225.

Hammond, R.T., Protheroe, R.J., Orford, K.J., Shearer, J.A.L., Turver, K.E., Waddoup, W.D. and Wellby, D.W., 1978, II Nuovo Cimento, IC, 315.

Hillas, A.M., 1975, Phys. Rep., 20, 59.

Hillas, A.M., 1979, Proc XVIth Int. Conf. Cosmic Rays, Kyoto, 8, 7.

James, M. and Roos, M., 1975, Comp. Phys. Comm., 10, 343.

Jelley, J.V., 1958, Cerenkov Radiation and its Applications, Pergamon Press, London.

Jelley, J.V., 1967, Prog. Cosmic Ray Phys., 10, 41.

Juliusson, E., 1975, Proc. XIVth Int. Conf. Cosmic Rays, Munich, 8, 2689

Kalmykov, N.N., Khristiansen, G.B., Nechin, Y.A., Prosin, V.V., Efimov, N.W. and Grigor'eV, V.M., 1976, paper presented to the European Symposium on Air Showers, Leeds.

Kalmykov, N.N., Kristiansen, G.B., Nichin Gn.A., Prosin, V.V., Grigor'eV, V.M., and Efimov, N.N., 1977, Proc., XVth Int. Conv. Cosmic Rays, Plovdiv, 8, 244.

Krasilnikov, D.D., 1979, Proc. XVIth Conf. Cosmic Rays, Kyoto, 2, 26.

Linsley, J., 1973, Proc XIIIth Int. Conf. Cosmic Rays, Denver, 5, 3207.

Linsley, J., 1977, Proc. XVth Int. Conf. Cosmic Rays, Plovdiv, Preprint.

Linsley, J., 1979, Proc. XVIth Int. Conf. Cosmic Rays, Kyoto, 9, 274.

Lloyd-Evans, J., Pollack, A.M.T. and Watson, A.A., 1980, Proc. XVIth Int. Conf. Cosmic Rays, Kyoto, 13, 130.

Marsden, R.G., Elliot, H., Hynds, R.J. and Thambyahpillai, T., 1976, Nature, 260, 491.

Orford, K.J., Stubbs, R.J. and Waddoup, W.D., 1977, Nucl. Inst. and Math., 146, 389.

Orford, K.J. and Turver, K.E., 1976, Nature, 264, 727.

Orford, K.J. and Turver, K.E., 1980, Phys. Rev. Lett., 44, 959.

Osborne, J.L., Wolfendale, A.W. and Wdowczyk, J., 1977, Proc. XVth Int. Conf. Cosmic Rays, Plovdiv, 2, 182.

Pollack, A.M.T. and Watson, A.A., 1975, Proc. XIVth Int. Conf. Cosmic Rays, Munich, 2, 298.

Protheroe, R.J., 1977, Ph.D. Thesis, University of Durham.

Protheroe, R.J. and Turver, K.E., 1977, Proc.XVth Int Conf. Cosmic Rays, 8, 275.

Shearer, J.A.L., 1978, M.Sc. Thesis, University of Durham.

Smith, G.J. and Turver, K.E., 1973, J. Phys. A., 6, L121.

Stubbs, R.J. and Waddoup, W.D., 1977, Nucl. Inst. and Meth., 146, 389.

Strong, A.W., Wdowczyk, J. and Wolfendale, A.W., 1974, J. Phys. A., 7, 1489.

Thornton, G.J. and Clay, R.W., 1978, J. Phys. G:Nucl. $\underline{4}$, 193.

Thornton, G.J. and Clay, R.W., 1979, Phys. Rev. Let., $\underline{43}$, 1622

Thornton, G.J., Kohlmann, J.D., Liebing, D.F., Clay, R.W.,
Gregory, A.G., Patterson, J.R. and Prescott, J.R.,
1979, Proc. XVIth Int. Conf. Cosmic Rays, Kyoto, $\underline{8}$, 103.

Waddoup, W.D. and Stubbs, R.J., 1975, Nucl. Inst. and Meth.,
$\underline{137}$, 133.

Waddoup, W.D. and Stubbs, R.J., 1977, Nucl. Inst. and Meth.,
$\underline{146}$, 561.

Webber, W.R., Lezniak, J.A., Kish, J. and Damle, S.V., 1973,
Astrophys. Space Sci., $\underline{24}$, 17.

Wellby, D.W., 1977, Ph.D. Thesis, University of Durham.